SKI Report 2004:54

Research

Studies of Corrosion of Cladding Materials in Simulated BWR-environment Using Impedance Measurements

Part II: Measurements in the Post-transition Region

Stefan Forsberg
Elisabet Ahlberg
Ulf Andersson

September 2004

ISSN 1104–1374
ISRN SKI-R-04/54-SE

SKI

SKI Perspective

Fuel rod cladding waterside corrosion is one of the phenomena that limits the life time of nuclear fuel. Corrosion performance depends on the cladding material properties as well as operating conditions during the irradiation of the fuel. The corrosion resistance of the cladding is affected by its chemical composition and the manufacturing process. Fuel rod power history, coolant temperature and water chemistry are among the operational parameters that influence corrosion. In an ideal situation, the oxide film formed on the surface of a material protects the material against further degradation. The degree of protection depends on the properties of the oxide. Since these properties change as the oxide grows, the oxidation process has stages of different growth rates. In order to understand the mechanisms it is therefore important to monitor the corrosion process of the material through the different stages. Available methods to measure oxide thickness, however, are designed to measure oxide in the late stages of oxidation when the oxide has grown thick, and they do not allow measurement simultaneously with growth.

The project was initiated to qualify a technique for measuring oxide in-situ in an autoclave in the different stages of growth. The technique is based on electrochemical impedance spectroscopy and allows, in addition to the oxide layer thickness, the measurement of several physical properties that characterise the oxide layer. The results of the project are presented in two separate reports. They concern measurements in the pre- and post-transition corrosion regimes, respectively.

SKI has participated in the project in order to encourage efforts to increase the understanding of corrosion mechanisms for fuel rod cladding and other Zirconium components. This in turn will support the ability to make fair judgements about consequences from changes in the operation of power plants and to validate the potential improvements of new cladding materials. An additional incentive for supporting this research is that it contributes to the development of knowledge and competence in the Swedish nuclear industry, institutes and universities.

Responsible for the project at SKI have been Ingrid Töcksberg and Jan-Erik Lindbäck.
SKI reference: 14.6-010346

Studsvik reference: STUDSVIK/N-04/117
2004-09-02, N64051, SKI/KP/STUDSVIK-B47:2

SKI Report 2004:54

Research

Studies of Corrosion of Cladding Materials in Simulated BWR-environment Using Impedance Measurements

Part II: Measurements in the Post-transition Region

Stefan Forsberg
Elisabet Ahlberg
Ulf Andersson

Studsvik Nuclear AB
SE-611 82 Nyköping
Sweden

September 2004

This report concerns a study which has been conducted for the Swedish Nuclear Power Inspectorate (SKI). The conclusions and viewpoints presented in the report are those of the author/authors and do not necessarily coincide with those of the SKI.

Stefan Forsberg
Elisabet Ahlberg
Ulf Andersson

Studies of corrosion of cladding materials in simulated BWR-environment using impedance measurements

Part II: Measurements in the post-transition region

Abstract

The corrosion of two pre-oxidized Zircaloy 2 cladding materials, LK2 and LK3, have been studied in-situ in an autoclave using electrochemical impedance spectroscopy. Measurements were performed in simulated BWR water at temperatures up to 288^{o}C. The impedance spectra were successfully modelled using an equivalent circuit with two time constants for the oxide. This shows that the oxide is composed of an inner and an outer layer. Less information has been possible to gain from the impedance measurements in the post-transition region compared to the measurements in the pre-transition region. However, the thickness of the inner oxide layer, oxide conductivity and oxide porosity were successfully evaluated from the impedance data. The values of these quantities did not differ significantly between the two investigated materials. The thickness of the inner protective layer was found to be about 2 μm. Porosities in the range 3.5-6.4 % and 3.0-10.9 % were derived in the present work for the LK2 and LK3 material, respectively.

Sammanfattning

Korrosionen hos två Zircaloy-2 kapslingsmaterial, LK2 och LK3, har studerats in-situ i en autoklav med användande av elektrokemisk impedansspektroskopi. Föreliggande rapport, som är den andra inom projektet, redovisar resultaten från mätningar på föroxiderade prover i eftertransitionsområdet. Mätningarna har genomförts i simulerat BWR-vatten vid temperaturer upp till 288^{o}C. Uppmätta impedansspektra har modellerats med hjälp av en ekvivalent elektriska krets med två tidskonstanter för oxiden. Det faktum att två tidskonstanter syns i uppmätta spektra visar att oxiden är skiktad och består av ett inre och ett yttre skikt. Mindre information har erhållits från impedansmätningarna i eftertransitionsområdet jämfört med mätningarna i förtransitionsområdet. Oxidtjockleken hos det inre skiktet, oxidkonduktiviteten och oxidens porositet har dock kunnat beräknas från uppmätta impedansdata. Inga signifikanta skillnader gällande dessa kvantiteter hittades mellan de två materialen. Den beräknade tjockleken på det inre oxidskiktet var ungefär 2 μm. Porositeter i området 3.5-6.4% och 3.0-10.9% härleddes för LK2- respektive LK3-materialet.

List of contents

		Page
1	**Introduction**	**1**
2	**Oxidation of Zirconium and its alloys**	**2**
3	**Experimental**	**5**
3.1	Materials	5
3.2	Experimental set-up and procedure	7
3.3	Chemistry	9
4	**Results**	**10**
4.1	The LK2 material	10
4.2	The LK3 material	25
5	**Discussion**	**38**
6	**Conclusions**	**42**
Acknowledgements		**43**
References		**44**
Appendices		
A	Data from potential measurements	
B	Measured impedance spectra	
C	Parameter values from equivalent circuit analysis	
D	Values of α-corrected (extrapolated) capacitance and accompanying values of the dispersion factor	

1 Introduction

Zirconium alloys are widely used as fuel cladding material in nuclear power plants because of their low thermal neutron cross section, mechanical properties and corrosion resistance. In pressurized water reactors (PWRs) Zircaloy 4 and in boiling water reactors (BWRs) Zircaloy 2 are used for fuel tubes. Corrosion performance is a very important parameter and a lot of work to improve the corrosion resistance has been done. The cladding material's resistance to corrosion may limit the lifetime of the fuel in the core. The corrosion performance is a function of the materials properties (alloy composition and heat treatment) and the environment, such as temperature and water chemistry. Irradiation has also an impact on the corrosion of the cladding.

Impedance measurements can be used to investigate in-situ the physical properties of the oxide formed on the zirconium alloy. Information on the following properties can be obtained from the measurements:

- Number of layers in the oxide
- Oxide thickness
- Oxide conductivity
- Oxide porosity
- Semi-conducting properties of the oxide

Equipment for in-situ impedance measurements of cladding materials at high temperature in simulated nuclear reactor water has previously been designed and built at Studsvik [1]. In the present work, in-situ impedance measurements were performed on three Zircaloy 2 materials, LK2, LK2+ and LK3, in simulated BWR water at high temperatures. These materials have different size distribution of secondary phase particles [2] and show differences in corrosion performance in actual plant. The purpose of the work was to qualify impedance measurements for in-situ studies of corrosion of cladding materials. Measurements have been conducted in both the pre-transition and the post-transition stage. The measurements in the pre-transition region have been accounted for in a previous report [3]. The present report presents the results from the measurements on specimens that have been pre-oxidized (post-transition stage). Measurements have not yet been conducted on the LK2+ sample in the post-transition region and, thus, this material is not accounted for in the present report. The work is a co-operation between Studsvik Nuclear AB and the Department of Inorganic Chemistry at Göteborg University. At Göteborg University, impedance measurements are performed on the same materials in simulated PWR water.

2 Oxidation of Zirconium and its alloys

Due to large affinity of oxygen for zirconium it is difficult to avoid that a thin oxide layer is formed on the metal, even at room temperature. This so-called air-formed film is a thin layer of 2-5 nm oxide. The solubility of oxygen in α-Zr is nearly 30 atomic percent ($ZrO_{0.4}$) at 500°C and does not vary much with temperature. At low oxygen contents the atoms are randomly distributed in the metal, and at higher oxygen contents the atoms are partly ordered. At the composition $ZrO_{0.33}$ the oxygen atoms are completely ordered. When the solubility limit is reached, zirconium oxide (zirconia, ZrO_2) is formed. ZrO_2 exists in three crystallographic modifications at normal pressure: monoclinic, tetragonal and cubic. The stable phase at room temperature is the monoclinic phase. The phase transformation from monoclinic to tetragonal occurs at 1205°C, and from tetragonal to cubic at 2370°C. High pressures stabilize the tetragonal phase so that the transformation from monoclinic to tetragonal phase occurs at lower temperature when the pressure increases.

The phase transformation from metal to oxide is followed by a volume expansion of approximately 50-60 %. This increase of volume results in large compressive stresses in the oxide and tension in the metal. When the oxide thickness has increased above a critical thickness, the large compressive stresses causes mechanical failure of the oxide, and cracks are formed in the outer oxide layer. This is the so-called transition (see also below). The high compressive stresses found at the metal/oxide interface stabilize the tetragonal phase. Therefore, in addition to the monoclinic phase, tetragonal phase may also form during oxidation of Zr. The amount of tetragonal phase is, however, probably small in most cases. In a study where five different zirconium alloys were tested in autoclave at 288°C and 360°C it was found that the amount of tetragonal phase was too low to be detected by x-ray diffraction (see Paper I in Oskarsson [4]). The tetragonal phase was, however, detected by selected area diffraction. The pressure in the oxide layer is highest at the metal/oxide interface and the pressure of an individual ZrO_2-layer decrease when it moves away from the interface during the oxidation process. At the point when the stresses in the oxide have decreased below the critical stress to stabilize the tetragonal phase, the tetragonal phase transforms to monoclinic.

The initial growth rate of the oxide decreases with time up to a transition point, after which the growth rate is linear with time, see Figure 1. The situation can be explained by an approximate equation describing oxidation rate with time as:

$$\Delta w = k\, t^n \qquad \text{(Eq 1)}$$

where Δw = weight gain and

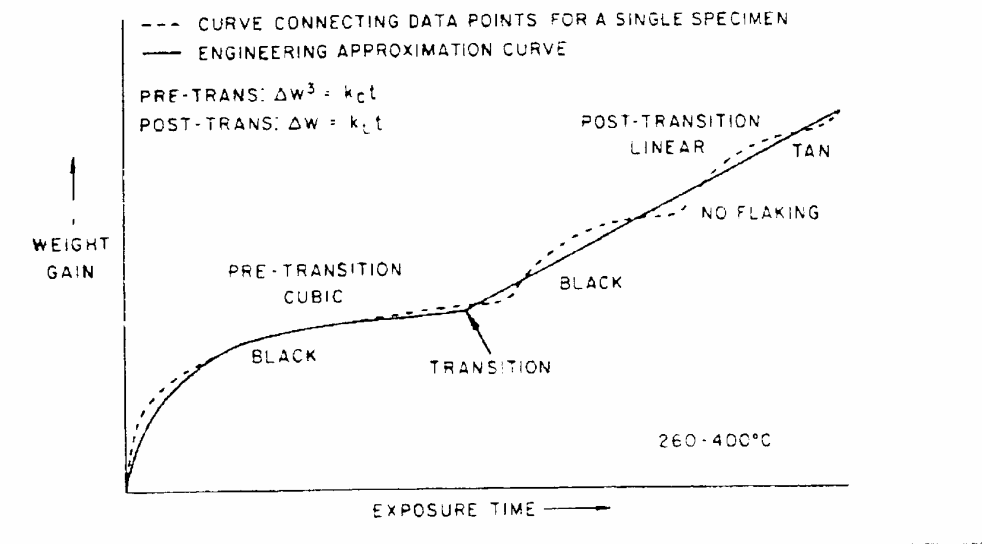

Figure 1
Schematic representation of the corrosion of Zircaloy (Reproduced from Oskarsson [4]).

n = 0.25 – 0.6 during pre-transition growth
n = 1 during post-transition growth

The transition of the oxide growth rate occurs at approximately 2 μm thickness. This is also accompanied by a visual change in appearance from black to grey/white oxide.

During oxide growth, splitting of water molecules to oxygen ions and hydrogen ions is believed to take place at the outer oxide surface. The oxygen ions diffuse through the oxide layer and reacts with zirconium at the metal/oxide interface. The formed electrons are transported in the opposite direction and combine with hydrogen ions at the oxide/water interface. These processes may be written

$$H_2O \rightarrow 2\,H^+ + O^{2-} \qquad \text{(Eq 2)}$$

$$\tfrac{1}{2}\,Zr + O^{2-} \rightarrow \tfrac{1}{2}\,ZrO_2 + 2\,e^- \qquad \text{(Eq 3)}$$

$$2\,H^+ + 2\,e^- \rightarrow H_2 \qquad \text{(Eq 4)}$$

Combining these reactions one obtains

$$\tfrac{1}{2}\,Zr + H_2O \rightarrow \tfrac{1}{2}\,ZrO_2 + H_2 \qquad \text{(Eq 5)}$$

Pre-transition oxidation

After the initially formed oxide with the appearance of interference colours, a black coherent oxide film is formed. The pre-transition oxidation rate is controlled by oxygen diffusion through the growing oxide layer. Diffusion along grain boundaries is significantly faster than bulk diffusion. The diffusion controlled oxidation rate continues up to a maximum oxide film thickness, when cracks start to form at the outside of the oxide. This is the transition point. The second phase particles (SPP) present in the metal are known to oxidize more slowly than the matrix. These intermetallics are believed to act as easy paths for electron migrating from the metal to the oxide surface. At the beginning of the pre-transition oxidation, the SPP precipitates may be larger than the oxide thickness, and therefore electron transfer cannot be the rate-limiting step.

Transition

When the oxide has grown to a thickness of about 2 μm, the kinetics is changed. This point is called the transition. Up to this point the growth is controlled by diffusion through the growing oxide layer, but after transition the growth is controlled by diffusion through an oxide layer of fairly constant thickness. The inner oxide layer remains dense and protects the metal. This protective oxide film is often called the barrier layer.

Post-transition oxidation

Post-transition oxidation is characterized by a growth rate proportional to time ($\Delta w = k\,t$). The oxidation rate is believed to be controlled by inward diffusion of oxygen through a barrier layer of constant thickness. The oxide layer outside the barrier layer is rather porous and is not believed to control the oxidation rate. The open network of pores and cracks allows water and oxygen to penetrate the oxide to the barrier layer.

3 Experimental

3.1 Materials

The materials used for the present investigations were two different Zircaloy-2 tubes: LK2 and LK3. Sandvik Steel AB manufactured the tubes, and their chemical composition is given in Table 1. Although listed in the table, no experiment has yet been performed using the LK2+ material. This material was, however, used in the pre-transition measurements [3]. All three materials are from the same ingot and, thus, their chemical composition is identical. The main difference between the three materials is the size distribution of second phase particles (SPP). The size distribution of SPPs in the LK2, LK2+ and LK3 fuel cladding before and after different amounts of irradiation in Forsmark 3 power plant has been measured by Nystrand and Lundström [2]. The results show that the LK2 non-irradiated material has the smallest particle diameter and the LK3 material has the largest particle diameter. The particle density in all three materials decreases with irradiation time. After a burn-up of about 40 MWd/kgU, the LK3 fuel cladding had 18 % of the particles left, the LK2+ had 9 % left and the LK2 fuel cladding had no particles left.

The samples used for the present experiments have been pre-oxidized in steam in an autoclave at 415^{o}C for 331 days. The weight gain observed is listed in Table 1. The colour of the oxide has changed from black to grey. The oxide thickness in Table 1, calculated from the weight gain (WG), is based on the rule of thumb that a weight gain of 15 mg/dm^2 corresponds to an oxide thickness of 1 μm.

Before the experiments, the samples were investigated by light optical microscopy (LOM) and, also, their hydrogen contents were measured using a method described previously [3]. Light optical micrographs are shown in Figure 2. For each sample, the oxide thickness was measured at approximately 10 different positions and the result is shown in Table 1.

Table 1
Chemical composition, weight gain, oxide thickness and hydrogen content of Zircaloy-2 tubes.

Sample	Lot No.	Alloying elements (wt.-%)					Weight gain (mg/dm^2)	Oxide thickness (μm)		Hydrogen content (ppm)
		Sn	Fe	Cr	Ni	O		WG	LOM	
LK2	44-186	1.3	0.18	0.10	0.05	0.13	228.4	15	14-19	1005
LK2+	99-107	1.3	0.18	0.10	0.05	0.13	268.9	18	15-20	1173
LK3	99-108	1.3	0.18	0.10	0.05	0.13	241.3	16	12-17	1066

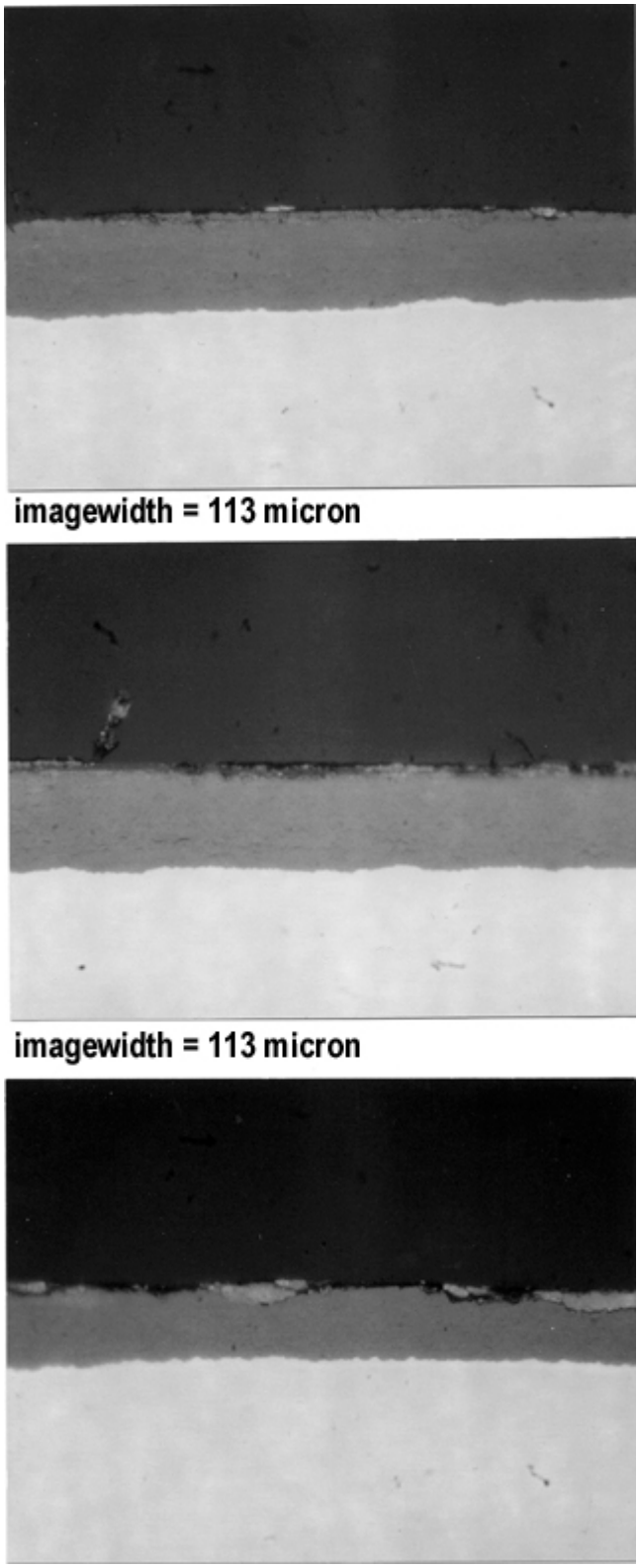

Figure 2
Light optical micrographs of the samples showing the oxide layer on the metal.

The measured hydrogen contents are also given in Table 1. The oxide thickness measured using LOM is in agreement with the thickness calculated from the weight gain and the difference between the materials is not large. It seems, however, that both the oxide thickness and hydrogen content of the LK2+ material are slightly larger compared to the other two materials.

After the first LOM investigation, the samples were chemically etched (using a mixture of HF, HNO_3, lactic acid and H_2O_2) in order for the hydrides to appear. Light optical micrographs of the etched samples are shown in Figure 3. It can be seen that the hydrides are mainly circumferentially orientated (parallel with the surface) and uniformly distributed in the metal.

Six Westinghouse Atom SVEA-96 fuel rods with LK2, LK2+ and LK3 cladding, irradiated for three and four years in Forsmark 3, have previously been examined in Studsvik. This examination showed that the LK3 material had the best corrosion resistance (thinnest oxide) and the LK2 material the least corrosion resistance (thickest oxide) (see for example [2]). The difference in corrosion behaviour was, however, not as significant as the difference in hydrogen uptake. The LK3 material had the lowest hydrogen uptake and the LK2 material the highest hydrogen uptake. Thus, the size distribution of SPPs seems to be important in regard to the in-reactor fuel cladding corrosion behaviour and hydrogen uptake.

The tubes used for the present experiments are 22 mm long and the diameter is 9.6 mm. Thus, the area exposed in the impedance measurements was 6.6 cm^2.

3.2 Experimental set-up and procedure

The impedance measurements were carried out in an autoclave at temperatures up to 288^{o}C. The experimental set-up and instrumentation have been described previously [3]. In short, high purity, degassed water with a conductivity of less than 0.07 μS/cm was pre-heated before it entered the autoclave (except for the room temperature measurements). A continuous water flow of about 2 litres per hour was used during the experiments. Dosage of chemicals to the water was possible. The autoclave and other wetted surfaces at high temperature are made of titanium in order to avoid influence from corrosion products of stainless steel.

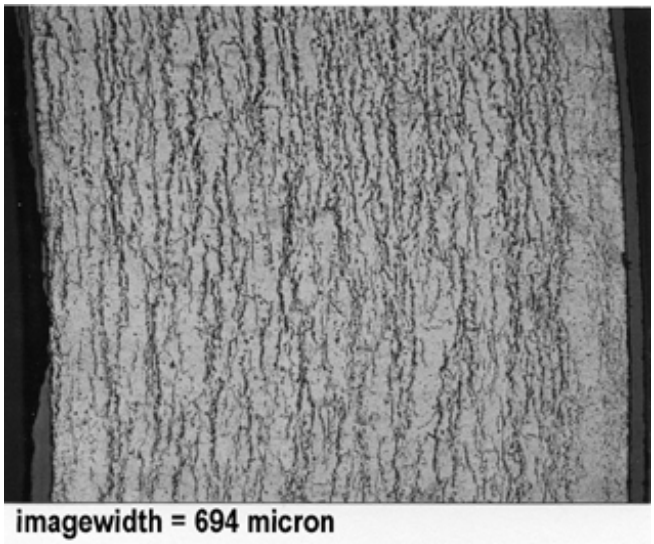

LK2

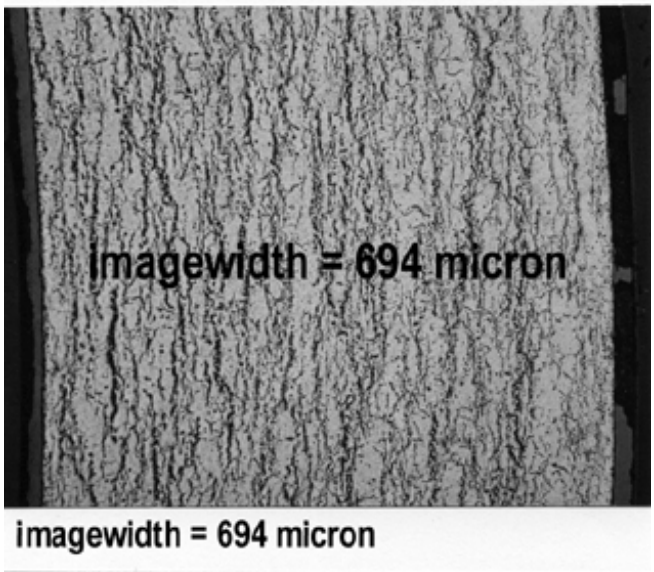

LK2+

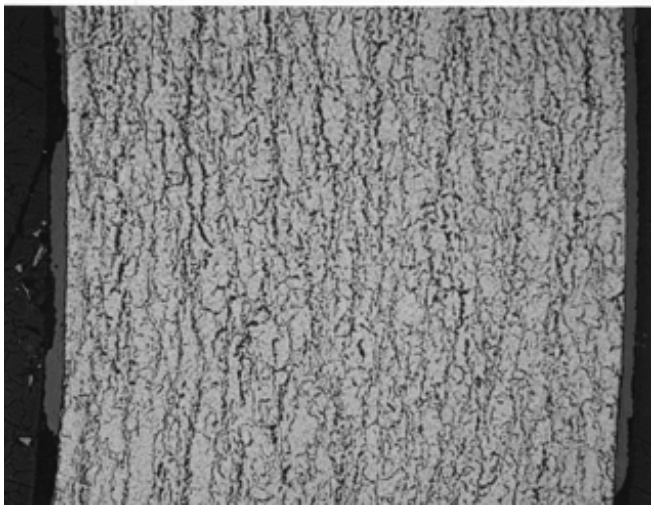

LK3

Figure 3
Light optical micrographs of the samples showing the hydride structure.

A two-electrode cell was used for the impedance measurements. The counter (outer) electrode was a platinum cylinder and the working (inner) electrode was the Zircaloy cylinder. The autoclave was also equipped with an Ag/AgCl reference electrode, used to measure the potentials of the platinum and Zircaloy electrodes. Data on electrode potentials, autoclave temperature and ambient temperature conductivity of pure water were collected during the periods between the impedance measurements.

At the start of an experiment, the electrodes were mounted in the autoclave, the water flow was started and the pressure was raised to 90 bar. Impedance measurements were then performed at room temperature, and a few other temperatures, before raising the temperature to 288^{o}C. During the measurements, an AC voltage (usually 10 mV) was applied between the CE and WE at the open circuit potential. Measurements were carried out in the frequency range 0.001 Hz – 100 000 Hz. The samples were kept for a prolonged time at 288^{o}C. This time was 46 days for LK2 and 54 days for the LK3 material. During this period, impedance measurements were usually carried out once a day. A few measurements were also carried out when the temperature was lowered at the end of the experiments. In addition to this, measurements were also performed at applied voltage in the range –1 to +1 V versus open circuit potential in order to obtain information about the electronic conductivity from so-called Mott-Schottky plots (see section 2.5 in [3]).

3.3 Chemistry

In order to simulate the oxidizing in-core environment of a BWR, 500 ppb hydrogen peroxide (H_2O_2) was dosed to the water in the present experiments. Some of the H_2O_2 decomposed. According to calculations using PEROX [5], 110 ppb H_2O_2 remained at the Zircaloy sample and 180 ppb O_2 was formed. In order to study the influence of the chemical environment on the oxidation of the Zircaloy samples, 2 ppb Fe and 0.5 ppb Ni were dosed to the water during the latter part of the experiments. Both elements were added in the form of nitrates. Throughout the experiments, 0.2 mM $NaNO_3$ was added in order to increase the conductivity of the water.

4 Results

In the present work, the oxidation of two different Zircaloy-2 materials, LK2 and LK3, have been studied in situ in an autoclave using electrochemical impedance spectroscopy (EIS). The results are accounted for below. During these experiments, the potentials of the platinum and Zircaloy electrodes as well as the potential of the autoclave (titanium) have been continuously monitored (in between the impedance measurements). Potentials measured are presented in Appendix A. All impedance spectra measured are given in Appendix B, and the results from the equivalent circuit analysis are tabulated in Appendix C. Values of the α-corrected (extrapolated) capacitance and the associated dispersion factor are tabulated in Appendix D.

4.1 The LK2 material

Impedance measurements were carried out in the temperature range 20-288^{o}C on the pre-oxidized material. Dosage of H_2O_2 (500 ppb) and $NaNO_3$ (0.2 mM) was made throughout this experiment. Dosage of Fe (2 ppb) and Ni (0.5 ppb) was made during the latter part of the experiment. The potentials measured are shown in Figure A.1 in Appendix A. The autoclave temperature is also displayed in this figure. The temperature is kept at 200^{o}C during the period December 6, 2002 – January 9, 2003 and, when raising the temperature further to 288^{o}C, the Zircaloy potential is instantaneously lowered by approximately 600 mV. The Zircaloy potential then increases with time at this temperature and, at the end of the experiment, the potential are 280-350 mV lower than potentials of platinum and ground. Thus, in spite of the oxidizing environment, the Zircaloy potential is approximately 200 mV below zero (versus the Standard Hydrogen Electrode) at the end of the experiment at 288^{o}C. When starting the addition of Fe and Ni (February 3, 2003) the potentials of all electrodes remain unaffected. All potentials measured are in agreement with the potentials measured during the experiment with the LK2 material in the pre-transition region [3].

All impedance spectra measured are given in Appendix B.1 –B.9. The numbers in the legends correspond to the date when the measurement was performed. For example, ”z021206” is a measurement conducted December 6, 2002. During the period January 10 – February 24, 2003, the temperature was 288^{o}C. Impedance spectra measured at three different temperatures at the beginning of the experiment are shown in Figure 4. It can be seen that the impedance decreases as the temperature increases.

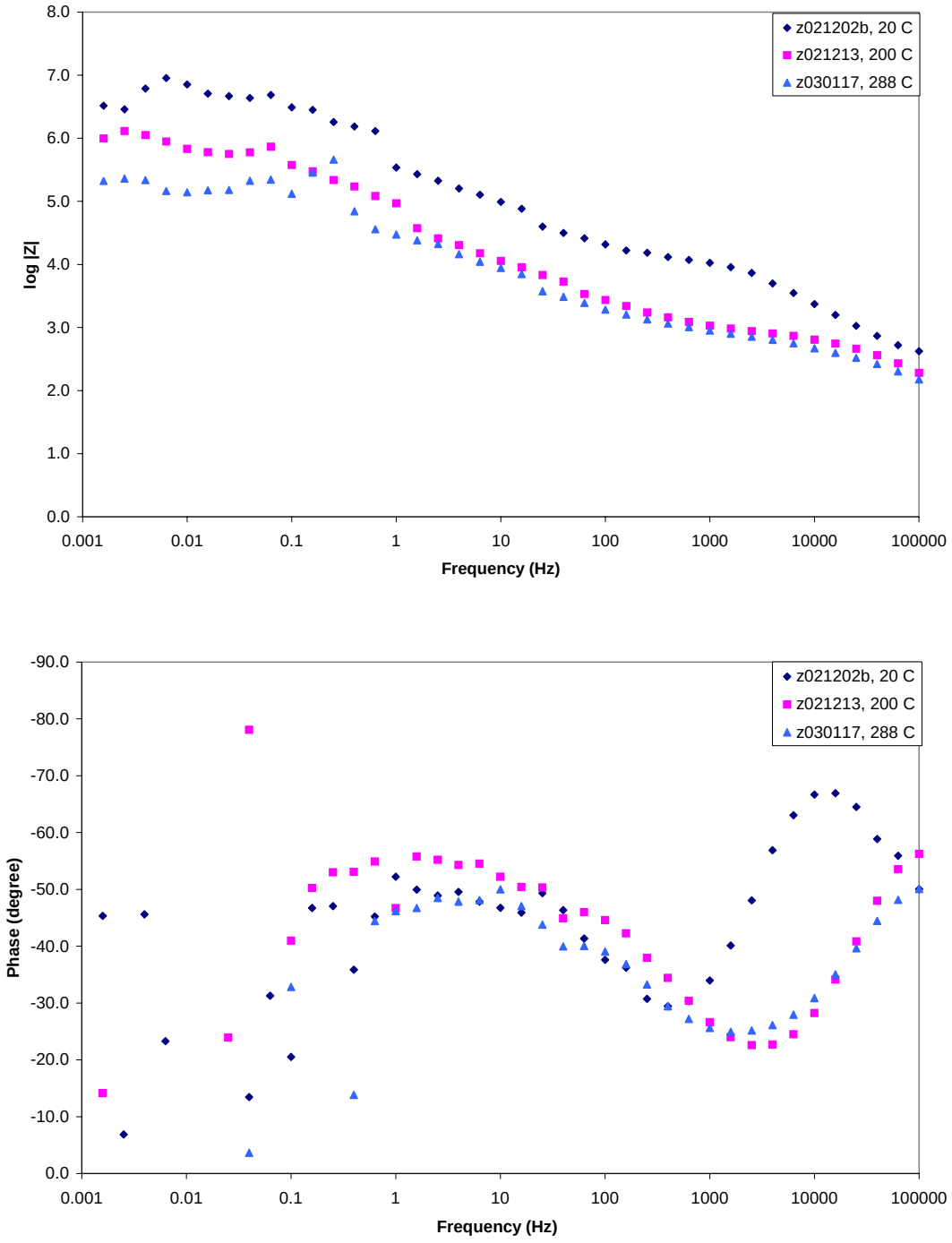

Figure 4
Impedance spectra of the LK2 material at three different temperatures at the beginning of the experiment.

From the phase angle plot, two maxima are clearly visible. This shows that the oxide is composed of two layers, an inner and an outer layer. In Figure 4, the maximum at low frequencies is associated with the inner layer and the maximum at high frequencies with the outer layer. From the phase angle plot it can also be seen that the maximum at high frequencies is displaced to higher frequencies with increasing temperature while the position of the other maximum remains unchanged. At 288^{o}C, the first-mentioned maximum is outside the measured frequency range.

Impedance spectra measured during the exposure at 200^{o}C and the subsequent exposure at 288^{o}C are shown in Figure 5 and 6. At 200^{o}C there are virtually no changes in the spectra with time. If the outer layer were porous, one would expect that water is allowed to penetrate this layer and, if so, there should be a gradual change in the impedance spectra. The fact that the spectra in Figure 5 remain unchanged indicates that this is a fast process, which probably is completed before the temperature was raised to 200^{o}C. At 288^{o}C small changes with time are seen in the spectra, especially in the phase angle. This is most likely a consequence of the oxide growth taking place at this higher temperature, and not due to the dosage of Fe and Ni starting on February 3rd.

All impedance spectra in the present work have been successfully modelled using the equivalent circuit displayed in Figure 7. On account of the layered structure of the oxide, two time constants (parallel combinations of a resistor, R, and a Constant Phase Element, Q) are needed in order to describe the impedance of the oxide. In Figure 7, Q2 and R3 are associated with the capacitance and resistance of the inner layer and, when written as in this figure, Q1 is the total capacitance of the oxide (inner and outer layer). The results from the equivalent circuit analysis are tabulated in Appendix C.1. The temperature of the measurements is also given.

An example of a modelled spectrum, measured at 288^{o}C, is presented in the Bode plot in Figure 8. The triangles are experimental data and the lines are the result from the equivalent circuit analysis. In Figure 9, this spectrum is displayed in a Nyquist plot. In the latter plot, a part of a semicircle is seen at high frequencies whereas a linear portion is seen at lower frequencies.

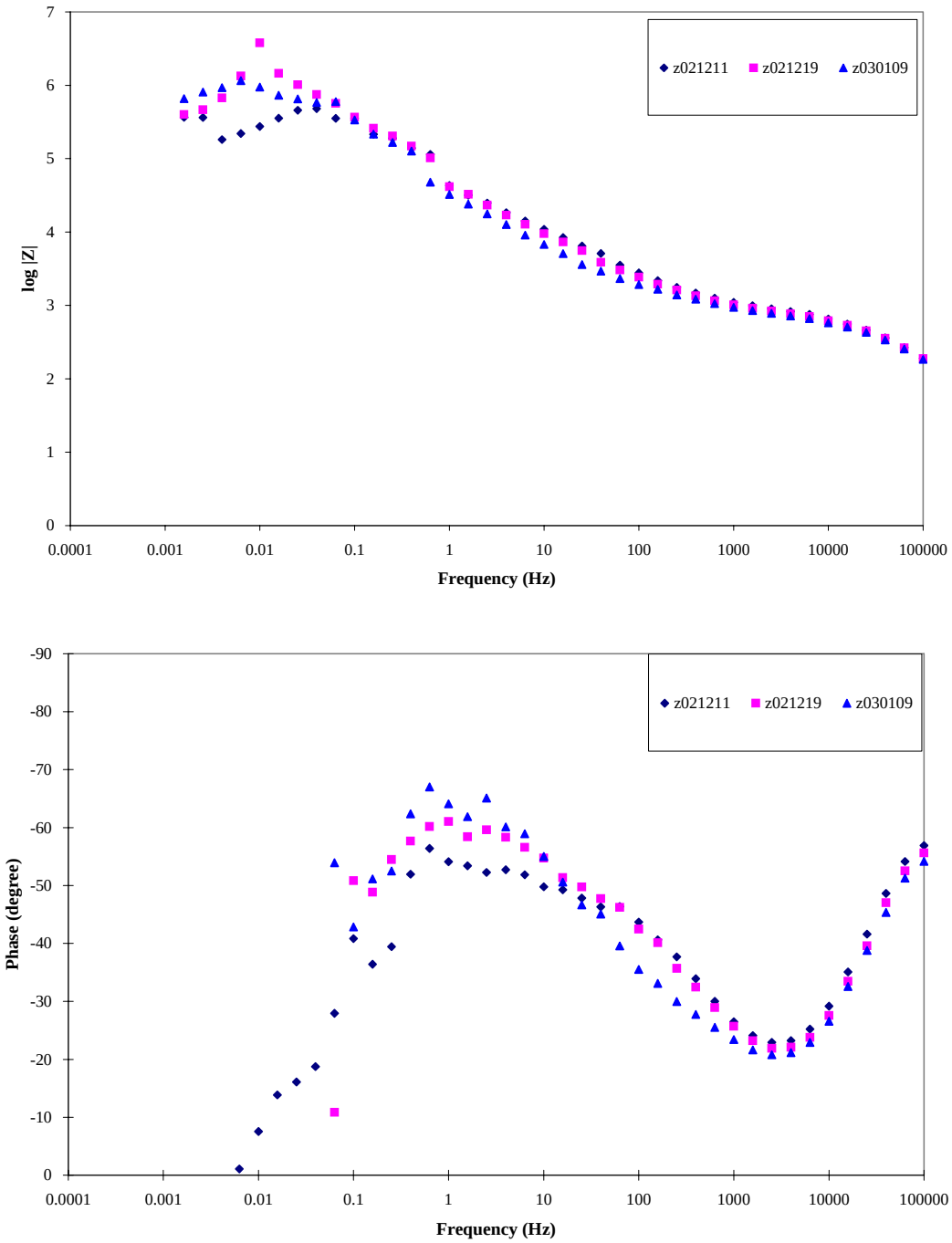

Figure 5
Impedance spectra at three different points of time at 200^{o}C.

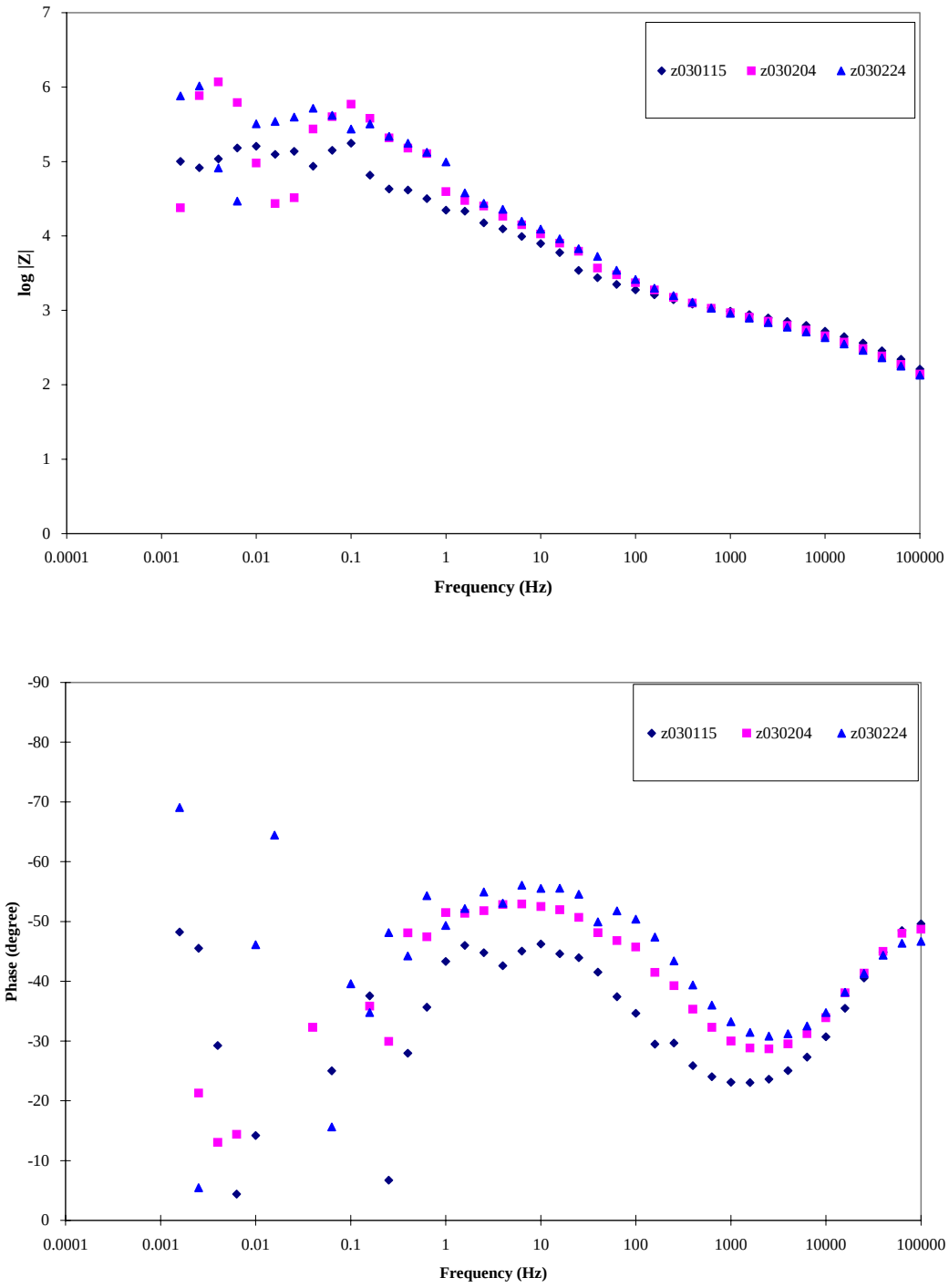

Figure 6
Impedance spectra at three different points of time at 288^{o}C. Dosage of Fe and Ni was started on February 3rd.

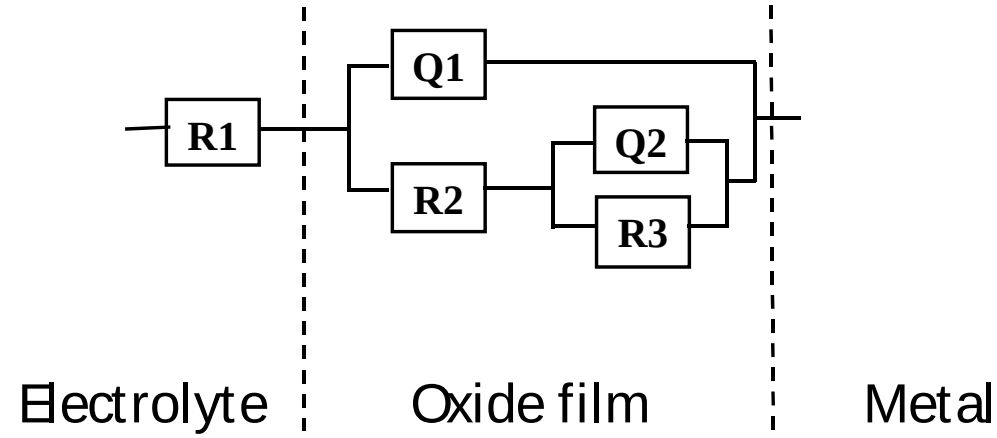

Figure 7
Equivalent circuit of a two-layer oxide film in high conductivity electrolyte. Q = Constant Phase Element and R = resistor.

Oxide thickness, conductivity and porosity

The calculated oxide thickness is shown as a function of test time in Figure 10. The oxide thickness was calculated from the fit parameters of the equivalent circuit analysis using the following equation [3]:

$$d = \frac{\varepsilon \varepsilon_0 A}{C_Q^{1/\alpha}} \qquad \text{(Eq 6)}$$

where

d	= oxide thickness
ε	= dielectric constant of ZrO_2 (= 22)
ε_0	= permittivity of a vacuum (= 8.854×10^{-12} F/m)
A	= area of Zircaloy sample (=6.635×10^{-4} m^2)
C_Q	= capacitance (of Q1 in Figure 7)
α	= dispersion factor (of Q1 in Figure 7)

The test time at 288^{o}C is indicated in Figure 10. Dosage of Fe and Ni was started at a test time of 66 days. Since the oxide thickness is known to be about 15 μm at the beginning of the experiment (see Table 1), the calculated thickness is obviously in most cases much too large, and some points also fall outside the scale of the diagram in Figure 10.

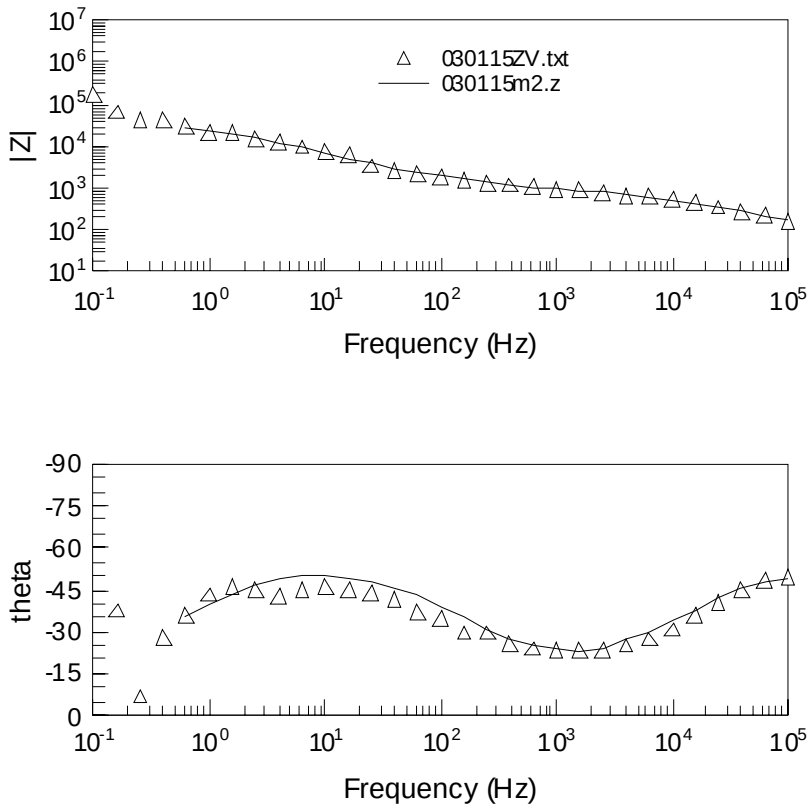

Figure 8
Impedance spectrum of the LK2 material measured at 288^{o}C and the result of the equivalent circuit analysis.

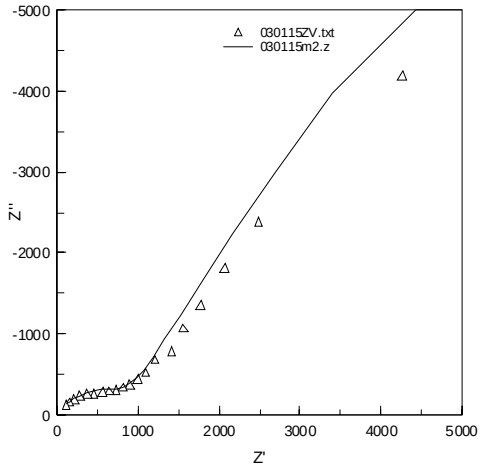

Figure 9
The impedance spectrum in Figure 8 presented in a Nyquist plot.

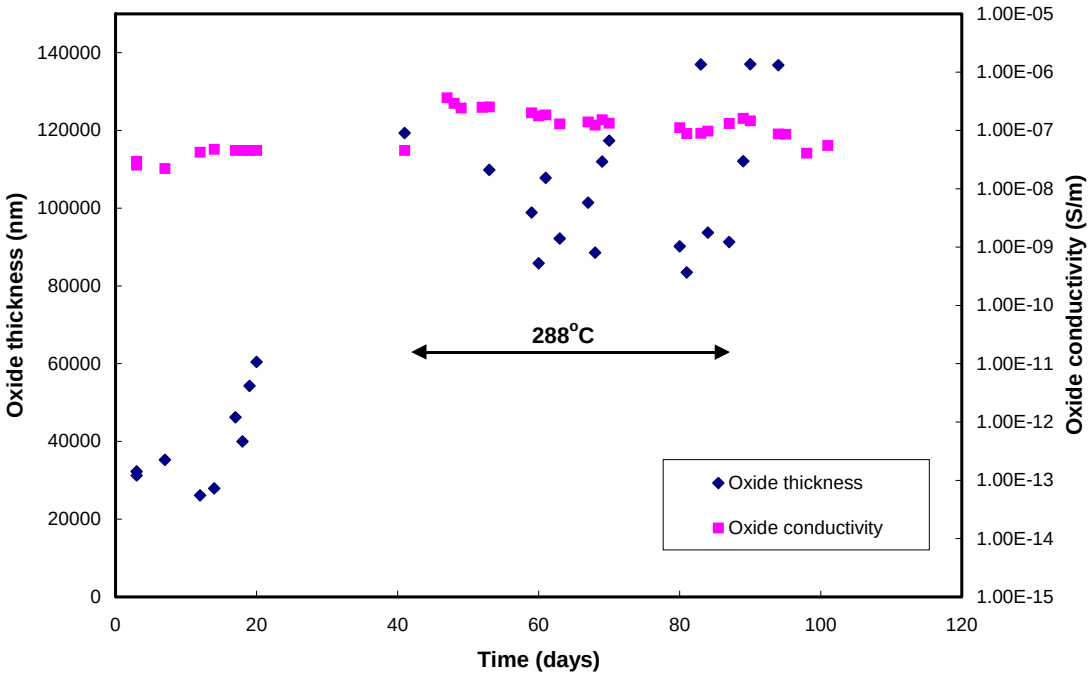

Figure 10
Calculated oxide thickness and conductivity for the LK2 material. The conductivity is based on a thickness of 15 μm.

Three possible explanations may be found for this:

- The dispersion factor (α) is too low.
- The oxide contains pores, which are filled by air at the beginning of the experiment.
- The time constant (maximum in phase angle) of the outer oxide layer falls outside the frequency range of the measurements.

When the dispersion factor is below a certain value (about 0.85-0.90 depending on the capacitance) oxide thickness cannot be calculated from the fit parameters using Eq 6. In this case, the calculated thickness will be too large. From Table C.1 in Appendix C.1 one may conclude that the dispersion factor is probably too low in all measurements except for the first five ones. For these first five measurements at 20°, 100° and 200°C, α is in the range of 0.90 – 0.95.

A likely explanation for the too large calculated thickness for the first five measurements is that the outer layer of the oxide is porous and the pores are filled by air at the beginning of the experiment. In this case, the relative dielectric constant of the oxide scale (ε_{app}) will depend on the porosity and, therefore, will deviate from the dielectric constant of ZrO_2. According to Paper IV in Oskarsson [4], the apparent relative dielectric constant of the oxide scale can be written:

$$\varepsilon_{app}^{-1} = x\,\varepsilon_{air}^{-1} + (1-x)\,\varepsilon_{ZrO_2}^{-1} \qquad \text{(Eq 7)}$$

where

x	= fraction of pores in the oxide
ε_{app}	= dielectric constant of oxide scale
ε_{air}	= dielectric constant of air (= 1)
ε_{ZrO_2}	= dielectric constant of ZrO_2 (= 22)

Eq 7 is of course only valid as long as the pores are filled by air. Thus, if the thickness of the oxide is known, the apparent dielectric constant can be obtained using Eq 6 (substituting ε with ε_{app}) and, subsequently, the porosity may be calculated from Eq 7.

By using the oxide thickness based on the measured weight gain in Table 1 (15 μm), the apparent dielectric constant and porosity at the beginning of the experiment were calculated, and the result is shown in Figure 11. The first two measurements were conducted at room temperature, the third at 100°C and the last two in the figure at 200°C. Porosities of pre-hydrided Zircaloy-2 samples oxidized in an autoclave at 400°C for different periods of time were reported by Oskarsson [4]. Porosities in the range 4.2 %- 6.1 % were found which is in excellent agreement with the present work. From Figure 11, a slight increase in the dielectric constant with time is seen. This is to be expected if water penetrates into the pores, since the dielectric constant of water is about 80 at room temperature. At 288°C, on the other hand, the dielectric constant of water is close to the dielectric constant of ZrO_2. Therefore, at this temperature, the dielectric constant of the oxide scale remains virtually unaffected if the oxide is porous and the pores are filled by water.

At 288°C, the time constant of the outer oxide layer falls outside the frequency range of the measurements – see Figure 4. The reason for this is a low resistance together with a small capacitance. In fact, if the resistance over the oxide is decreasing due to electrolyte penetration, the time constant will move to higher frequencies. This may be part of the explanation for the displacement of this time constant seen in Figure 4. The fact that a part of the spectra associated with the outer oxide layer falls outside the measured frequency range makes the determination of capacitance and dispersion factor more difficult. As a consequence, these parameters will be more uncertain and the calculated oxide thickness will be less reliable.

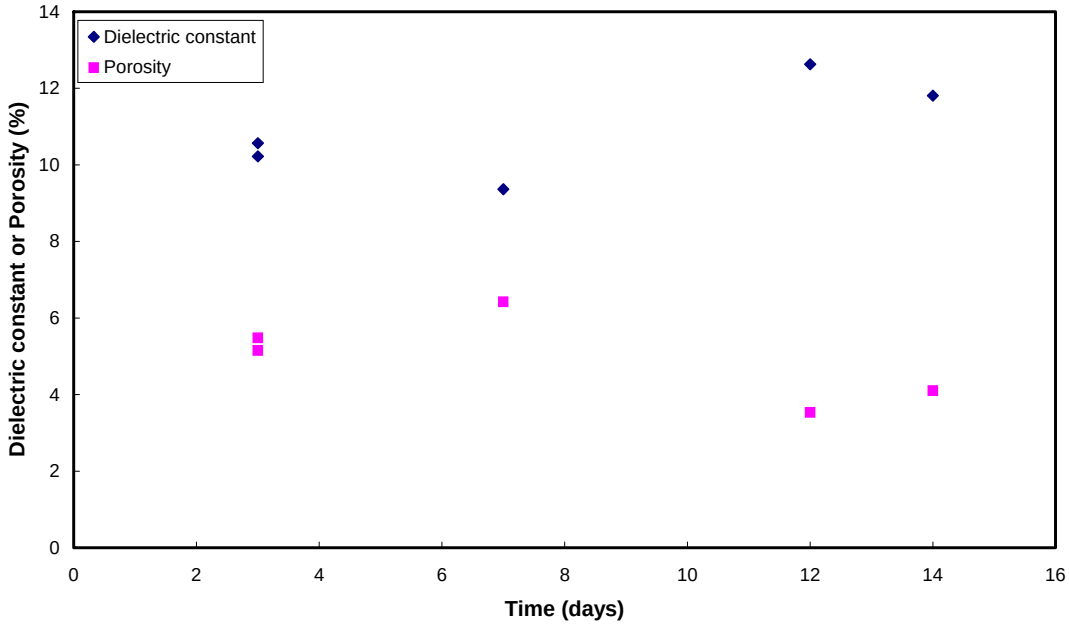

Figure 11
Apparent dielectric constant of the oxide scale and oxide porosity at the beginning of the experiment.

As explained in the previous report [3], an α-corrected capacitance may be obtained from plots of log capacitance vs log frequency, where the capacitance is calculated from the imaginary component of the impedance. An example of such a plot, based on the measurement at 100°C, is shown in Figure 12. The α-corrected capacitance, $C_{\alpha\text{-corr}}$, is obtained by extrapolating the linear section(s) to high frequencies (10^5 Hz is used in the present work). By substituting $C_{\alpha\text{-corr}}$ for $C_Q^{1/\alpha}$, Eq 6 may then be used to calculate oxide thickness. The dispersion factor is obtained from the slope of the linear section(s). From Figure 12, it is evident that two linear sections are present. The linear section at low frequencies is associated with the inner oxide layer and the one at high frequencies with the outer oxide layer. Unfortunately, at temperatures higher than 100°C, the linear section at high frequencies falls outside the measured frequency range. This is due to the fact that the time constant is displaced to higher frequencies (see Figure 4). Therefore, at high temperatures, only the thickness of the inner oxide layer can be obtained using this method. Values of the α-corrected (extrapolated) capacitance and the dispersion factor are tabulated in Appendix D.1.

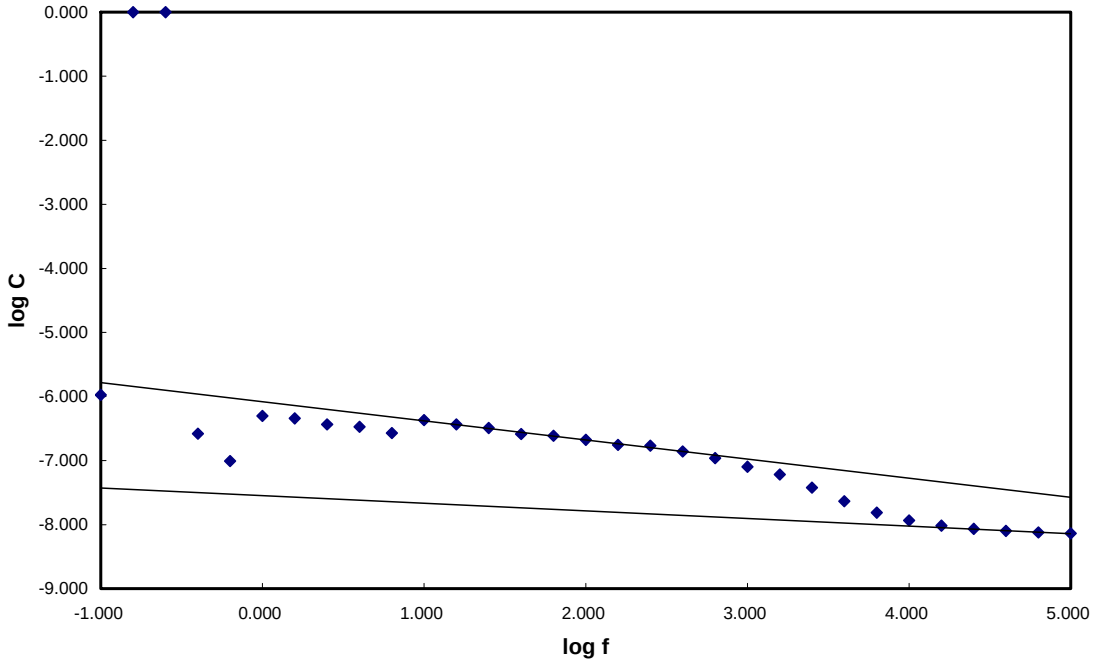

Figure 12
An example of a plot of log C versus log f from the measurement at 100°C.

The oxide thickness calculated from the high frequency α-corrected (extrapolated) capacitance at low temperatures is given in Table 2. The last three values in the table are in reasonable agreement with the weight gain value (15 μm). The oxide thickness for the inner oxide layer, calculated from the low frequency α-corrected (extrapolated) capacitance, is shown in Figure 13. The test time at 288°C is marked in the diagram. Dosage of Fe and Ni was started at a test time of 66 days. The calculated thickness exhibits some spread but the majority of the data points lie within the range 1.6 – 2.4 μm. This is in good agreement with the thickness at which the

Table 2
Oxide thickness calculated from the high frequency α-corrected (extrapolated) capacitance at the beginning and at the end of the experiment.

Date	Test time (days)	Temperature (°C)	Oxide thickness (nm)
2002-12-02	3	20	24 570
2002-12-02	3	20	23 464
2002-12-06	7	100	17 881
2003-03-07	98	20	18 941
2003-03-10	101	20	19 743

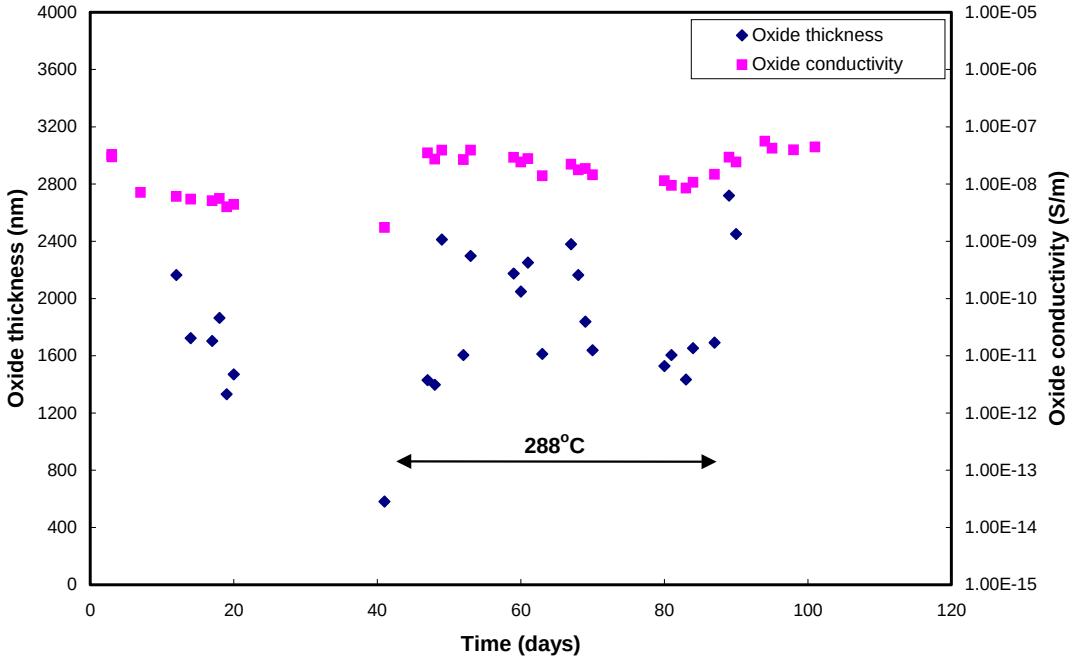

Figure 13
Oxide thickness and conductivity of the inner layer of the LK2 material.

transition from pre- to post-transition growth usually occurs (see Chapter 2). The inner layer may thus be identified with the protective barrier layer.

The conductivity may be calculated using the following equation:

$$\sigma = \frac{d}{RA} \qquad \text{(Eq 8)}$$

where

σ	= specific conductivity of the oxide
d	= oxide thickness
R	= resistance of the oxide (=R2+R3 in Figure 7)
A	= area of Zircaloy sample (=6.635×10^{-4} m^2)

The conductivity is not readily obtainable using only the impedance data since, from most measurements, the total oxide thickness has not been possible to calculate. However, by using the weight gain value of the thickness (15 μm) and the resistance from the impedance measurements (R2+R3 in Figure 7), the conductivity can be calculated. The result has been introduced in Figure 10. The conductivity of the inner oxide layer was calculated using the thickness and resistance (R3 in Figure 7) of this layer and the result is shown in Figure 13.

Arrhenius plots of the oxide conductivity as a function of inverse temperature at the beginning and at the end of the experiment are shown in Figure 14. The conductivity is based on an oxide thickness of 15 μm, as explained above. The activation energy for conduction deduced from these plots is 10.5 and 5.3 kJ mol^{-1} at the beginning and end, respectively. The calculated activation energies are based on all data points although the linear relationship may be questioned, especially at the beginning of the experiment.

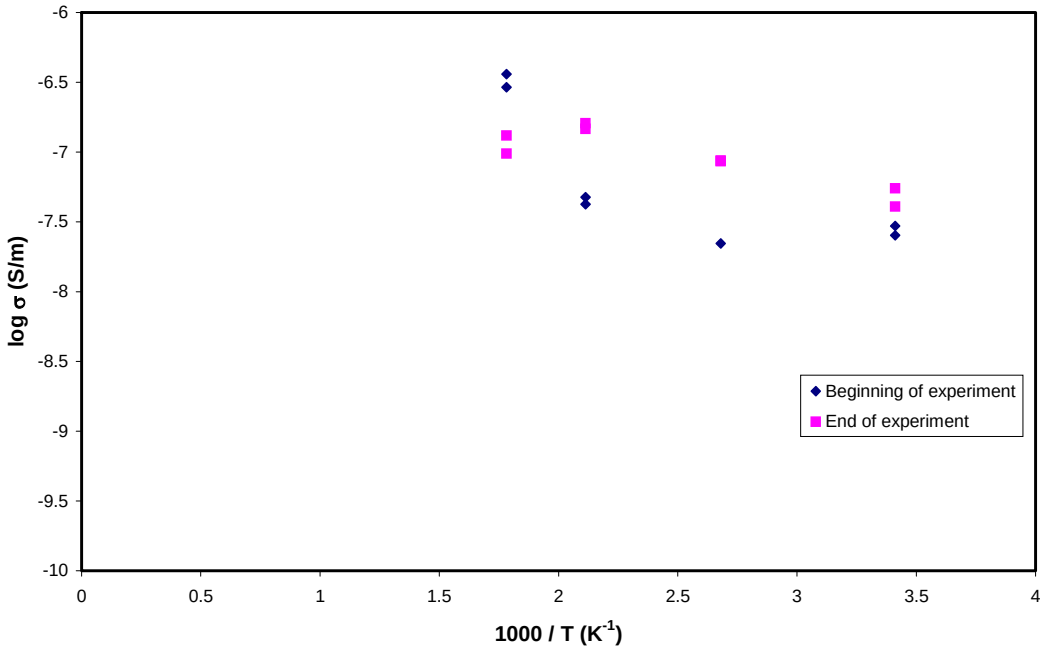

Figure 14
Oxide conductivity as a function of inverse temperature for the LK2 material at the beginning and at the end of the experiment.

Effective donor density

Capacitance versus voltage profiles were measured on two occasions at 288°C and on two occasions when the temperature was lowered at the end of the experiment. Mott-Schottky plots (MS-plots) were constructed at three different frequencies, 100, 1000 and 10 000 Hz. For details regarding construction of MS-plots and the derivation of effective donor densities, see the previous report [3]. MS-plots from the measurements at 288°C are shown in Figure 15 and 16. The effective donor densities derived from these plots are given in Table 3. It was not possible to find linear sections in the plots at 10 000 Hz that could be used for evaluation of donor densities and, therefore, these plots are not shown in Figure 15 and 16.

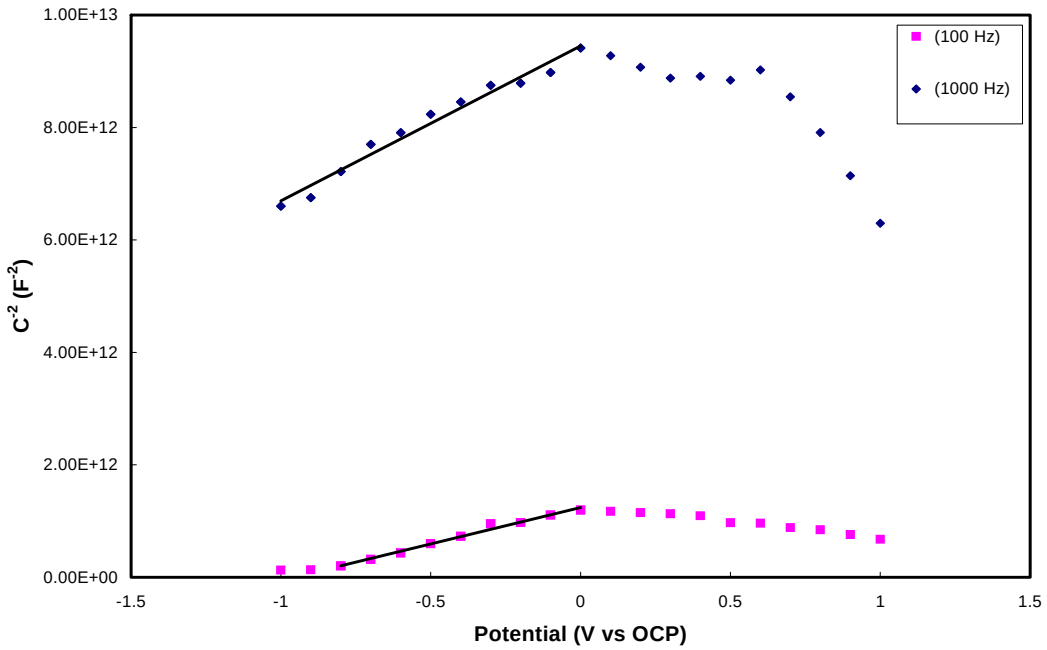

Figure 15
Mott-Schottky plots for the LK2 material at 288°C. The measurements were conducted at a total test time of 63 days.

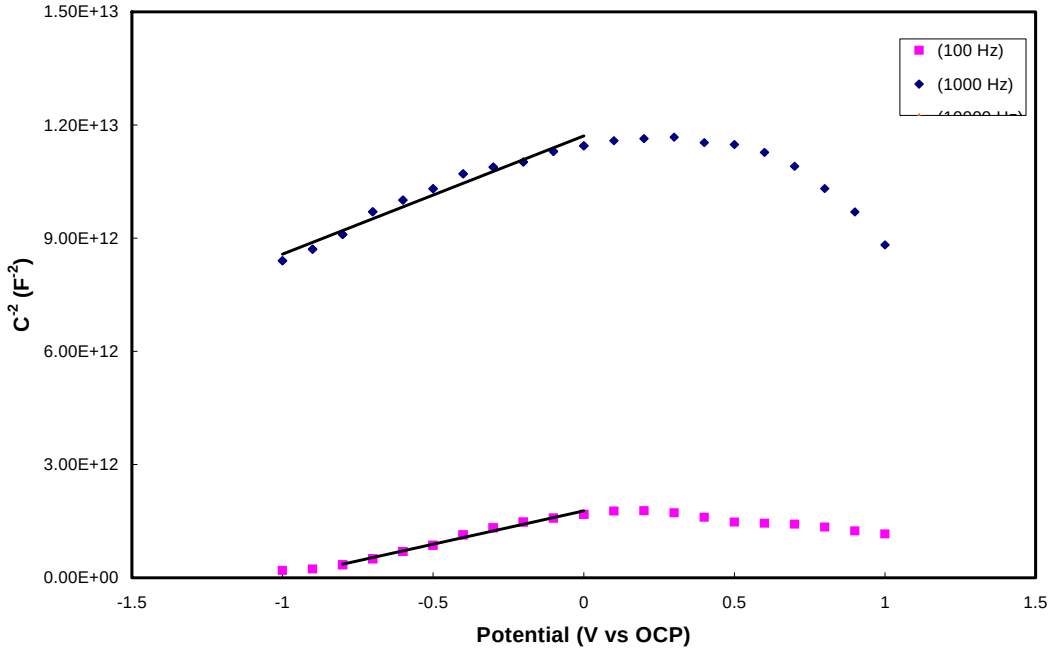

Figure 16
Mott-Schottky plots for the LK2 material at 288°C. The measurements were conducted at a total test time of 84 days. Dosage of Fe and Ni was made during this experiment.

Table 3
Effective donor density calculated for the LK2 material.

Test time (days)	Temperature (^oC)	Frequency (Hz)	Effective donor density $N_D \times 10^{-23}$ (m^{-3})
63	288	100	1.125
63	288	1000	0.528
63	288	10 000	---
84	288	100	0.824
84	288	1000	0.465
84	288	10 000	---

From Figure 15 and 16 it can be seen that the MS-plots are not linear over the whole potential regions. Therefore, the slopes used to derive the effective donor densities shown in Table 3 are based on a part of these plots. At 100 Hz the potential range –0.8 to 0 V versus open circuit potential was used, whereas the range –1 to 0 V was used at 1000 Hz. Due to the limited linear regions in the MS-plots in Figure 15 and 16, an attempt was made to use capacitances from equivalent circuit analysis to construct MS-plots. Therefore, all impedance spectra measured during the first Mott-Schottky experiment at a test time of 63 days were fitted to the equivalent circuit in Figure 7, and the capacitances (with respectively without correction for the dispersion factor) were used for the MS-plots. However, the data points in these plots were very scattered and it was not possible to use them in order to derive donor densities. As explained above, it is not possible to obtain α-corrected capacitances from plots of log capacitance vs log frequency since the linear section at high frequencies falls outside the measured frequency range. For the measurements at a test time of 63 days, a MS-plot was also constructed at 100 000 Hz (which is close to the maximum for the high frequency time constant). However, derivation of donor density was not successful at this frequency.

When the temperature was lowered, the appearance of the MS-plots is not good and, further, their slopes are negative. Calculations of effective donor densities at 100^o and 20^oC were therefore not successful.

4.2 The LK3 material

Impedance measurements were carried out in the temperature range 20-288°C on the pre-oxidized material. Dosage of H_2O_2 (500 ppb) and $NaNO_3$ (0.2 mM) was made throughout this experiment. Dosage of Fe (2 ppb) and Ni (0.5 ppb) was made during the latter part of the experiment. The potentials measured are shown in Figure A.2 in Appendix A. The autoclave temperature is also displayed in this figure. It can be seen that, at 288°C, the Zircaloy potential increases strongly with time at the beginning of the experiment. At the end of the experiment, the Zircaloy potential is about 220-280 mV lower than the potentials of ground (titanium) and platinum. The measured potentials are in good agreement with potentials measured for the LK3 material in the pre-transition region [3]. When starting the addition of Fe and Ni on October 14th, 2002, all potentials remain unaffected. The potential drop seen on November 3rd is due to a malfunction of the HPLC-pump used for dosage. The pump was dispatched for repair and the dosage of H_2O_2, $NaNO_3$ and Fe/Ni was restarted on November 15th.

All impedance spectra measured are given in Appendix B.10–B.18. The numbers in the legends correspond to the date when the measurement was performed. For example, ”z020904” is a measurement conducted September 4, 2002. During the period September 14 – November 6, 2002, the temperature was 288°C. Impedance spectra measured at three different temperatures at the beginning of the experiment are shown in Figure 17. It can be seen that the impedance decreases as the temperature increases. From the phase angle plot, two maxima are clearly visible. This shows that the oxide is composed of two layers, an inner and an outer layer. In Figure 17, the maximum at low frequencies is associated with the inner layer and the maximum at high frequencies with the outer layer. From the phase angle plot it can also be seen that the maximum at high frequencies is displaced to higher frequencies with increasing temperature and, at high temperature, this maximum is outside the measured frequency range.

Impedance spectra measured during the exposure at 288°C are shown in Figure 18. A gradual change in the spectra with time is seen between September 16th and October 31st. The impedance increases and changes are also noticeable in the phase angle plot. This is most likely a consequence of the oxide growth taking place at this temperature, and not due to the dosage of Fe and Ni starting on October 14th. No sudden change is seen in the spectra when the addition of Fe and Ni was started – see Appendix B.15. The last spectrum in the figure (on November 6th) was measured after all dosages had been stopped due to problems with the HPLC pump. It can be seen that, when interrupting the addition of $NaNO_3$ and H_2O_2, this has a great impact on the impedance spectra. The increased impedance at high frequencies is a natural consequence of the reduced electrolyte conductivity.

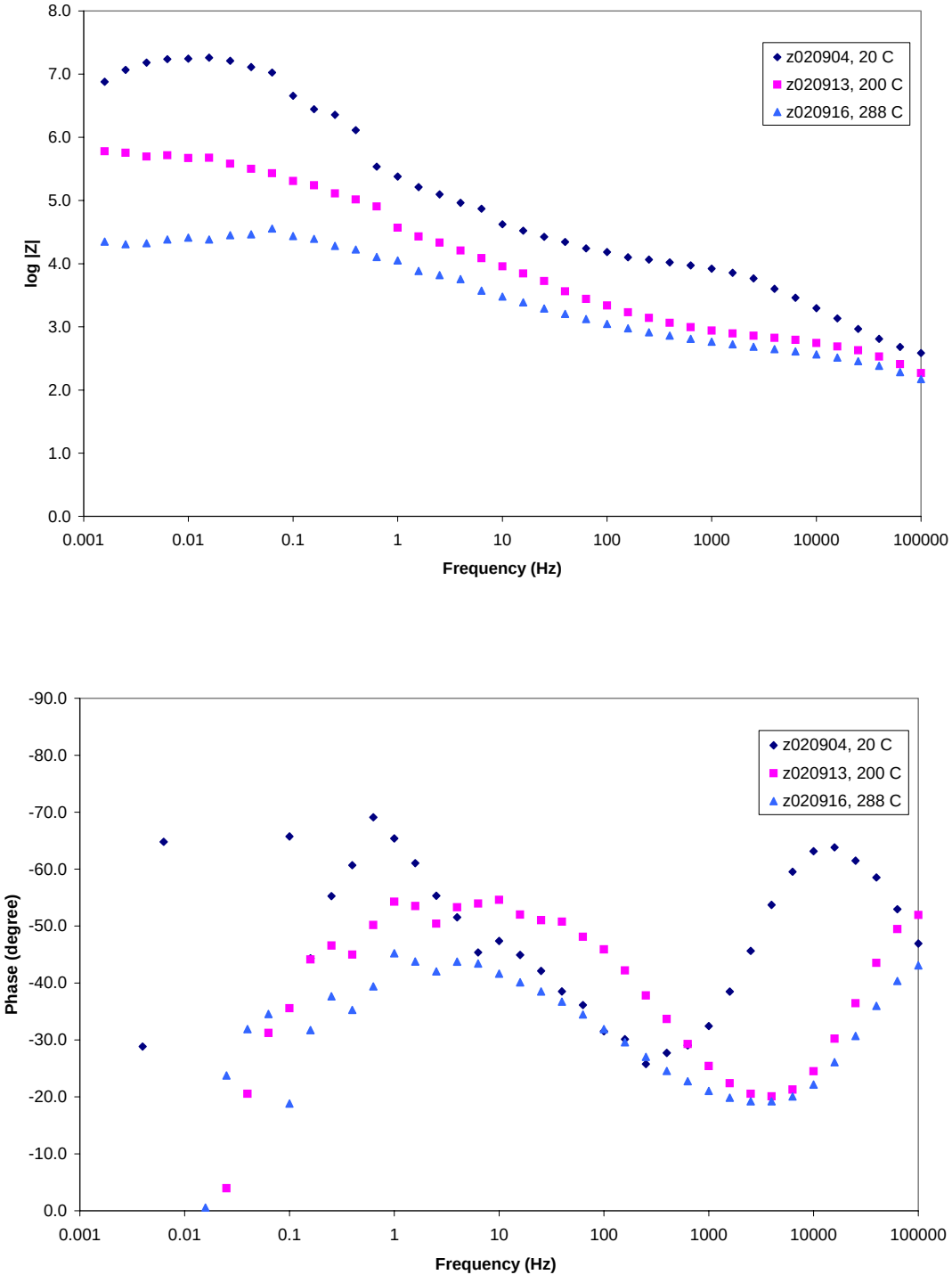

Figure 17
Impedance spectra of the LK3 material at three different temperatures at the beginning of the experiment.

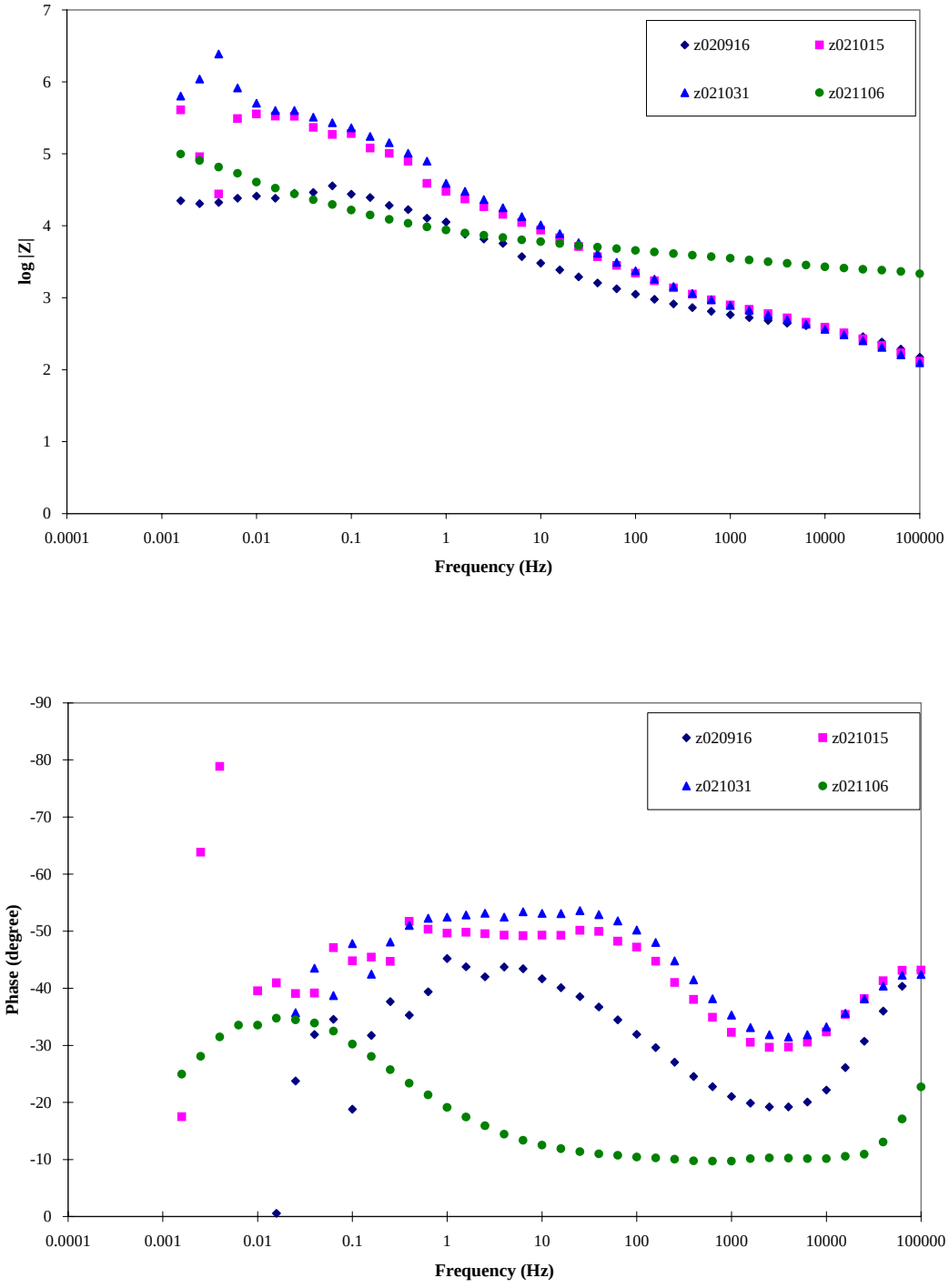

Figure 18
Impedance spectra at four different points of time at 288°C. Dosage of Fe and Ni was started on October 14th. The dosage pump was out of order on November 6th.

The impedance spectra have been successfully modelled using the equivalent circuit displayed in Figure 7. On account of the layered structure of the oxide, two time constants are needed in order to describe the impedance of the oxide. The results from the equivalent circuit analysis are tabulated in Appendix C.2. The temperature of the measurements is also given. Equivalent circuit analysis was not successful for the last two measurements at 288^{o}C. At the time of these two measurements, the dosage pump was out of order. An example of a modelled spectrum, measured at 288^{o}C, is presented in the Bode plot in Figure 19. The triangles are experimental data and the lines are the result from the equivalent circuit analysis. In Figure 20, this spectrum is displayed in a Nyquist plot. In the latter plot, a part of a semicircle is seen at high frequencies whereas a linear portion is seen at lower frequencies.

Oxide thickness, conductivity and porosity

The calculated oxide thickness of the LK3 material is shown as a function of test time in Figure 21. The oxide thickness was calculated from the fit parameters of the equivalent circuit analysis using Eq 6. The test time at 288^{o}C is also indicated in Figure 21. Dosage of Fe and Ni was started at a test time of 41 days. Since the oxide thickness is known to be about 16 μm at the beginning of the experiment (see Table 1), one may conclude that the calculated thickness is in most cases much to large, and some points also fall outside the scale of the diagram in Figure 21. Some interesting features are seen in Figure 21. At the beginning of the experiment, below 288^{o}C, the calculated oxide thickness decreases with time. When increasing the temperature to 288^{o}C (at day 11), the calculated thickness first increases strongly and then once more starts to decrease with time. When starting the addition of Fe and Ni at day 41, the calculated thickness increases with time.

Possible reasons for the too large calculated oxide thickness have been discussed in section 4.1 above. Three explanations were suggested, namely:

- The dispersion factor (α) is too low.
- The oxide contains pores, which are filled by air at the beginning of the experiment.
- The time constant (maximum in phase angle) of the outer oxide layer falls outside the frequency range of the measurements.

At the beginning of the experiment, in the temperature range 20^{o} – 200^{o}C, the dispersion factor is between 0.87 – 0.90 (except for one measurement). This is somewhat lower than for the LK2 material but should allow for a reasonable oxide thickness to be calculated using Eq 6. As discussed in section 4.1, a possible explanation for the too large calculated thickness is that the outer layer of the oxide is porous and the pores are filled by air at the beginning of the experiment. In this case, the dielectric constant of the

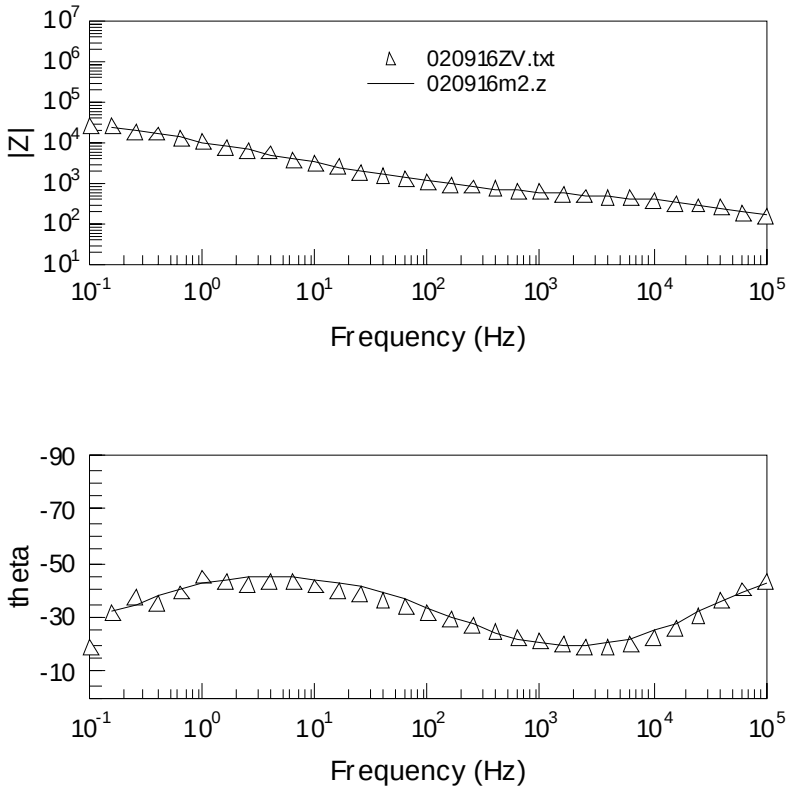

Figure 19
Impedance spectrum of the LK3 material measured at 288^{o}C and the result of the equivalent circuit analysis.

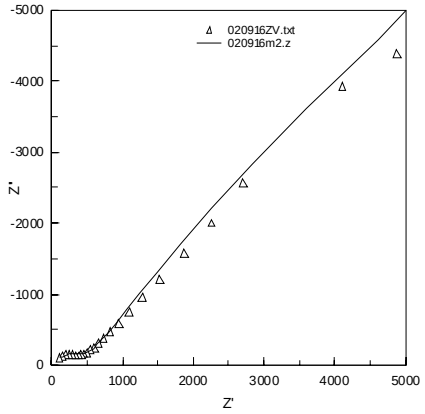

Figure 20
The impedance spectrum in Figure 19 presented in a Nyquist plot.

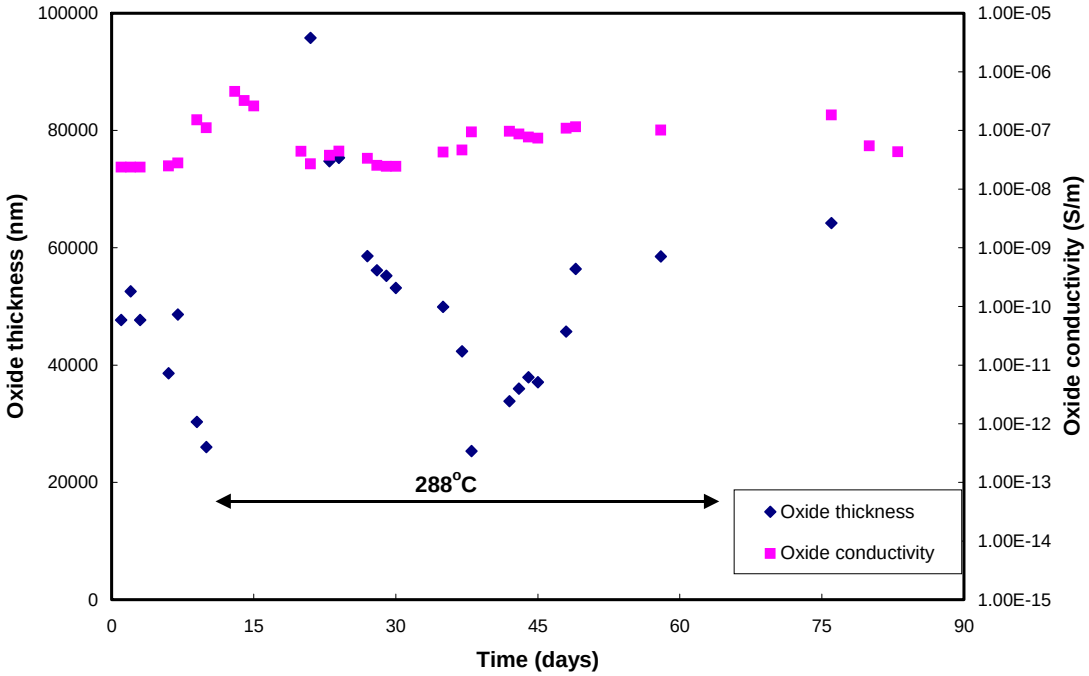

Figure 21
Calculated oxide thickness and conductivity for the LK3 material. The conductivity is based on a thickness of 16 μm.

oxide scale (ε_{app}) will be lower than the value (ε_{ZrO2} = 22) used to calculate the thickness in Figure 21. When electrolyte penetrates into the pores, the dielectric constant of the scale approaches to the value used in the calculations. As a result, the calculated thickness approaches the correct value.

By using the oxide thickness based on the measured weight gain in Table 1 (16 μm), the apparent dielectric constant and porosity at the beginning of the experiment were calculated using Eq 6 and Eq 7. The result is shown in Figure 22. The first three measurements were conducted at room temperature, the next two at 100°C and the last two in the figure at 200°C. It can be seen that the dielectric constant increases with time, which is expected as electrolyte penetrates into the air filled pores. The porosity varies in the range 3.0-10.9 % compared to 3.5-6.4 % for the LK2 material. It is possible that the dispersion factor in the present experiment is slightly too low to allow Eq 6 to be used. If this is the case, the value of the dielectric constant in Figure 22 would be underestimated and the porosity overestimated. Instead of $C_Q^{1/\alpha}$, α-corrected capacitances obtained from plots of log capacitance vs log frequency can be used to evaluate the dielectric constant and porosity (see below).

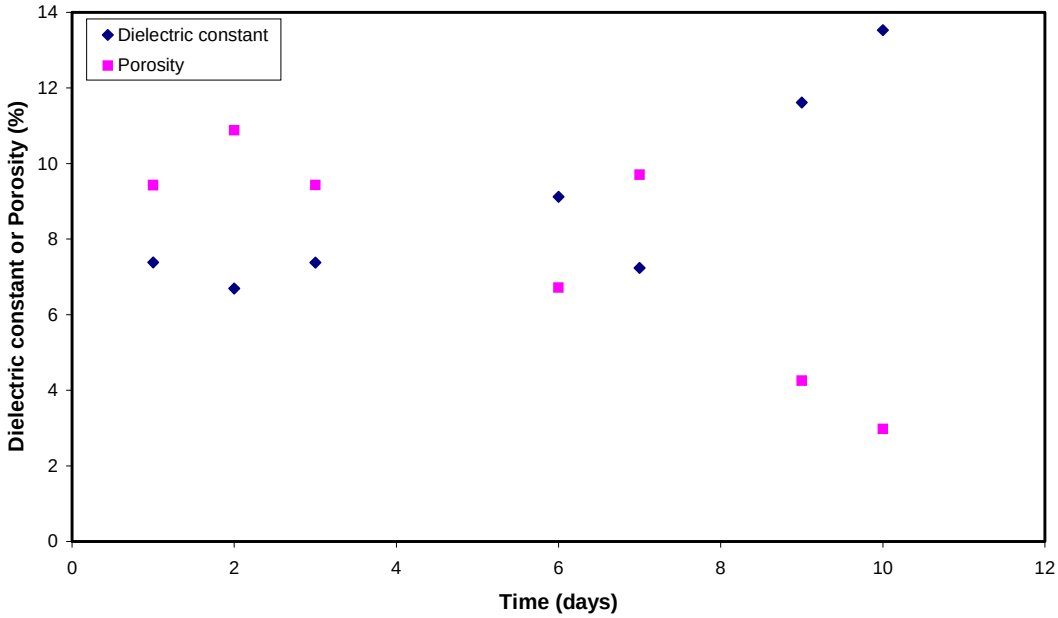

Figure 22
Apparent dielectric constant of the oxide scale and oxide porosity at the beginning of the experiment.

The strong increase in the calculated oxide thickness, seen in Figure 21 when increasing the temperature to 288°C, is probably due to a decrease in the dispersion factor from about 0.90 to about 0.63 (see Table C.2 in Appendix C.2). From Table C.2 one may conclude that the dispersion factor is probably too low in all measurements at 288°C to allow for the thickness to be calculated using Eq 6. This also applies when the temperature was lowered at the end of the experiment. During the exposure at 288°C, the dispersion factor increases gradually with time so that the calculated thickness decreases and approaches the correct value. The reason may be that pores are choked up so that the oxide becomes more homogeneous. When the addition of Fe and Ni is started at day 41, the trend is broken. The dispersion factor decreases again and the calculated oxide thickness increases. Thus, it seems that the addition of Fe and Ni affects the pore structure of the oxide.

As explained in section 4.1, an α-corrected capacitance may be obtained from plots of log capacitance vs log frequency, where the capacitance is calculated from the imaginary component of the impedance. The α-corrected capacitance, $C_{\alpha\text{-corr}}$, is obtained by extrapolating the linear section(s) in these plots to high frequencies (10^5 Hz is used in the present work) and this value can then be used to calculate the oxide thickness. The dispersion factor is obtained from the slope of the linear section(s). In conformity with the measurements on The LK2 material, two linear sections are present in the plots at low temperatures. The linear section at low

frequencies is associated with the inner oxide layer and the one at high frequencies with the outer oxide layer. At temperatures higher than 100°C, the linear section at high frequencies falls outside the measured frequency range. This is due to the fact that the time constant is displaced to higher frequencies (see Figure 17). Therefore, at high temperatures, only the thickness of the inner oxide layer can be obtained using this method. Values of the α-corrected (extrapolated) capacitance and the dispersion factor are tabulated in Appendix D.2.

By substituting $C_{\alpha\text{-corr}}$ for $C_Q^{1/\alpha}$, Eq 6 may be used to calculate the oxide thickness from the α-corrected (extrapolated) capacitance. The thickness calculated from the high frequency α-corrected (extrapolated) capacitance at low temperatures is given in Table 4. The calculated thickness is in reasonable agreement with the weight gain value (16 μm), especially the last four values. Taking only these four values into account, the oxide growth in the course of the present experiment seems to be about 1.1-1.3 μm. In view of a test time of 53 days at 288°C, this appears to be reasonable. The oxide thickness for the inner oxide layer, calculated from the low frequency α-corrected (extrapolated) capacitance, is shown in Figure 23. The test time at 288°C is also marked in the diagram. Dosage of Fe and Ni was started at a test time of 41 days. At 288°C, the calculated thickness of the inner layer increases from about 1.2 μm to about 2.0 μm at the point when the addition of Fe and Ni was started. The reason may be that pores are choked up so that the oxide becomes more homogeneous. After the dosage of Fe and Ni was started, the thickness is relatively constant around 2 μm, except for the last three measurements (when the temperature is lowered) where the data points fall outside the scale of the diagram in Figure 23. This is in good agreement with the thickness at which the transition from pre- to post-transition growth usually occurs (see Chapter 2). The inner layer may thus be identified with the protective barrier layer.

Table 4
Oxide thickness calculated from the high frequency α-corrected (extrapolated) capacitance at the beginning and at the end of the experiment.

Date	Test time (days)	Temperature (°C)	Oxide thickness (nm)
2002-09-04	1	20	20 961
2002-09-05	2	20	20 912
2002-09-06	3	20	21 009
2002-09-09	6	100	15 538
2002-09-10	7	100	15 538
2002-11-22	80	20	16 650
2002-11-25	83	20	16 842

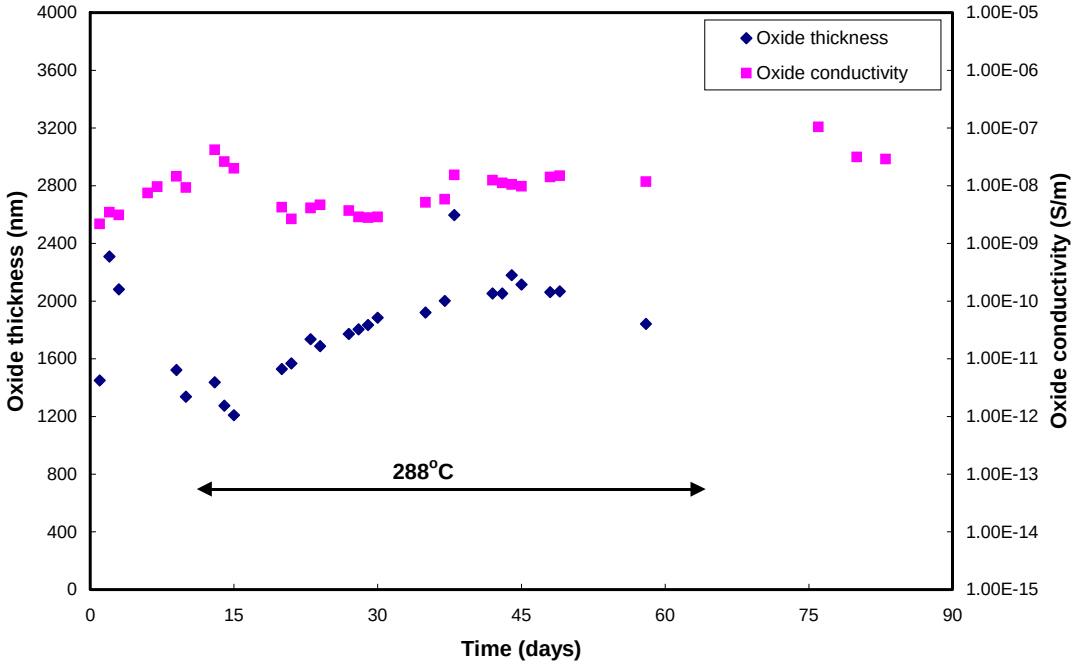

Figure 23
Oxide thickness and conductivity of the inner layer of the LK3 material.

As stated above, the high frequency α-corrected (extrapolated) capacitance may be used to evaluate the dielectric constant and porosity of the oxide scale at the beginning of the experiment. The apparent dielectric constant is obtained from Eq 6 (substituting $C_{\alpha\text{-corr}}$ for $C_Q^{1/\alpha}$) and the porosity from Eq 7. The oxide thickness was assumed to be 16 μm (the weight gain value from Table 1). The dielectric constant and porosity is accounted for in Table 5. The values of the dielectric constant is about twice as large as

Table 5
Dielectric constant and porosity of the oxide scale at the beginning of the experiment, evaluated from the high frequency α-corrected (extrapolated) capacitance.

Test time (days)	Temperature (°C)	ε_{app}	Porosity (%)
1	20	16.79	1.48
2	20	16.83	1.46
3	20	16.75	1.49
6	100	22.65	-0.14
7	100	22.65	-0.14

the values shown in Figure 22 and, consequently, the calculated porosity are smaller. A value of the dielectric constant exceeding 22 (the value for ZrO_2) is possible if water penetrate into the pores, since the dielectric constant of water is around 80 at room temperature. The reason for the negative porosity at 100^{o}C may be that the pores are no longer filled only by air and, thus, Eq 7 is no longer valid.

As is the case with the LK2 material, the conductivity of the oxide is not readily obtainable using only the impedance data since the total oxide thickness has not been possible to calculate. However, by using the weight gain value of the thickness (16 μm) and the resistance from the impedance measurements (R2+R3 in Figure 7), the conductivity can be calculated using Eq 8. The result has been introduced in Figure 21. The conductivity of the inner oxide layer was calculated using the thickness and resistance (R3 in Figure 7) of this layer and the result is shown in Figure 23.

Arrhenius plots of the oxide conductivity as a function of inverse temperature at the beginning and at the end of the experiment is shown in Figure 24. The conductivity is based on an oxide thickness of 16 μm, as explained above. The activation energy for conduction deduced from these plots is 13.6 and 3.6 kJ mol^{-1} at the beginning and end, respectively. It should be mentioned that, for the first measurements at room temperature, equivalent circuit analysis were not successful at first due to difficulties in determining the value of R3. This problem was solved by keeping the value of R3 fixed at 10^6 Ω during the analysis. As a consequence, the values at room temperature at the beginning of the experiment shown in Figure 24 are somewhat uncertain.

Effective donor density

Capacitance versus voltage profiles were measured at two occasions at 288^{o}C and at two occasions when the temperature was lowered at the end of the experiment. Mott-Schottky plots (MS-plots) were constructed at three different frequencies, 100, 1000 and 10 000 Hz. For details regarding construction of MS-plots and the derivation of effective donor densities, see the previous report [3]. MS-plots from the measurements at 288^{o}C are shown in Figure 25 and 26. The effective donor densities derived from these plots are given in Table 6. It was not possible to find linear sections in the plots at 10 000 Hz that could be used for evaluation of donor densities and, therefore, these plots are not shown in Figure 25 and 26.

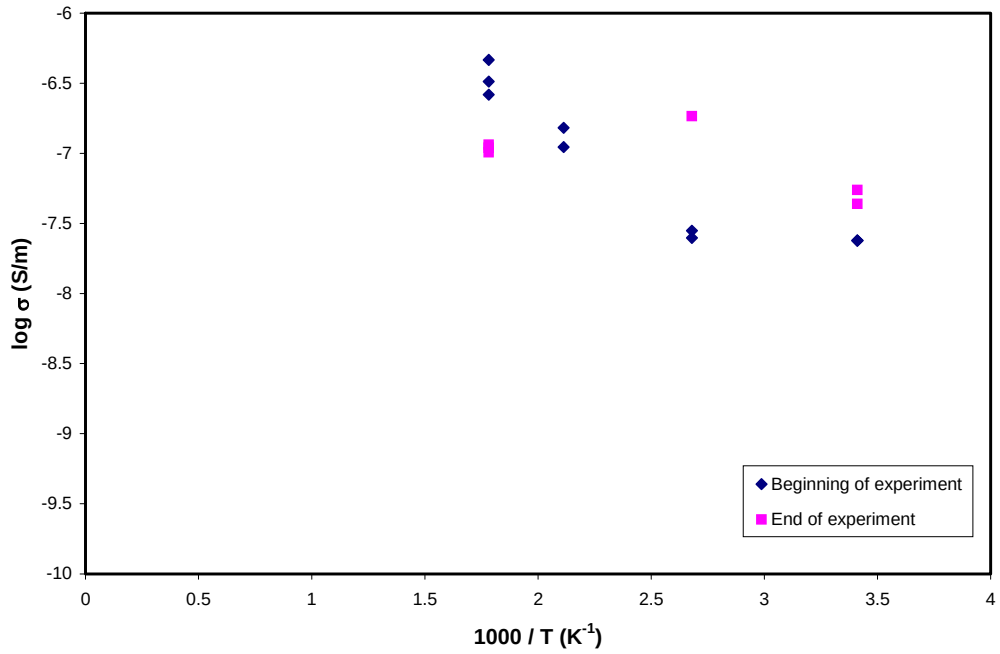

Figure 24
Oxide conductivity as a function of inverse temperature for the LK3 material at the beginning and at the end of the experiment.

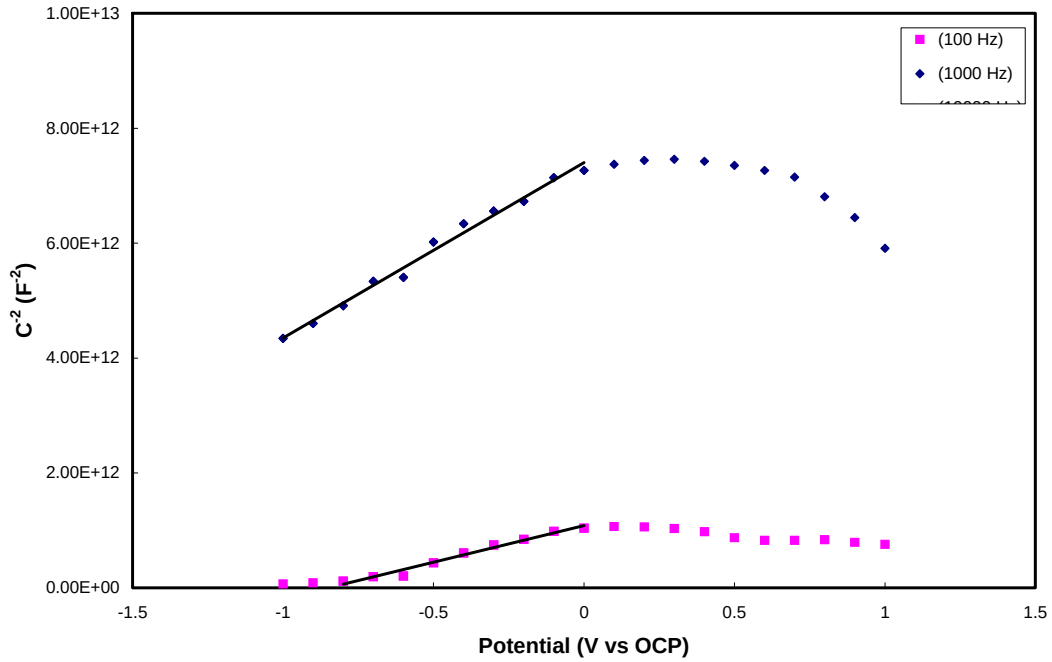

Figure 25
Mott-Schottky plots for the LK3 material at 288°C. The measurements were conducted at a total test time of 37 days.

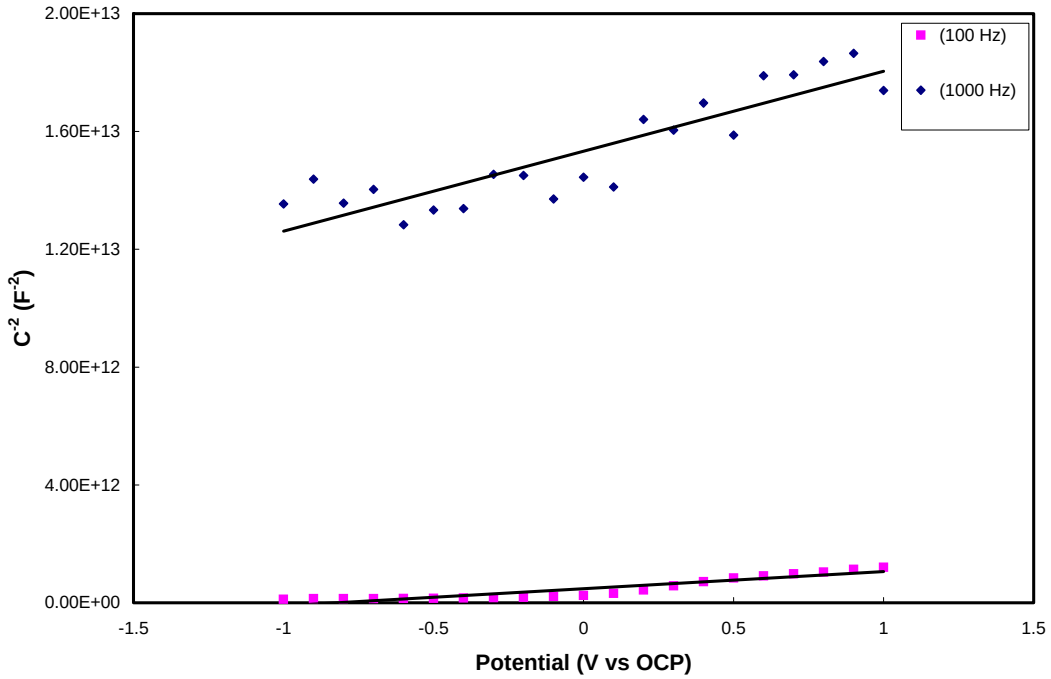

Figure 26
Mott-Schottky plots for the LK3 material at 288°C. The measurements were conducted at a total test time of 63 days. No dosage was made during this experiment.

From Figure 25 it can be seen that the MS-plots are not linear over the whole potential regions. Therefore, for the measurements conducted at a test time of 37 days, the slopes used to derive the effective donor densities shown in Table 6 are based on a part of these plots. At 100 Hz the potential range –0.8 to 0 V versus open circuit potential was used, whereas the range –1 to 0 V was used at 1000 Hz. For the measurements performed at a test

Table 6
Effective donor density calculated for the LK3 material.

Test time (days)	Temperature (°C)	Frequency (Hz)	Effective donor density $N_D \times 10^{-23}$ (m^{-3})
37	288	100	1.145
37	288	1000	0.477
37	288	10 000	---
63	288	100	2.495
63	288	1000	0.537
63	288	10 000	---

time of 63 days, the whole potential region was used to derive the donor densities. The last-mentioned measurements where performed when the dosage pump was out of order and, thus, dosage of H_2O_2, $NaNO_3$, Fe and Ni was not made during this experiment. As explained above, it is not possible to obtain α-corrected capacitances from plots of log capacitance vs log frequency since the linear section at high frequencies falls outside the measured frequency range. When the temperature was lowered, the slopes of the MS-plots are negative. Calculations of effective donor densities at 100^o and 20^oC were therefore not successful.

5 Discussion

Impedance spectra for the two materials investigated in the present work are compared in Figure 27. The measurements were performed at 288^{o}C at the end of the experiments. Fe and Ni were dosed to the water at the time of the measurements. The total test time was 87 and 58 days for the LK2 and LK3 material, respectively. It can be seen that there are no major differences between the materials, neither regarding the magnitude of the impedance nor the positions of the time constants. For comparison, a spectrum measured for the LK2 material in the pre-transition region [3] is also shown in Figure 27.

As explained above, reliable values of the total oxide thickness have not been obtainable from the impedance measurements. However, from the low frequency α-corrected (extrapolated) capacitance, the thickness of the inner oxide layer was successfully calculated. In Figure 28, the thickness of the inner layer is shown as a function of test time for the investigated materials. The values are in reasonable agreement although the calculated thickness of the LK2 material exhibits some spread. As stated above, the calculated values (about 2 μm) agree with the thickness at which the transition from pre- to post-transition growth usually occurs and, thus, the inner layer may be identified with the protective barrier layer.

The oxide conductivity is displayed in two figures. In Figure 29, the conductivity of the whole oxide is shown as a function of test time. As explained above, the conductivity is based on a thickness of 15 μm and 16 μm for the LK2 and LK3 material, respectively. The conductivity of the inner oxide layer of the investigated materials is shown in Figure 30. In this diagram, the conductivity of the LK2 material in the pre-transition region is also shown for comparison. It can be concluded that the difference between the investigated materials is small. The conductivity of the inner oxide layer is roughly one order of magnitude lower than the conductivity of the whole oxide and, further, the conductivity seem to be almost identical with the conductivity of the pre-transition oxide.

The porosity of the materials, derived according to the procedure described in section 4.1 and 4.2, is in the range 3.5-6.4 % and 3.0-10.9 % for the LK2 and LK3 material, respectively. It is possible that the dispersion factor is slightly too low in some of the measurements using the LK3 material to allow the porosity to be evaluated according to this procedure. In this case, the porosity would be overestimated. The porosities found in the present work are in good agreement with porosities of pre-hydrided Zircaloy-2 samples oxidized in an autoclave at 400^{o}C for different periods of time reported by Oskarsson [4]. Porosities in the range 4.2 %- 6.1 % are given in this work.

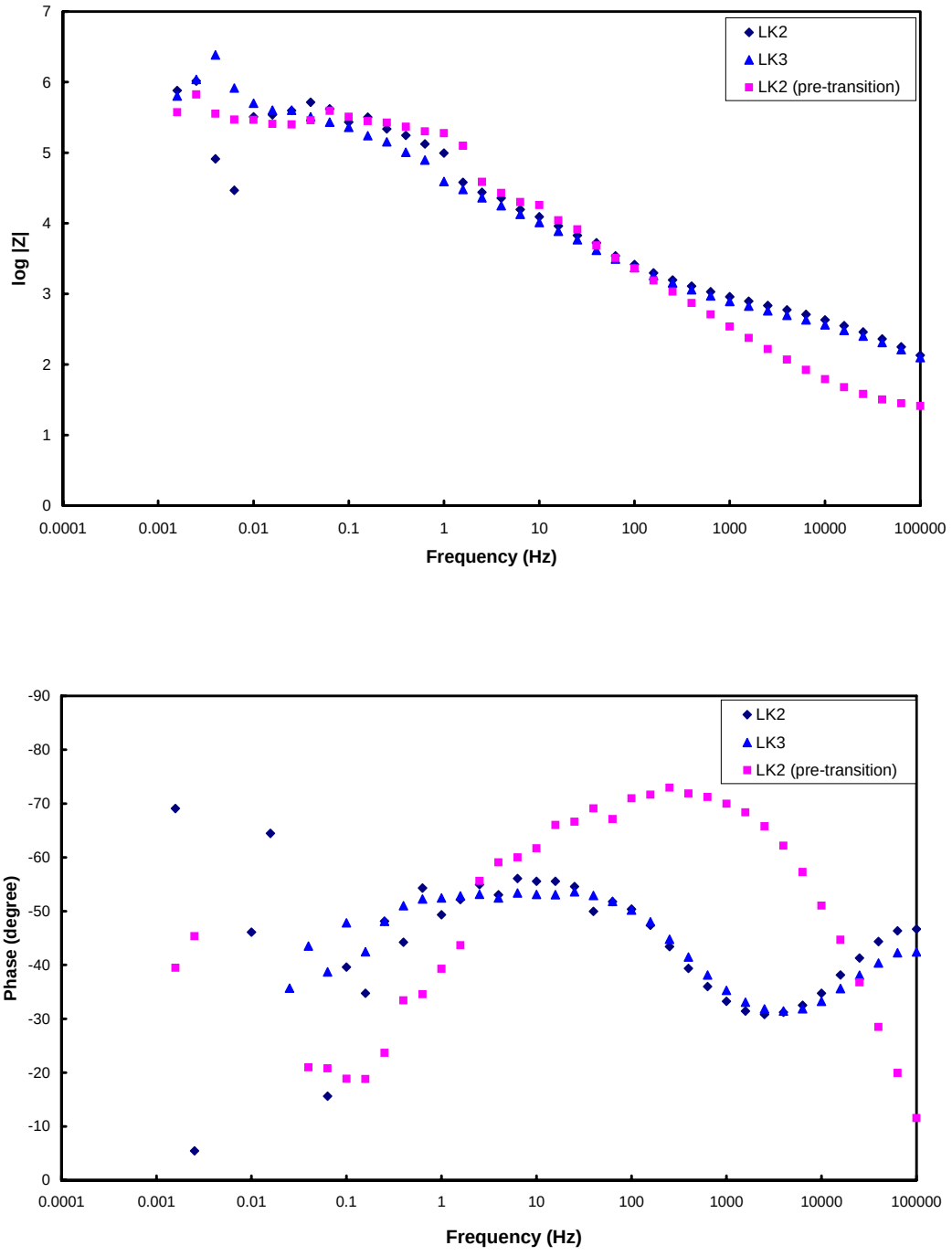

Figure 27
Impedance spectra of the investigated materials at the end of the experiments. The temperature was 288^{o}C.

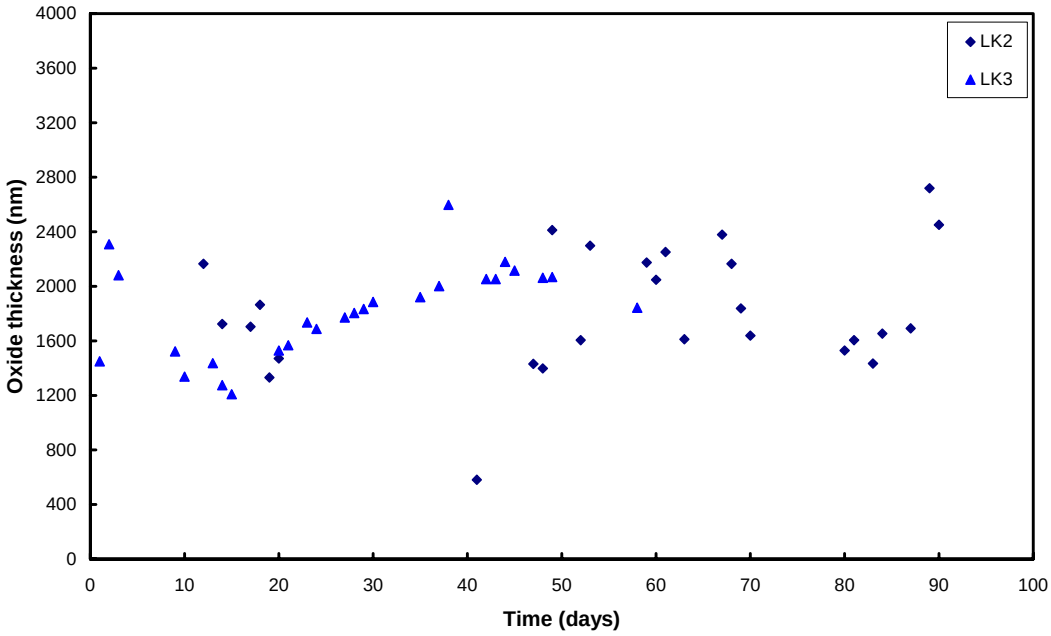

Figure 28
Calculated thickness of the inner oxide layer as a function of test time.

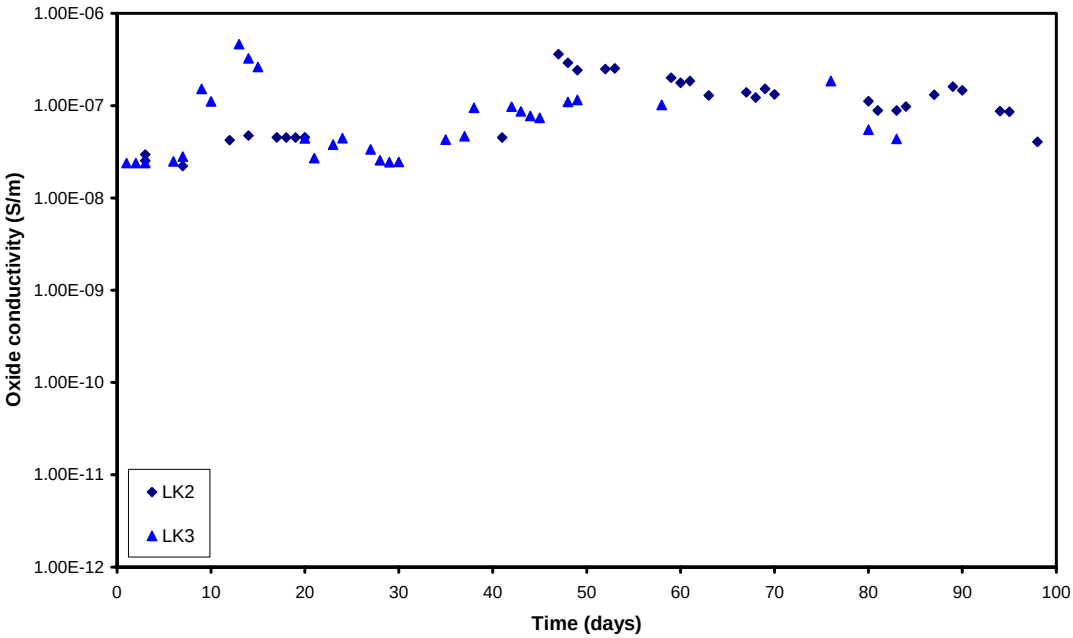

Figure 29
Calculated oxide conductivity of the whole oxide as a function of test time.

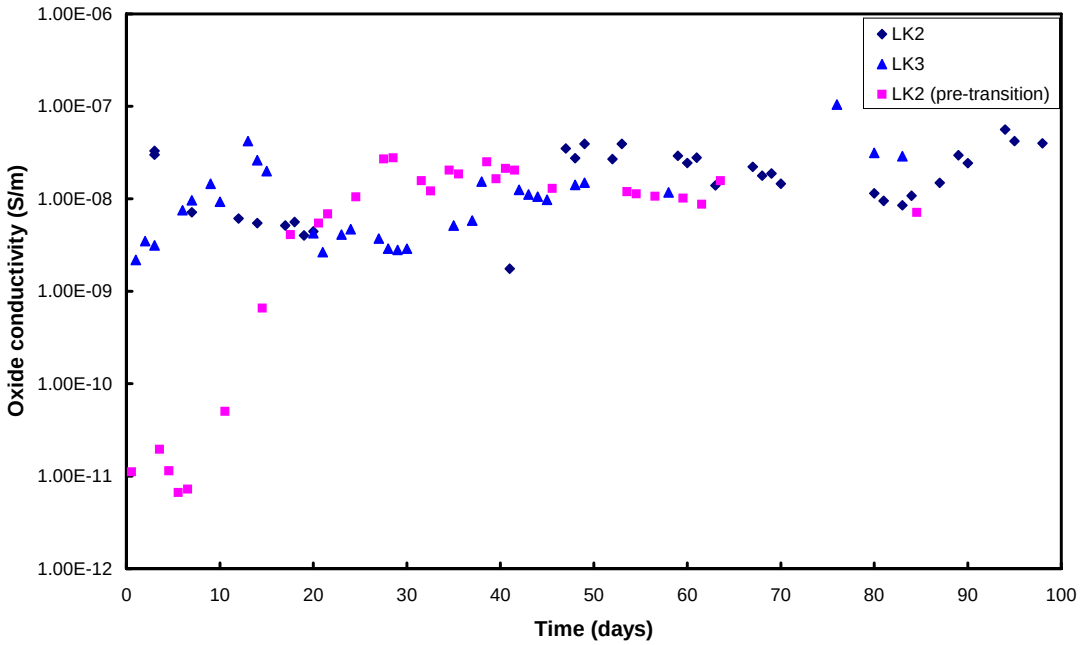

Figure 30
Calculated oxide conductivity of the inner oxide layer as a function of test time.

Values of the activation energy and the effective donor density found in the present work exhibit a greater spread compared to the values derived in the pre-transition region [3]. The first-mentioned values are thus afflicted with a greater uncertainty. The values obtained in the post-transition region are (in most cases) lower than the corresponding values in the pre-transition region.

The dosage of Fe and Ni during the latter part of the experiments does not appear to have any great influence on the oxide properties studied in the present work. For the LK3 material, however, it seems that the addition of Fe and Ni affects the pore structure of the oxide. At the point of time when the dosage was started, a change-over from increasing to decreasing values of the dispersion factor was seen.

6 Conclusions

- The oxide thickness of the LK2 and LK3 material is of comparable magnitude (≈ 15 μm) after a pre-oxidation in steam in an autoclave at 415^{o}C for 331 days.
- Their hydrogen contents are also in good agreement (≈ 1000 ppm) and the hydrides are mainly circumferentially orientated (parallel with the surface) and uniformly distributed in the metal.
- All impedance spectra have been successfully modelled using an equivalent circuit with two time constants for the oxide.
- This shows that the oxide is composed of an inner and an outer layer.
- Less information has been possible to gain from the impedance measurements in the post-transition region compared to the measurements in the pre-transition region.
- However, the following properties have been successfully evaluated from the impedance data:
  - thickness of the inner oxide layer
  - oxide conductivity
  - oxide porosity
- The values of these quantities did not differ significantly between the two investigated materials.
- The thickness of the inner protective layer is about 2 μm.
- The conductivity of the inner oxide layer is approximately one order of magnitude lower than the conductivity of the whole oxide and, further, this conductivity is in accordance with the conductivity of the pre-transition oxide.
- Porosities in the range 3.5-6.4 % and 3.0-10.9 % were derived in the present work for the LK2 and LK3 material, respectively.
- The present work has clearly demonstrated that impedance spectroscopy can be used for in-situ studies of the corrosion of Zircaloy cladding materials in the pre-transition region. Also in the post-transition region useful information has been obtained from the measurements (see above).

Acknowledgements

The authors would like to acknowledge the following persons:

Stig Karlgren, Studsvik Nuclear AB Sweden, for taking daily care of the experiments.
Eva Ögren, Studsvik Nuclear AB Sweden, for preparing solutions.
Hans Ericsson, Studsvik Nuclear AB Sweden, for performing the light optical microscopy investigations.
Roger Lundström, Studsvik Nuclear AB Sweden, for scanning the light optical micrographs.
Sören Karlsson, Studsvik Nuclear AB Sweden, for measurements of hydrogen contents.
Thomas Andersson, AB Sandvik Steel, Sweden, for supplying the pre-oxidized Zircaloy-2 tubes.

This work has been funded by the Swedish Nuclear Power Inspectorate, Sweden, Vattenfall Bränsle AB, Sweden, OKG AB, Sweden and Studsvik Nuclear AB, Sweden.

References

[1] YAMAMOTO, S and PEIN, K
Studsvik Nuclear AB, Sweden 2001,
STUDSVIK/N(K)-01/016

[2] NYSTRAND, A-C and LUNDSTRÖM, R
Studsvik Nuclear AB, Sweden 2000,
STUDSVIK/N(H)-00/020

[3] FORSBERG, S, AHLBERG, E and ANDERSSON, U
Studsvik Nuclear AB, Sweden 2003,
STUDSVIK/N(K)-03/17

[4] OSKARSSON, M
Study on the Mechanisms for Corrosion and Hydriding of Zircaloy.
Doctoral Thesis, The Royal Institute of Technology, Stockholm, Sweden, 2000.

[5] BERGSTRÖM, C and LUNDGREN, K
PEROX – Användarhandledning och teoribeskrivning.
ALARA Engineering, Report 98-0036R and 98-0035R, 1998, in Swedish.

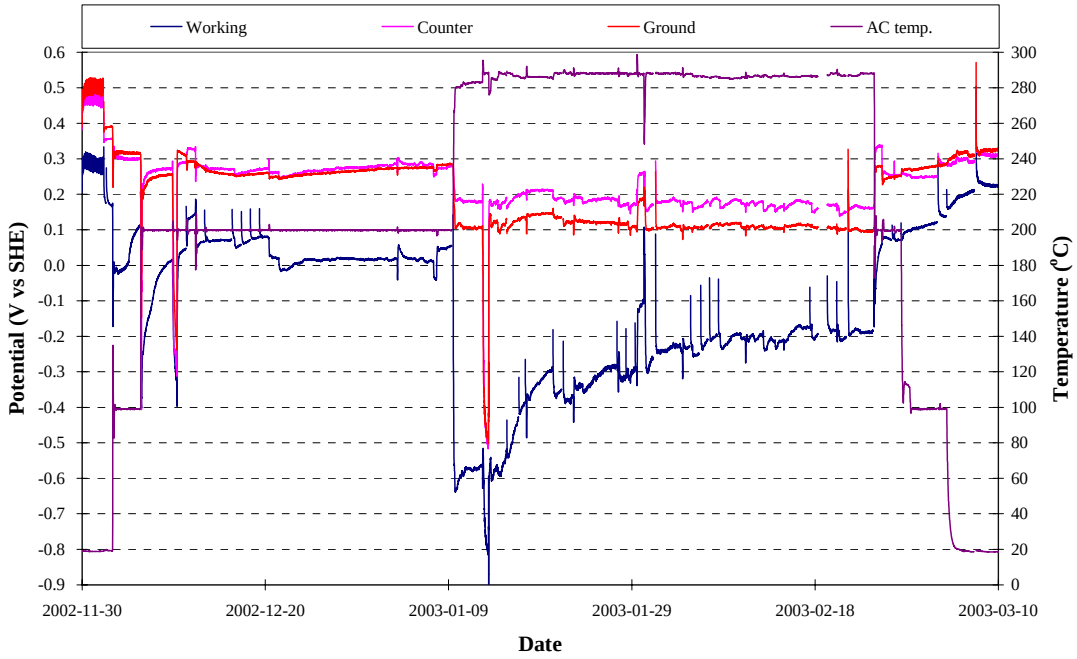

Figure A.1
Potentials measured during experiment with the LK2 material.

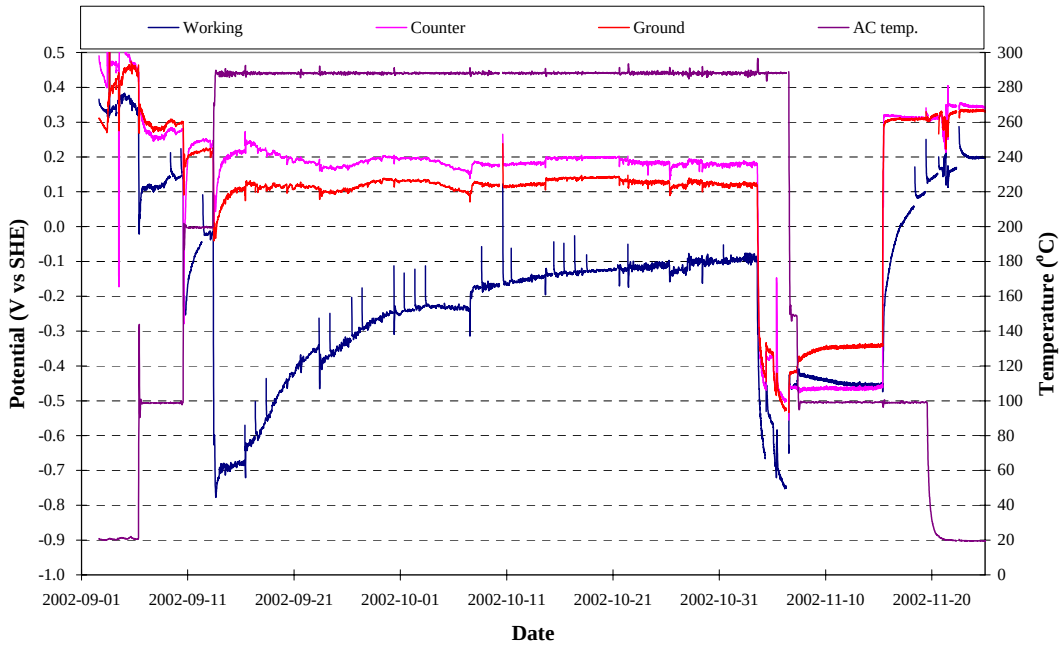

Figure A.2
Potentials measured during experiment with the LK3 material.

Impedance spectra measured during experiments with the LK2 material

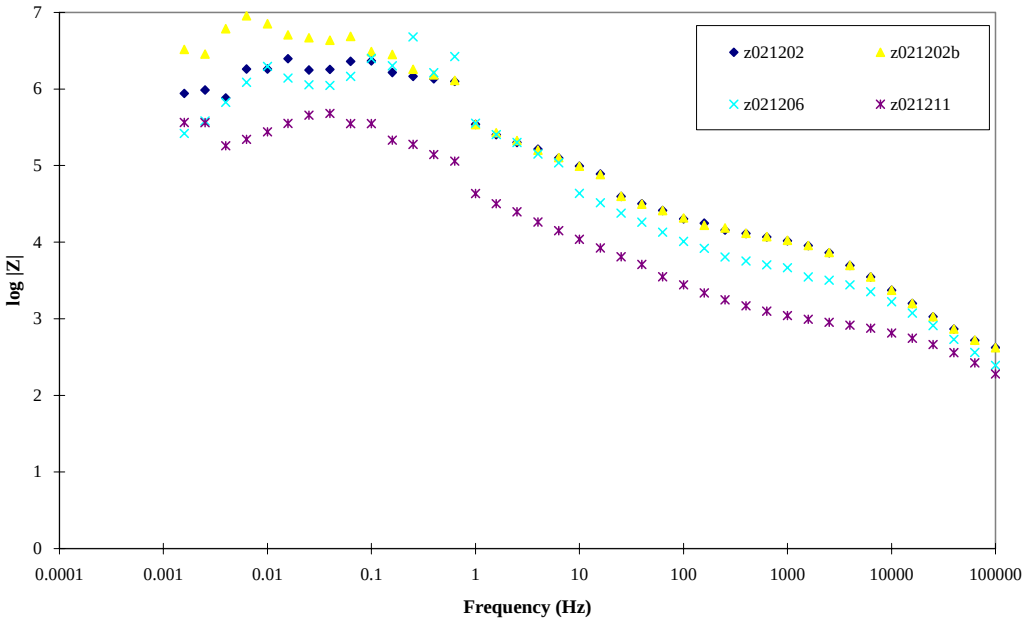

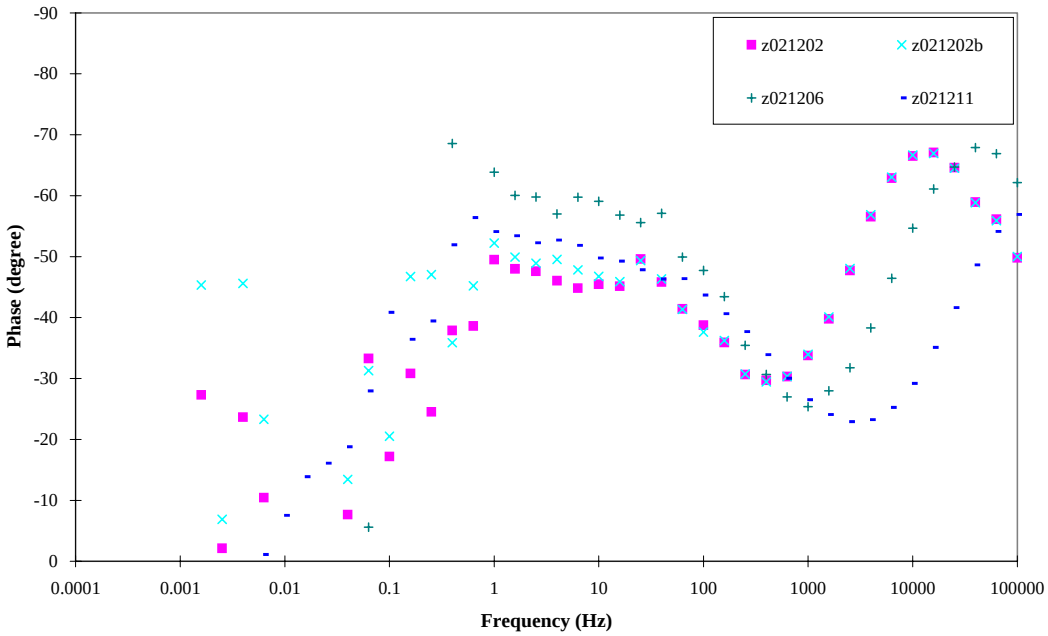

Impedance spectra measured during experiments with the LK2 material (cont.)

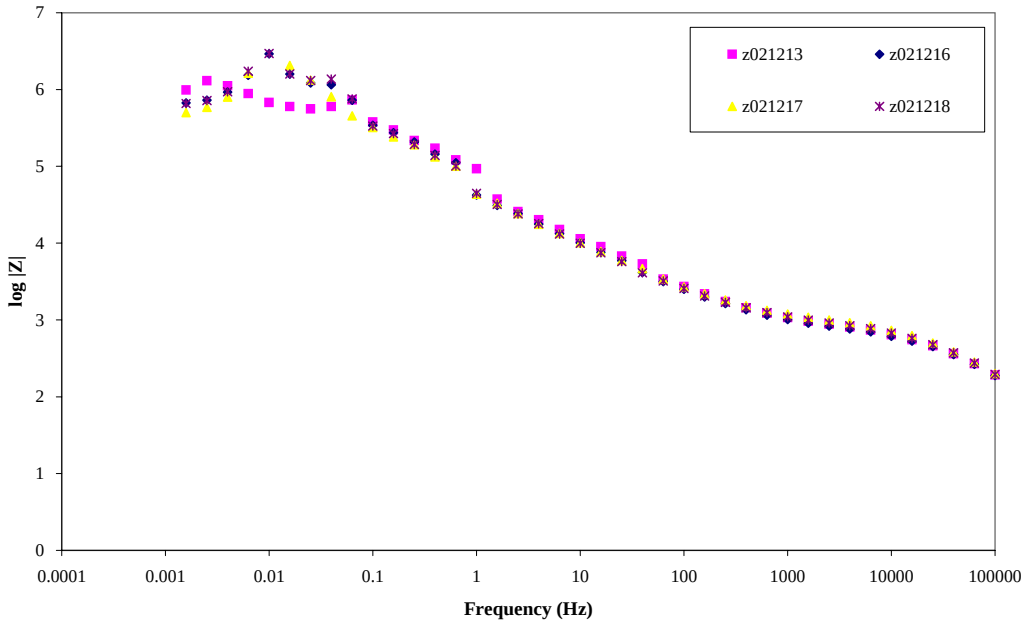

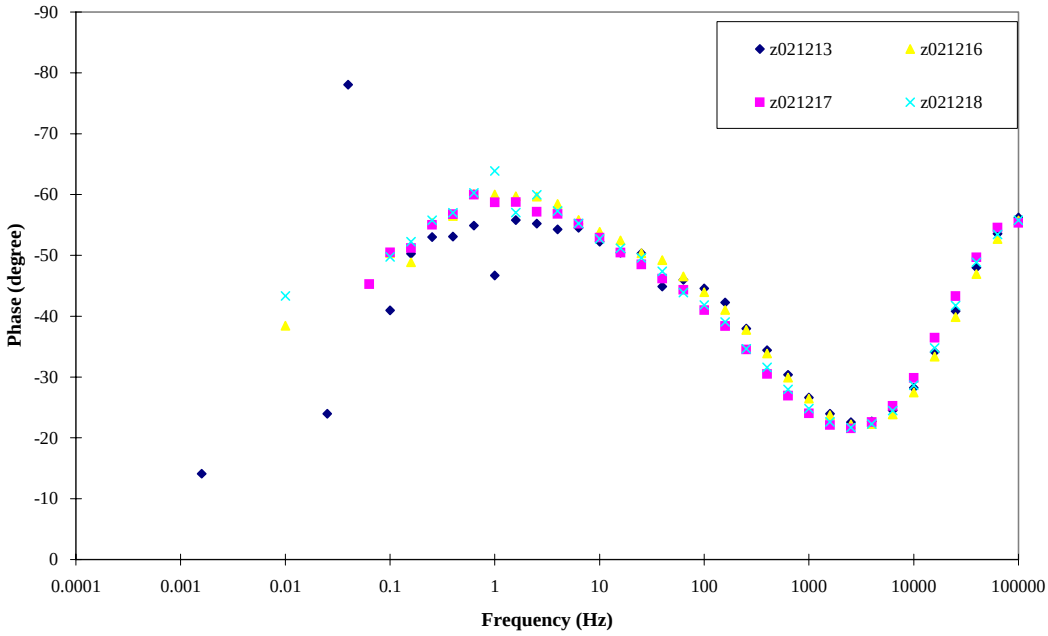

Impedance spectra measured during experiments with the LK2 material (cont.)

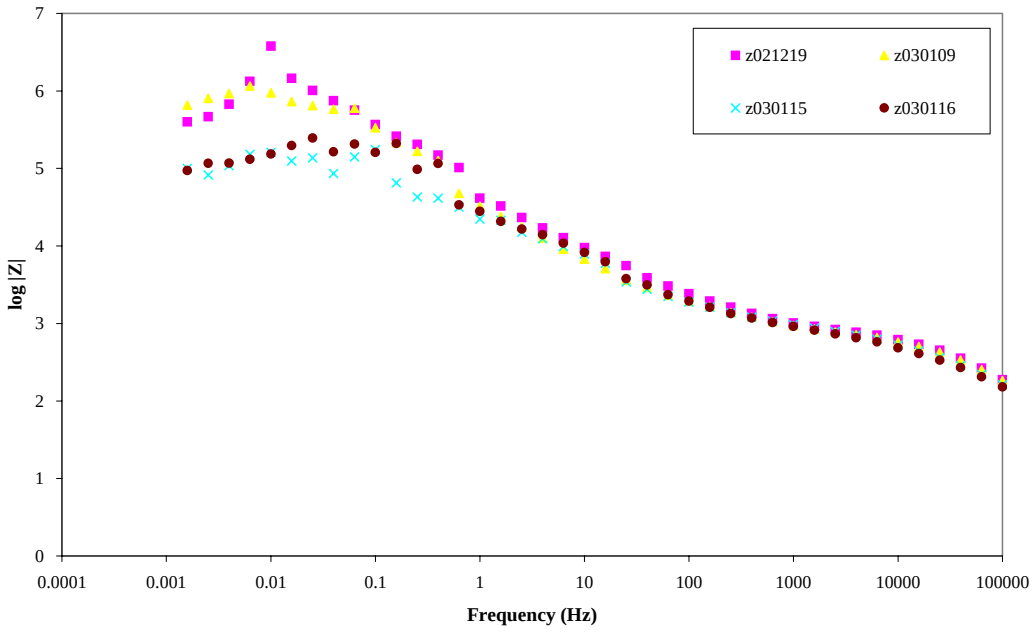

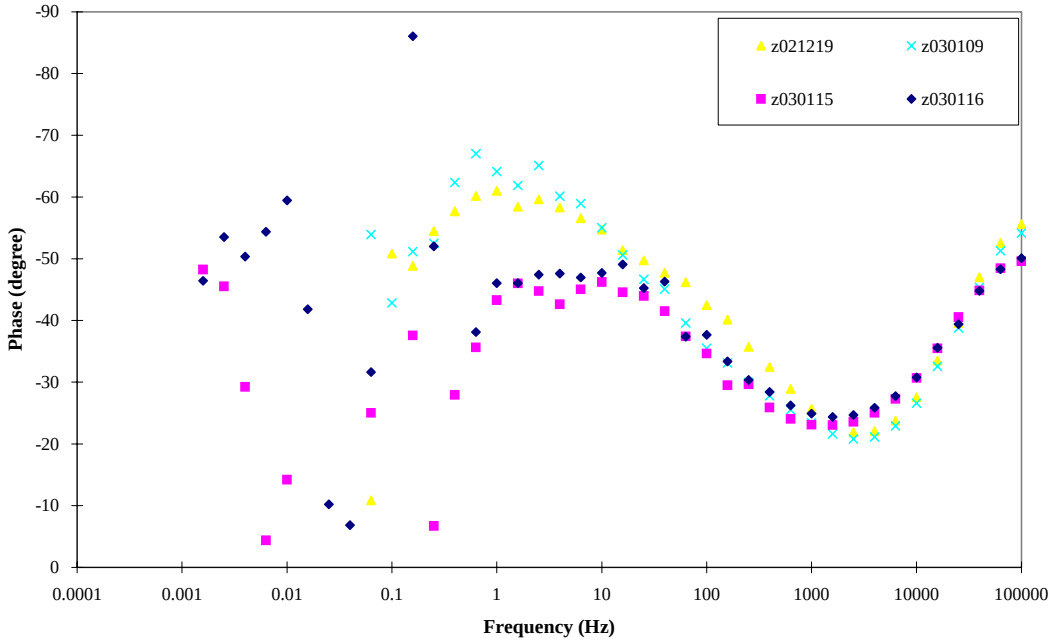

Impedance spectra measured during experiments with the LK2 material (cont.)

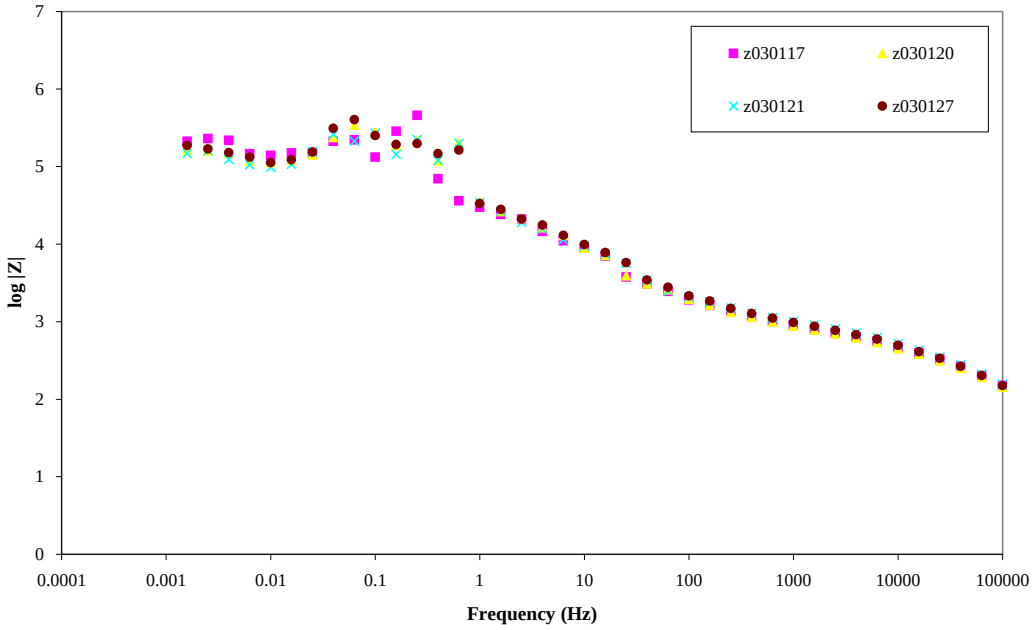

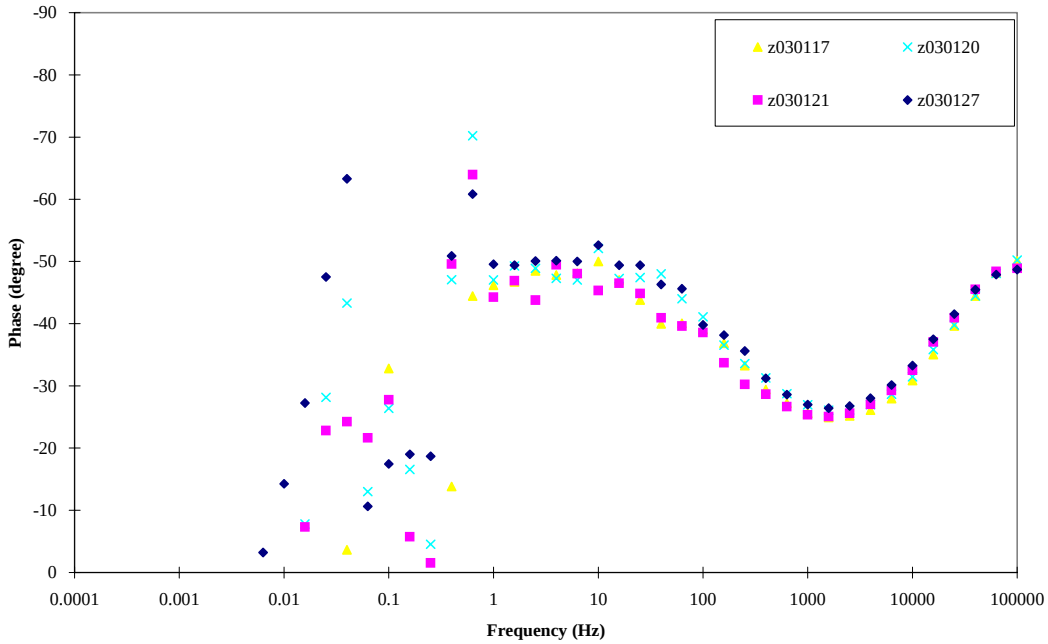

Impedance spectra measured during experiments with the LK2 material (cont.)

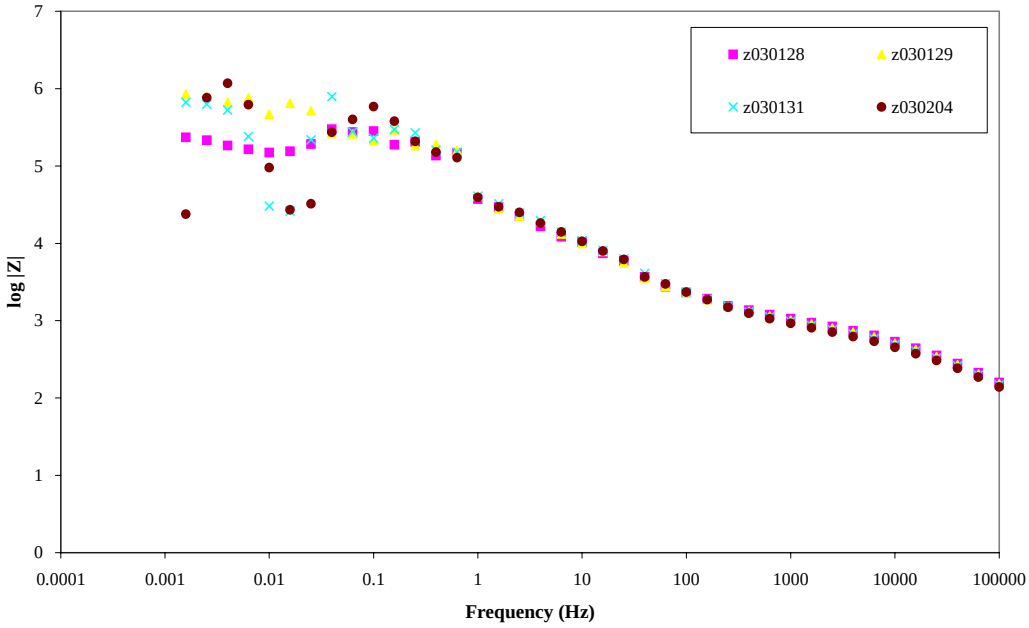

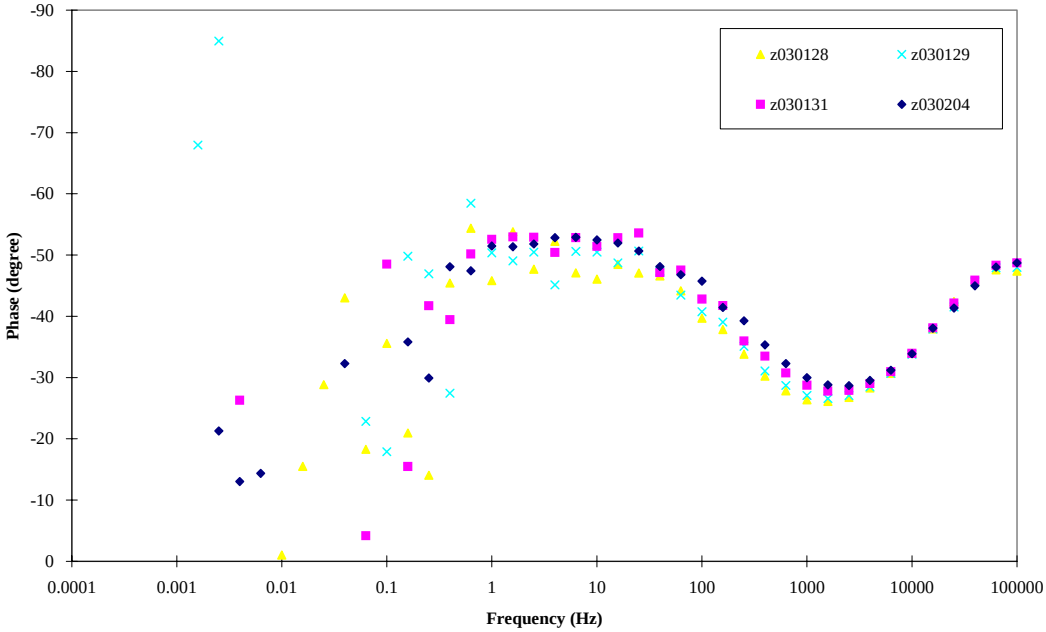

Impedance spectra measured during experiments with the LK2 material (cont.)

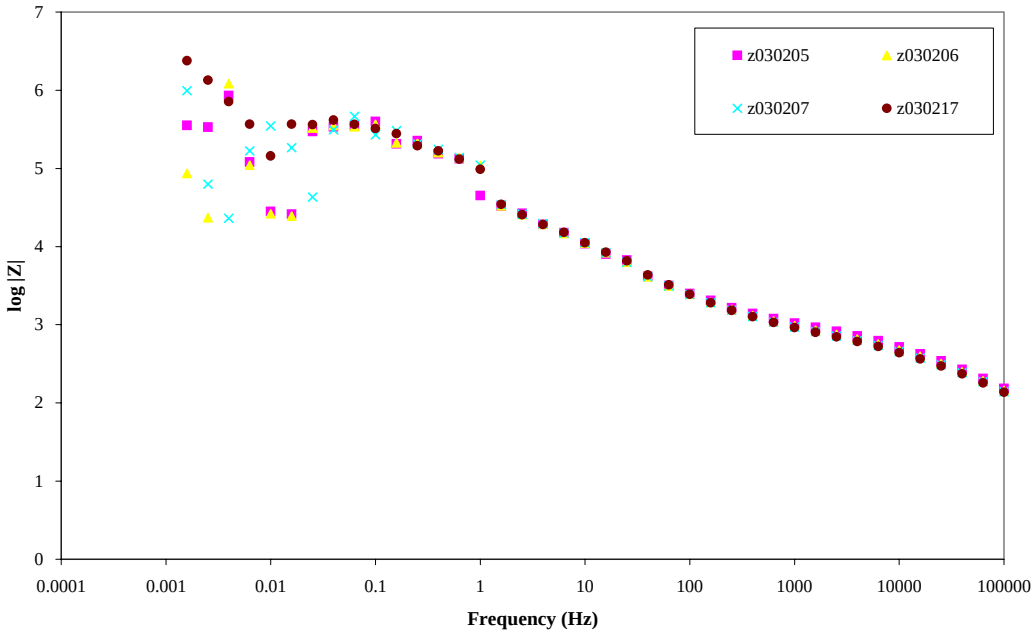

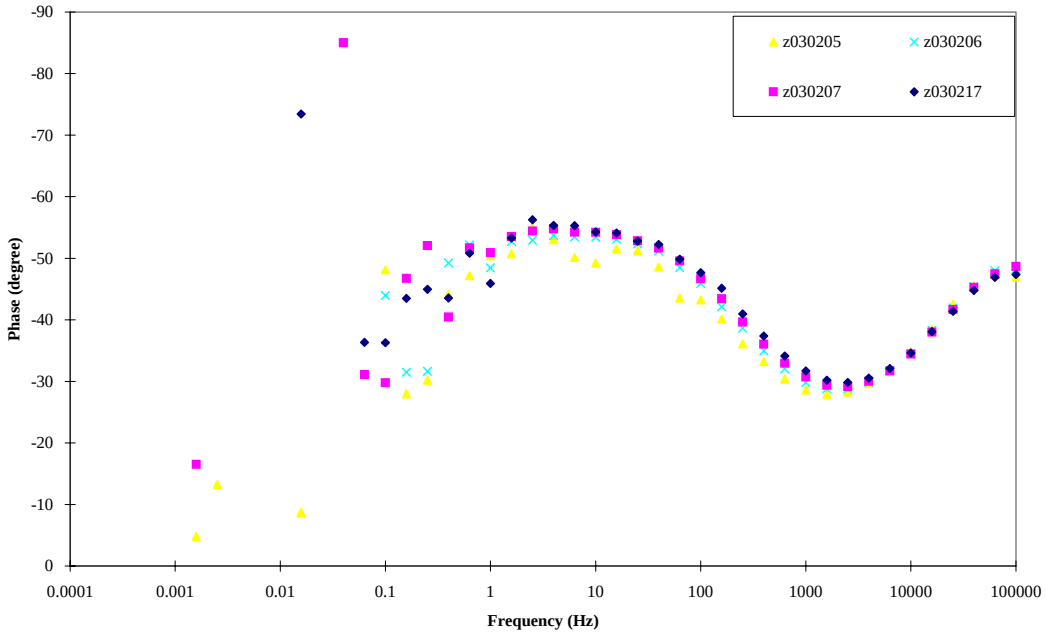

Impedance spectra measured during experiments with the LK2 material (cont.)

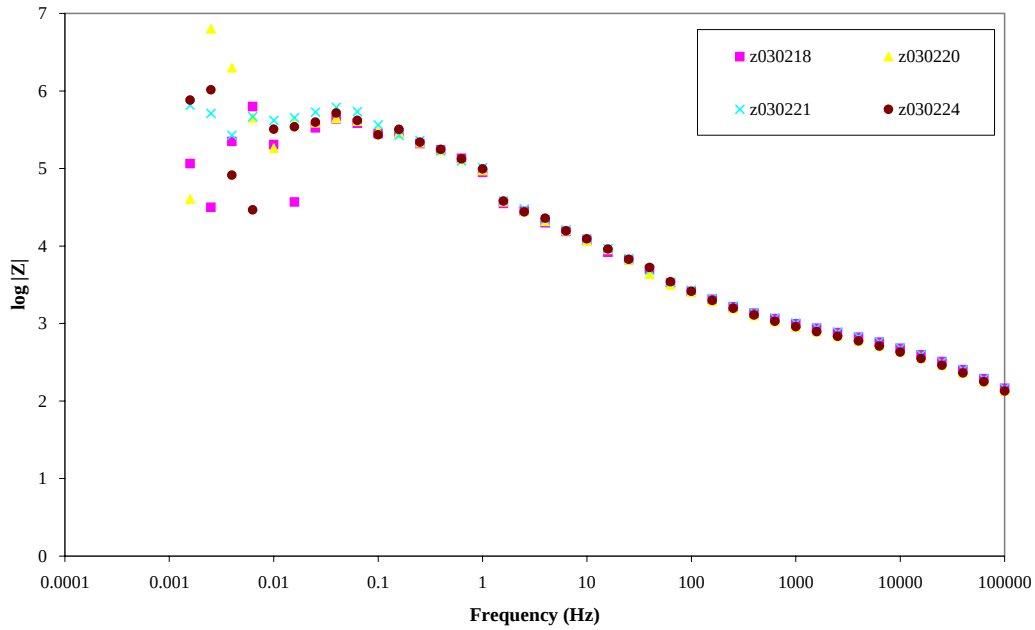

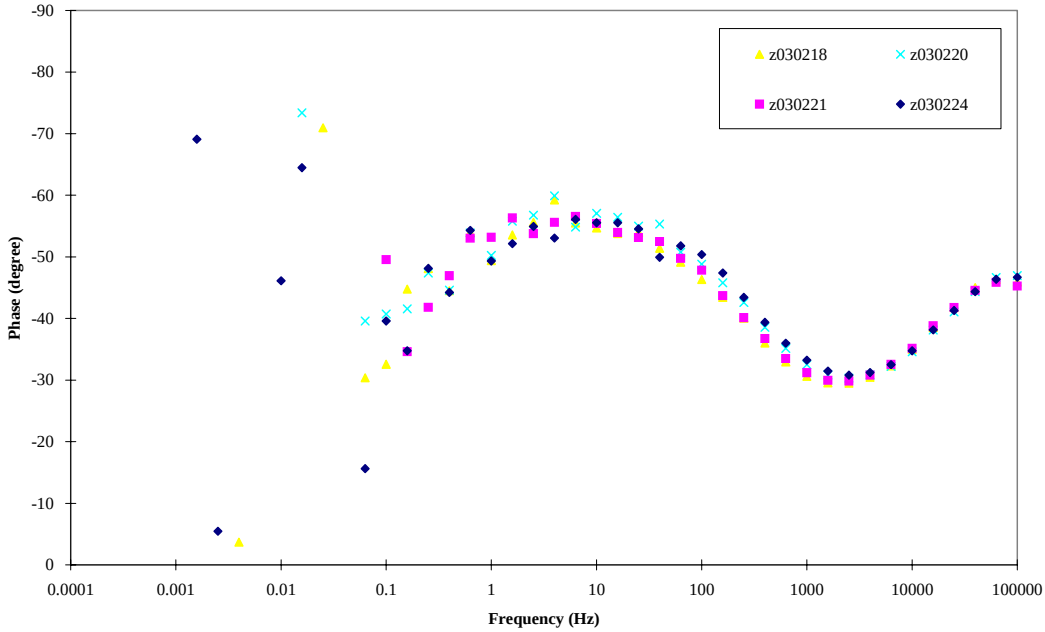

Impedance spectra measured during experiments with the LK2 material (cont.)

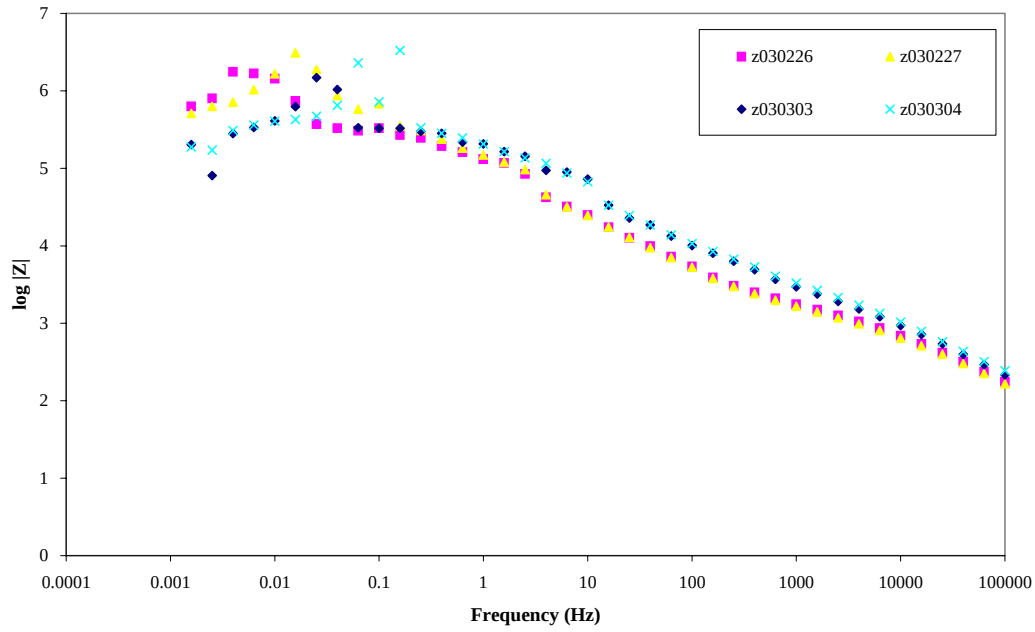

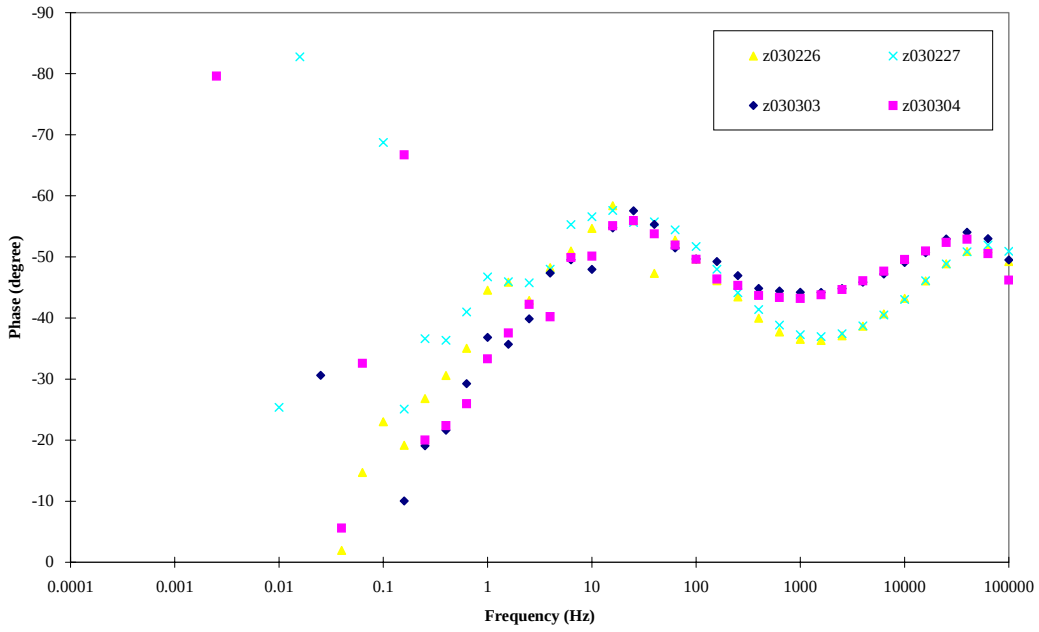

Impedance spectra measured during experiments with the LK2 material (cont.)

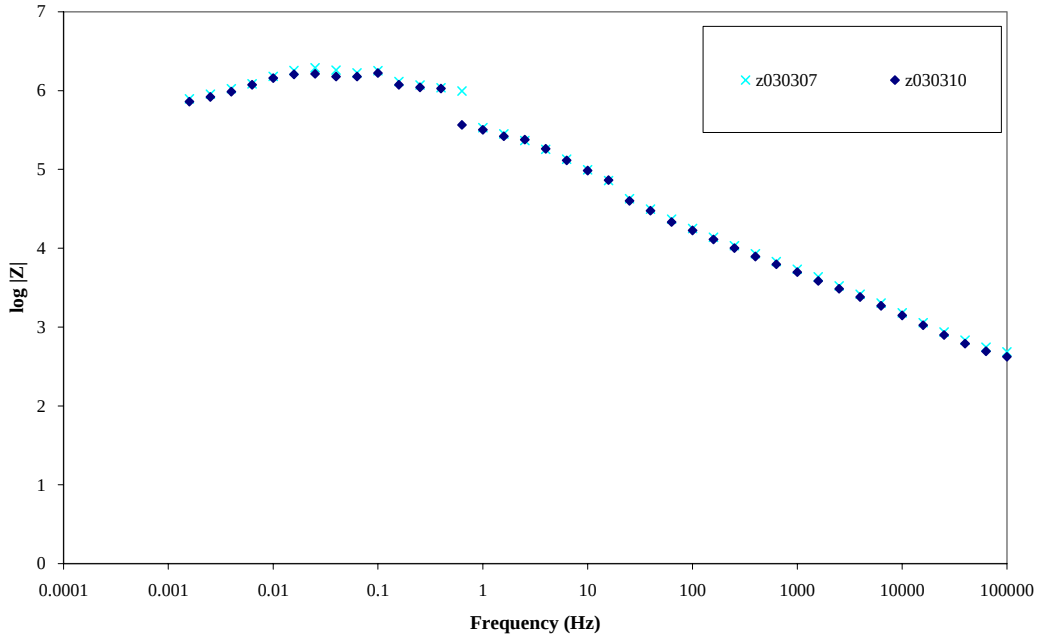

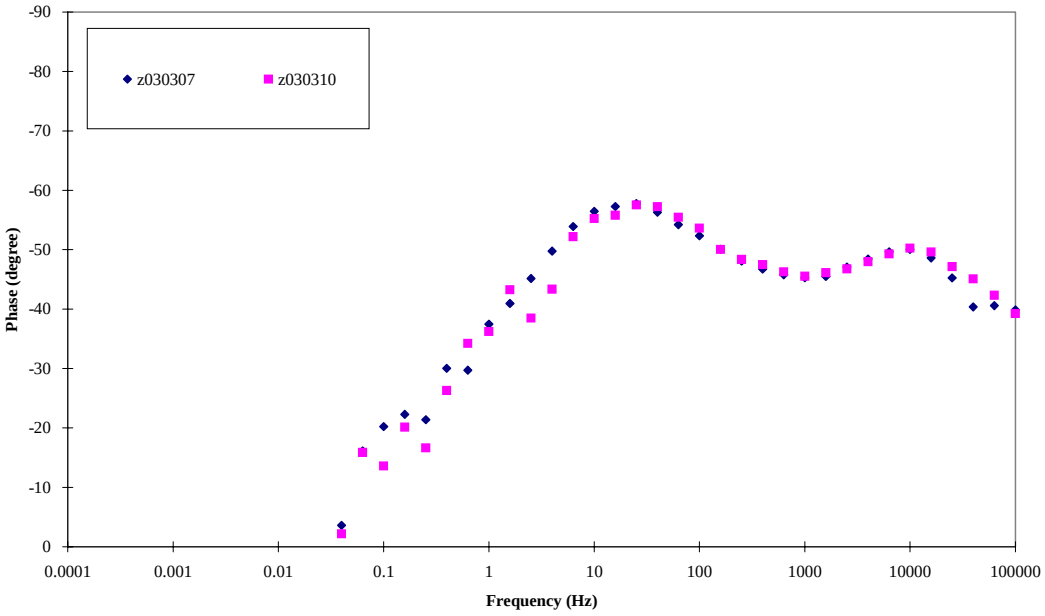

Impedance spectra measured during experiments with the LK3 material

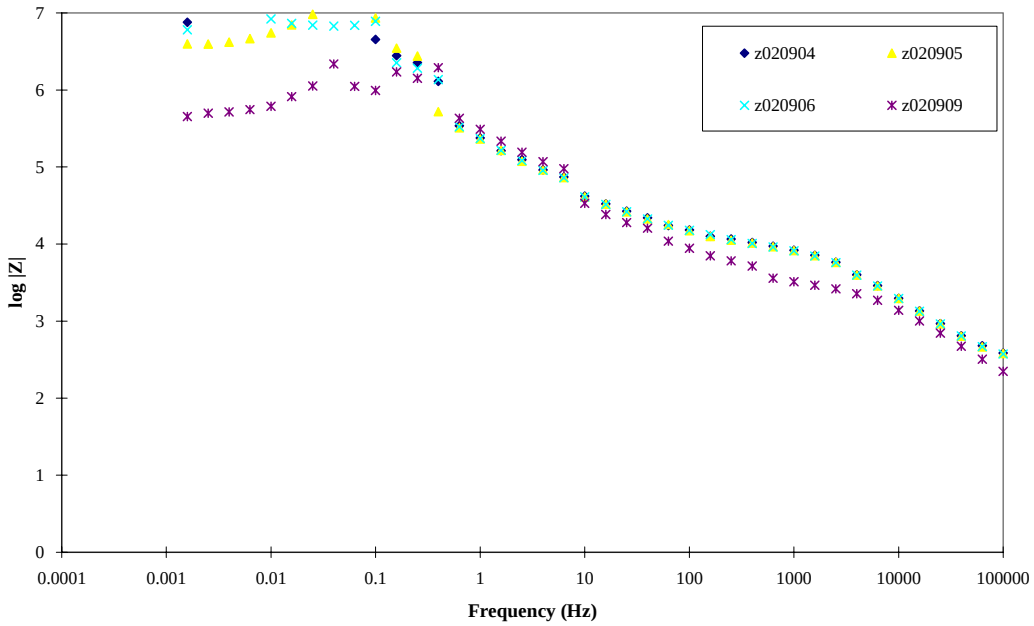

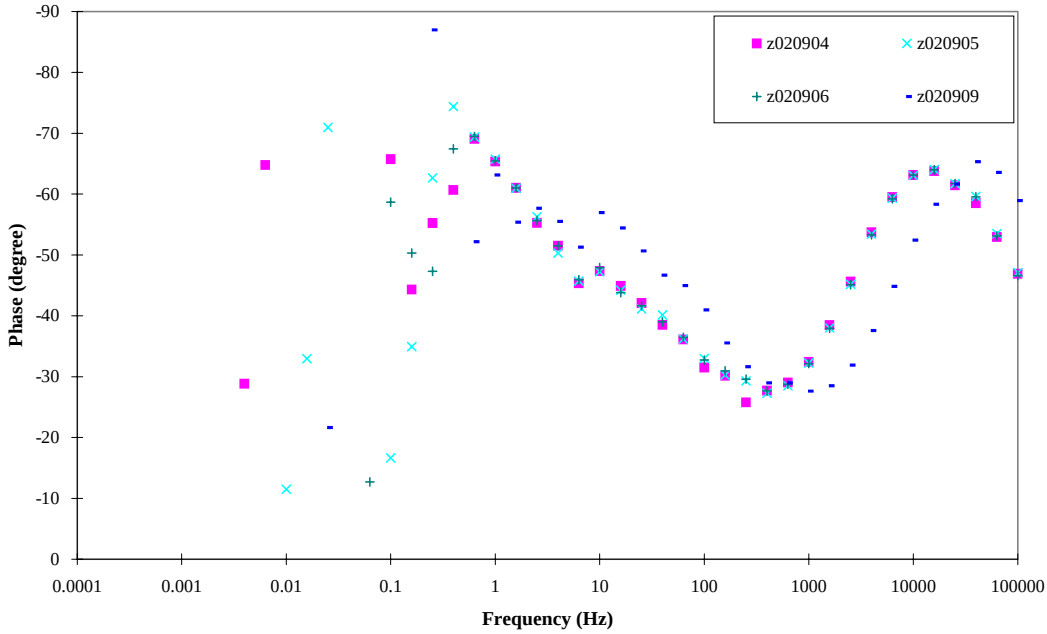

Impedance spectra measured during experiments with the LK3 material (cont.)

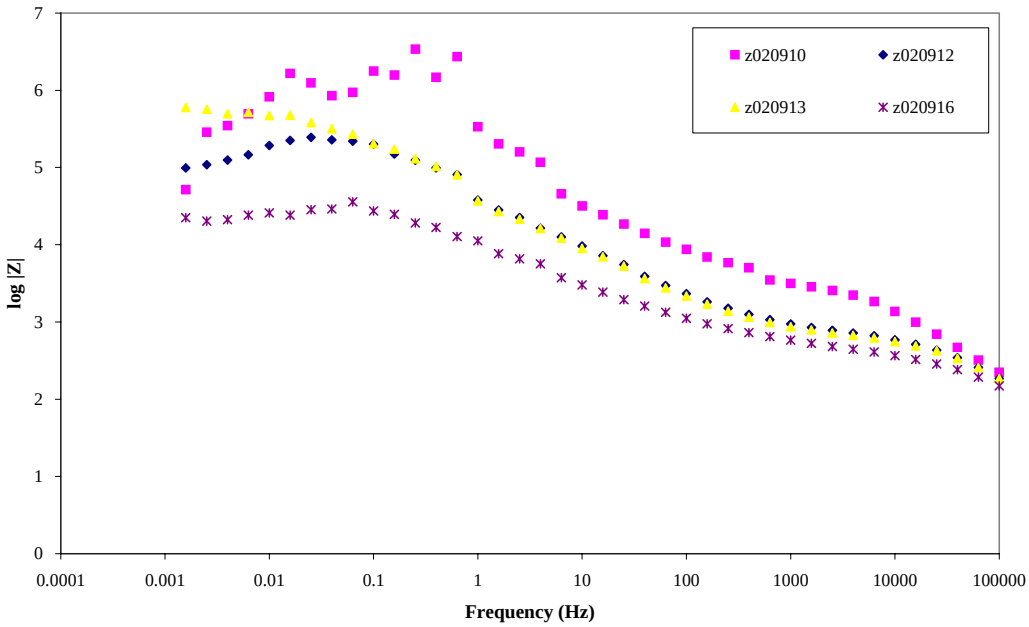

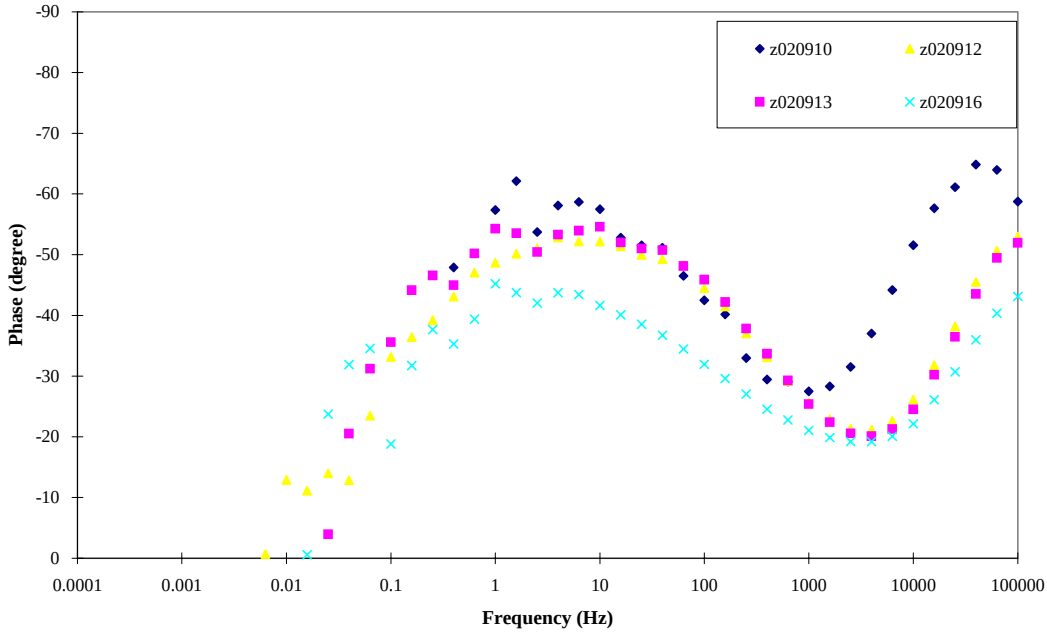

Impedance spectra measured during experiments with the LK3 material (cont.)

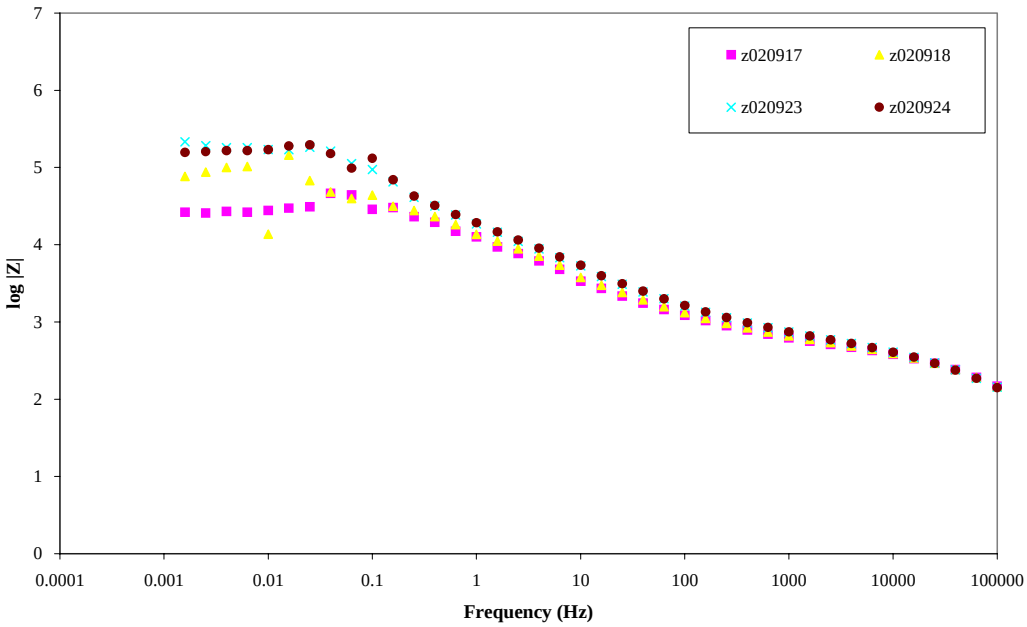

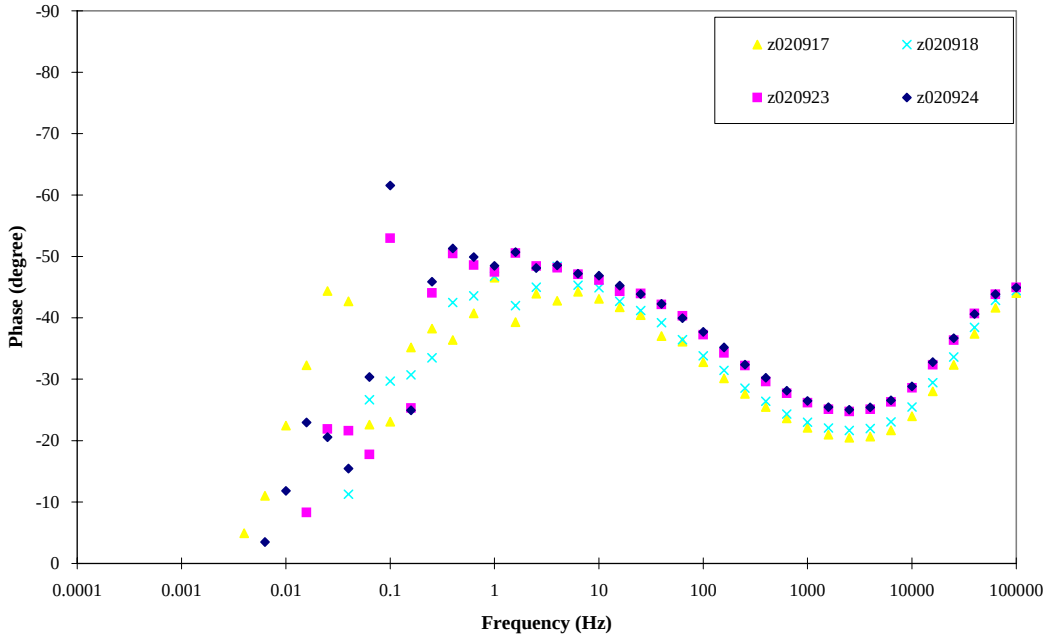

Impedance spectra measured during experiments with the LK3 material (cont.)

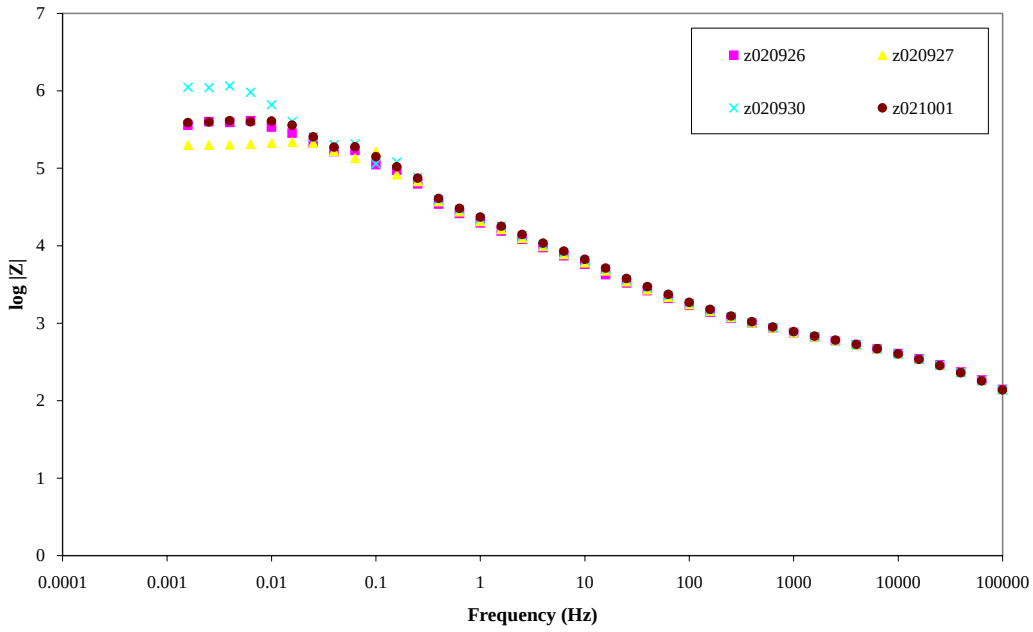

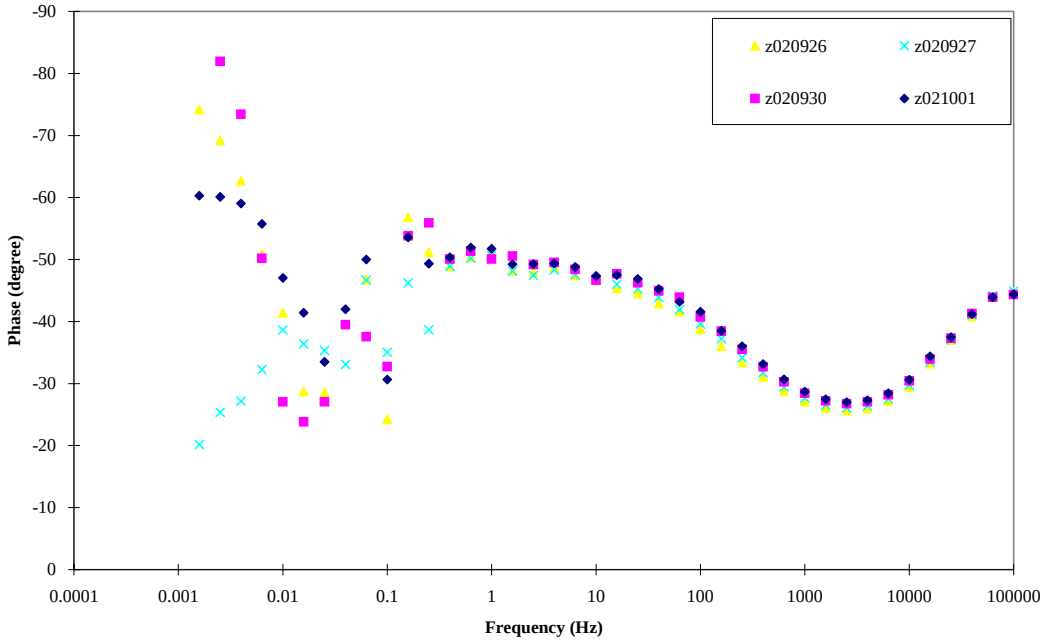

Impedance spectra measured during experiments with the LK3 material (cont.)

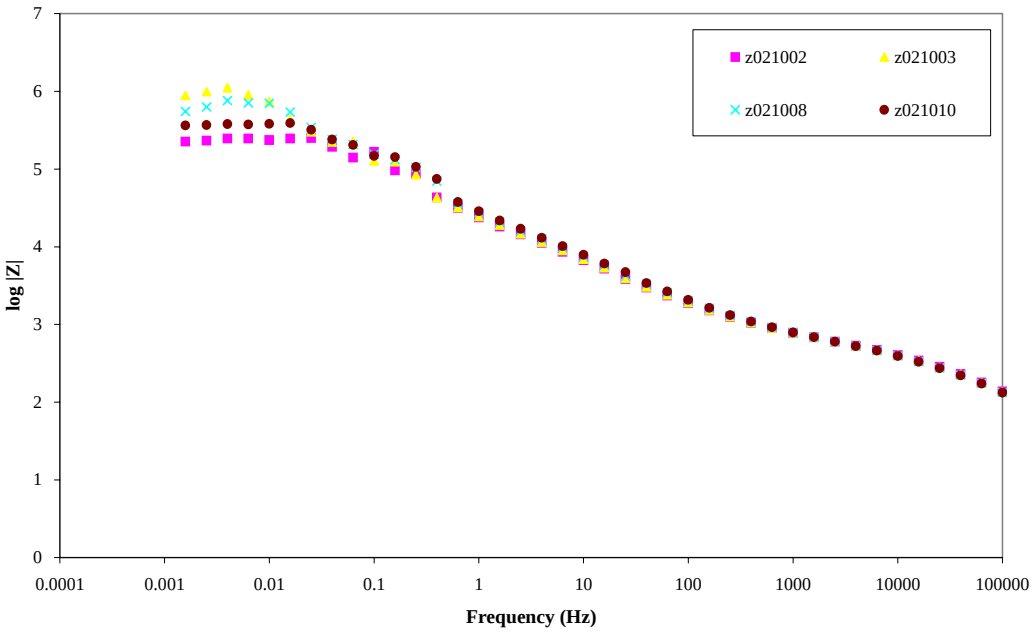

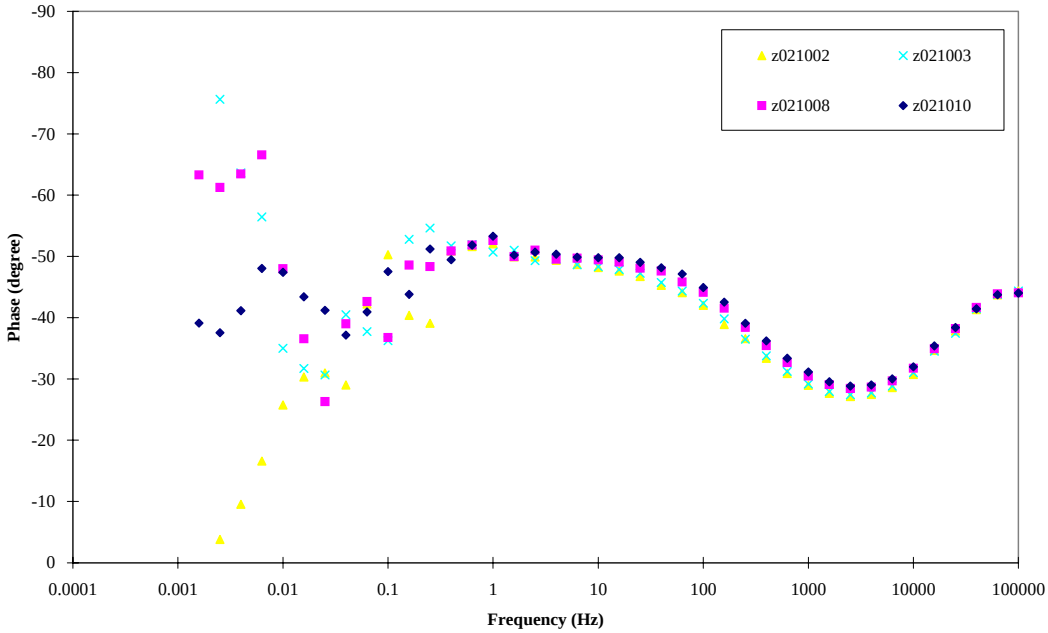

Impedance spectra measured during experiments with the LK3 material (cont.)

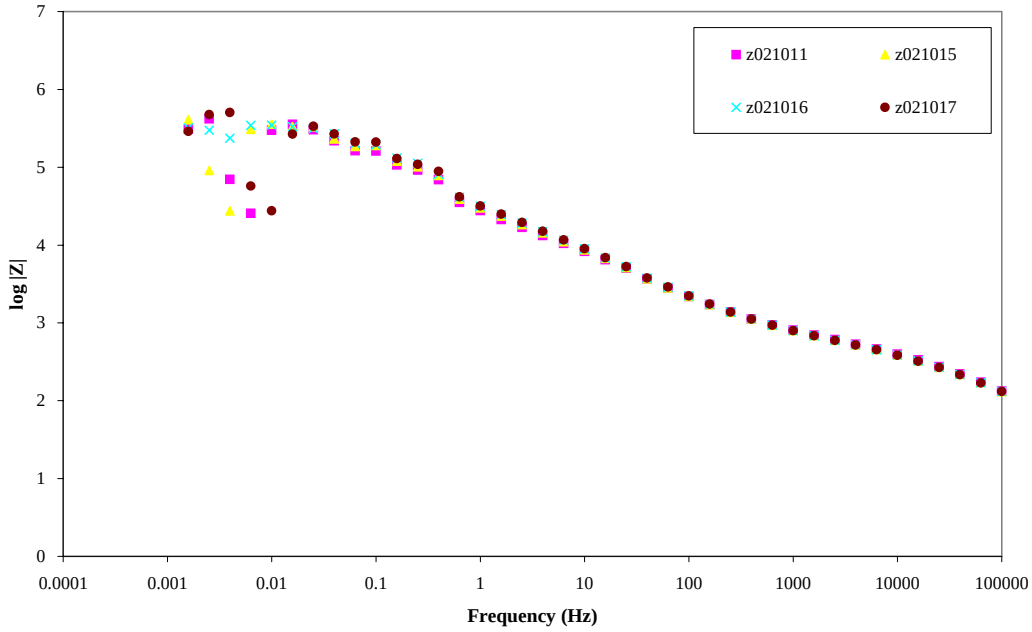

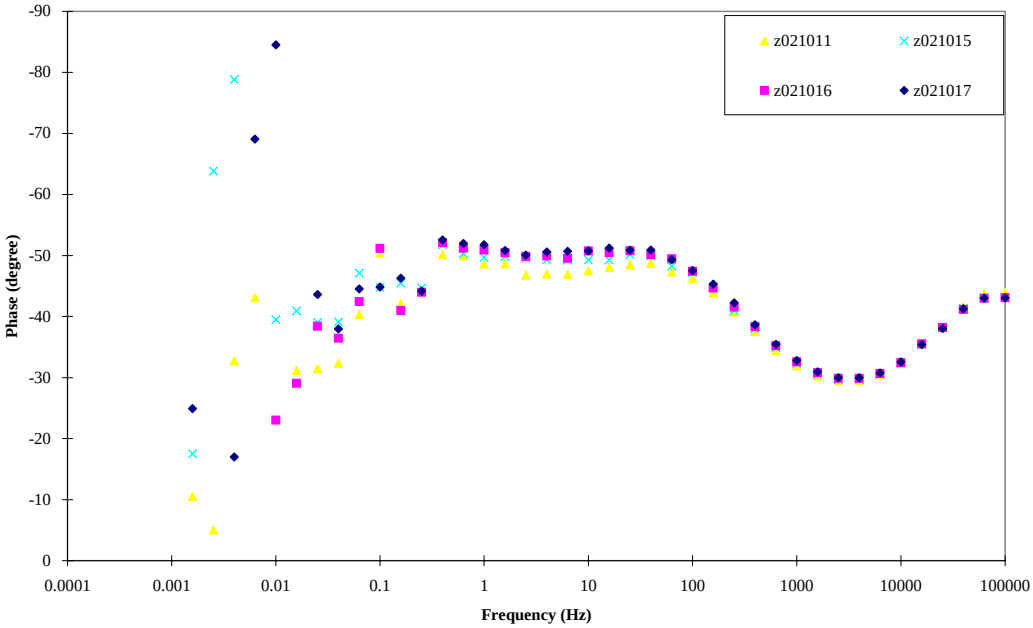

Impedance spectra measured during experiments with the LK3 material (cont.)

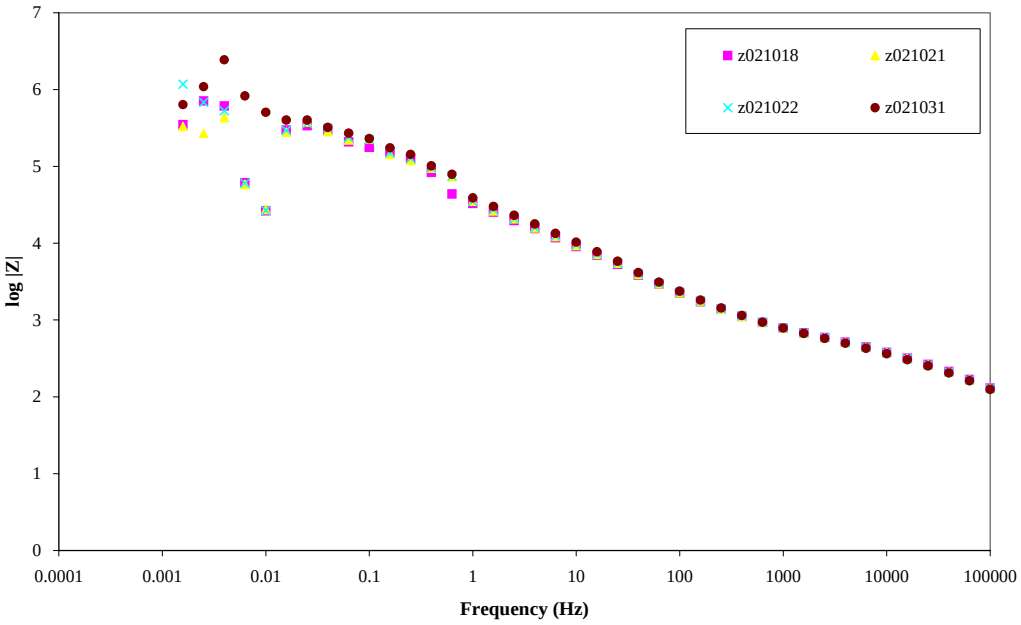

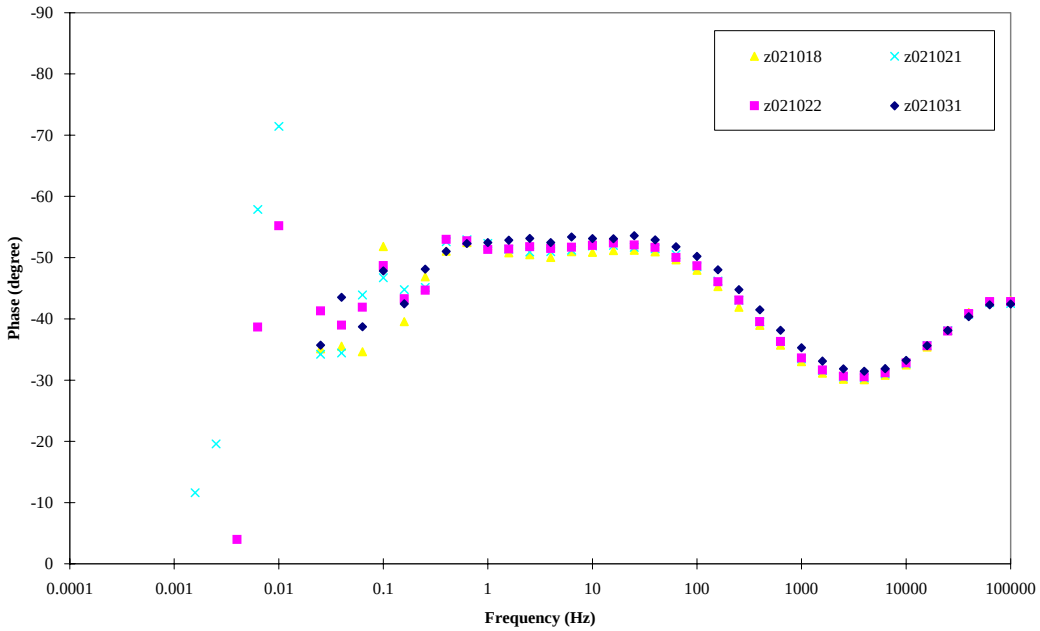

Impedance spectra measured during experiments with the LK3 material (cont.)

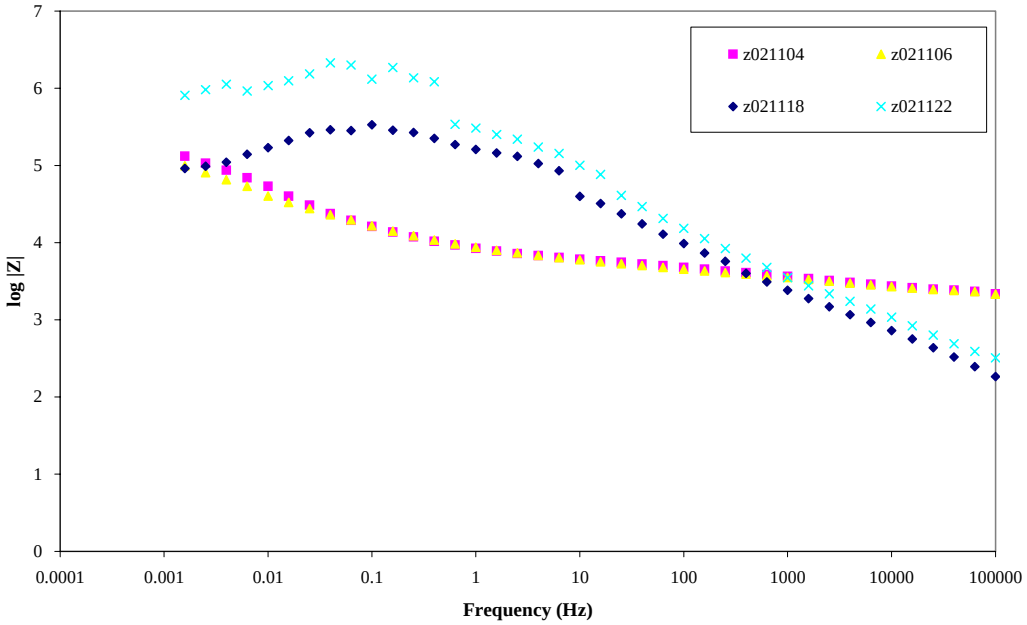

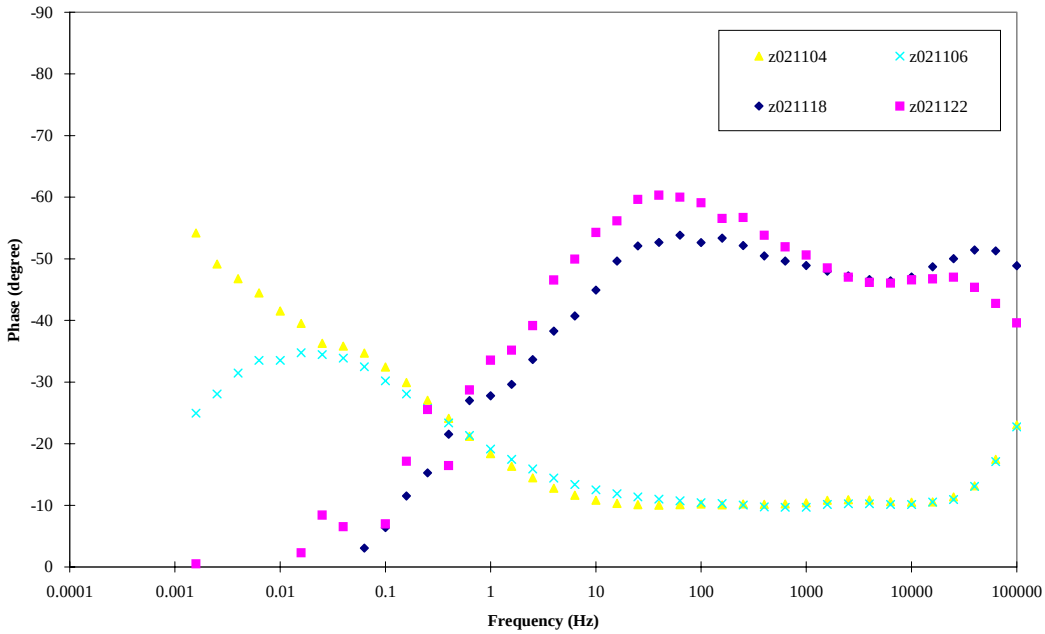

Impedance spectra measured during experiments with the LK3 material (cont.)

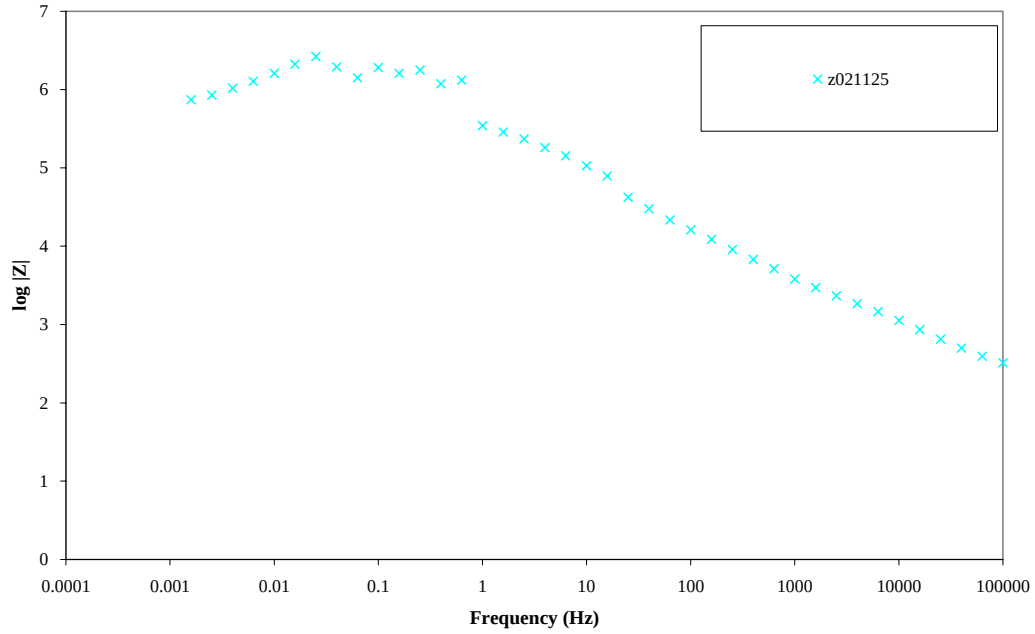

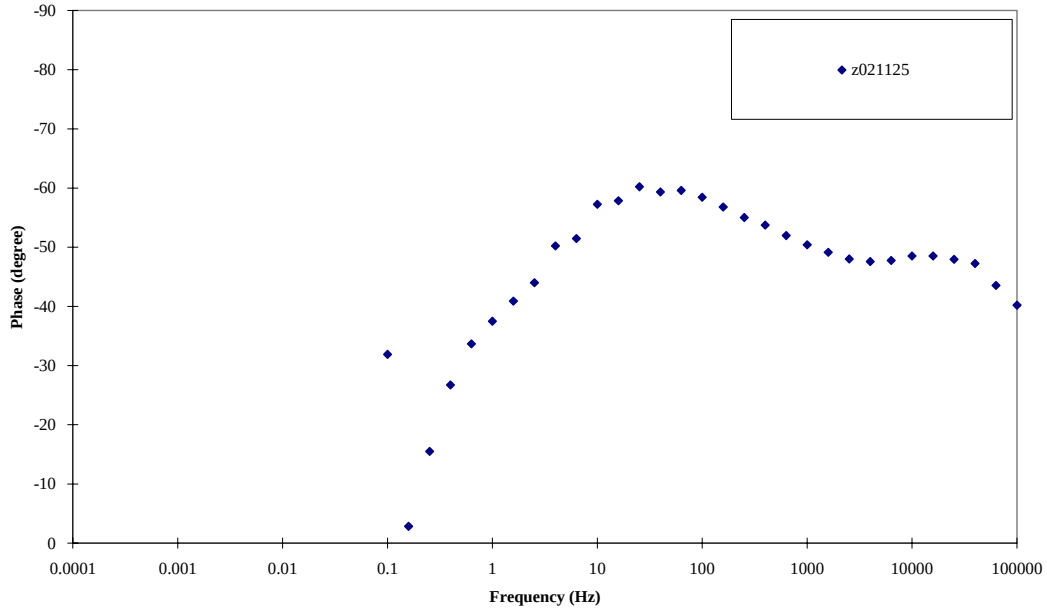

Table C.1
Parameter values from the equivalent circuit analysis for the LK2 material.

Date	Temp. (^{o}C)	R1 (Ω)	Q1 - C_Q (F)	Q1 - α	R2 (Ω)	Q2 - C_Q (F)	Q2 - α	R3 (Ω)
2002-12-02	20	250.0	1.13E-08	0.948	11202	5.95E-07	0.718	754750
2002-12-02	20	249.5	1.18E-08	0.944	11584	5.90E-07	0.722	880970
2002-12-06	100	69.9	2.61E-08	0.899	4518	5.29E-07	0.831	1017000
2002-12-11	200	42.9	3.15E-08	0.903	710	7.11E-06	0.629	534570
2002-12-13	200	41.9	3.43E-08	0.896	708	6.07E-06	0.651	475920
2002-12-16	200	24.8	7.18E-08	0.835	743	6.56E-06	0.663	500000
2002-12-17	200	41.1	5.70E-08	0.853	922	6.60E-06	0.658	500000
2002-12-18	200	25.6	8.62E-08	0.819	874	6.41E-06	0.670	500000
2002-12-19	200	18.8	1.01E-07	0.807	798	6.59E-06	0.671	500000
2003-01-09	200	20.0	3.08E-07	0.726	910	7.88E-06	0.707	500000
2003-01-15	288	12.0	6.49E-07	0.679	963	8.41E-06	0.676	61669
2003-01-16	288	6.6	7.83E-07	0.667	900	7.61E-06	0.676	76839
2003-01-17	288	7.1	7.58E-07	0.672	851	6.98E-06	0.680	92643
2003-01-20	288	10.0	9.18E-07	0.662	874	5.50E-06	0.710	90208
2003-01-21	288	24.3	5.12E-07	0.704	941	6.61E-06	0.675	88315
2003-01-27	288	24.1	5.14E-07	0.708	884	6.00E-06	0.680	112190
2003-01-28	288	35.1	4.23E-07	0.722	956	6.22E-06	0.673	126810
2003-01-29	288	26.3	5.63E-07	0.700	959	5.51E-06	0.690	121850
2003-01-31	288	23.7	5.00E-07	0.712	867	5.34E-06	0.683	174360
Dosage of Fe and Ni started on February 3rd.								
2003-02-04	288	18.9	6.28E-07	0.697	808	5.46E-06	0.677	161650
2003-02-05	288	33.6	4.85E-07	0.715	951	5.22E-06	0.679	183740
2003-02-06	288	21.1	6.75E-07	0.690	906	4.64E-06	0.697	147580
2003-02-07	288	17.9	7.48E-07	0.684	866	4.51E-06	0.699	170080
2003-02-17	288	23.7	6.38E-07	0.701	789	4.80E-06	0.685	201460
2003-02-18	288	33.1	5.32E-07	0.712	862	4.77E-06	0.682	254530
2003-02-20	288	16.9	9.91E-07	0.665	855	3.91E-06	0.708	253810
2003-02-21	288	34.3	6.13E-07	0.701	917	4.16E-06	0.696	230990
2003-02-24	288	24.1	6.80E-07	0.697	764	4.04E-06	0.695	171270
2003-02-26	200	36.6	4.74E-07	0.708	1962	1.53E-06	0.730	138490
2003-02-27	200	24.0	6.33E-07	0.687	1963	1.28E-06	0.754	152390
2003-03-03	100	55.4	4.05E-07	0.708	5416	2.91E-07	0.837	254690
2003-03-04	100	70.7	4.54E-07	0.693	7598	2.41E-07	0.870	256130
2003-03-07	20	282.4	2.75E-07	0.711	13962	1.61E-07	0.841	542910
2003-03-10	20	203.2	3.07E-07	0.705	13345	1.03E-07	0.912	398510

Table C.2
Parameter values from the equivalent circuit analysis for the LK3 material.

Date	Temp. (°C)	R1 (Ω)	Q1 - C_Q (F)	Q1 - α	R2 (Ω)	Q2 - C_Q (F)	Q2 - α	R3 (Ω)
2002-09-04	20	202.3	3.04E-08	0.877	11219	9.41E-07	0.767	1000000
2002-09-05	20	183.9	3.60E-08	0.865	11562	8.68E-07	0.795	1000000
2002-09-06	20	194.5	3.13E-08	0.876	11014	9.67E-07	0.763	1000000
2002-09-09	100	62.2	4.60E-08	0.866	3810	6.79E-07	0.813	964580
2002-09-10	100	51.8	6.24E-08	0.840	3948	6.87E-07	0.829	855280
2002-09-12	200	45.0	4.51E-08	0.878	648	6.84E-06	0.664	157980
2002-09-13	200	48.9	3.51E-08	0.898	578	7.22E-06	0.666	216860
2002-09-16	288	0.0	1.08E-06	0.634	523	2.81E-05	0.592	51548
2002-09-17	288	11.4	7.29E-07	0.672	522	2.53E-05	0.586	73705
2002-09-18	288	7.6	9.45E-07	0.652	585	2.10E-05	0.599	91447
2002-09-23	288	22.5	5.56E-07	0.703	571	1.79E-05	0.580	544400
2002-09-24	288	23.6	5.33E-07	0.707	564	1.77E-05	0.578	892290
2002-09-26	288	28.3	4.31E-07	0.727	543	1.67E-05	0.578	636020
2002-09-27	288	27.6	4.38E-07	0.725	542	1.56E-05	0.580	543170
2002-09-30	288	33.3	3.63E-07	0.744	523	1.45E-05	0.584	719100
2002-10-01	288	34.6	3.52E-07	0.747	524	1.40E-05	0.584	944340
2002-10-02	288	35.1	3.49E-07	0.748	563	1.35E-05	0.588	986700
2002-10-03	288	35.6	3.35E-07	0.752	519	1.32E-05	0.587	983250
2002-10-08	288	36.0	3.41E-07	0.753	515	1.15E-05	0.596	562320
2002-10-10	288	39.1	2.90E-07	0.768	496	1.08E-05	0.599	517590
2002-10-11	288	47.2	1.40E-07	0.827	420	1.12E-05	0.585	254870
Dosage of Fe and Ni started on October 14th.								
2002-10-15	288	44.2	2.33E-07	0.788	461	9.56E-06	0.606	247590
2002-10-16	288	43.5	2.55E-07	0.781	468	9.04E-06	0.612	277620
2002-10-17	288	42.0	2.75E-07	0.775	471	8.87E-06	0.613	311390
2002-10-18	288	42.2	2.75E-07	0.776	465	8.64E-06	0.616	326480
2002-10-21	288	40.3	3.87E-07	0.750	502	7.55E-06	0.632	219760
2002-10-22	288	35.7	4.85E-07	0.731	525	7.28E-06	0.635	208670
2002-10-31	288	35.2	5.66E-07	0.722	518	6.24E-06	0.647	236580
2002-11-04	288							
2002-11-06	288							
2002-11-18	100	54.4	2.24E-07	0.765	1522	1.03E-06	0.663	129550
2002-11-22	20	153.5	2.63E-07	0.733	4265	1.57E-07	0.826	435830
2002-11-25	20	152.5	2.48E-07	0.736	5075	1.69E-07	0.808	548530

Table D.1
Values of α-corrected (extrapolated) capacitance and accompanying values of the dispersion factor for the LK2 material.

Date	Temp. (^{o}C)	High frequencies		Low frequencies	
		log $C_{\alpha\text{-corr}}$	α	log $C_{\alpha\text{-corr}}$	α
2002-12-02	20	-8.279	0.845	-8.107	0.602
2002-12-02	20	-8.259	0.869	-8.133	0.594
2002-12-06	100	-8.141	0.881	-7.572	0.702
2002-12-11	200			-7.224	0.623
2002-12-13	200			-7.125	0.657
2002-12-16	200			-7.120	0.647
2002-12-17	200			-7.159	0.639
2002-12-18	200			-7.013	0.673
2002-12-19	200			-7.056	0.659
2003-01-09	200			-6.653	0.723
2003-01-15	288			-7.044	0.592
2003-01-16	288			-7.034	0.612
2003-01-17	288			-7.271	0.538
2003-01-20	288			-7.094	0.605
2003-01-21	288			-7.250	0.553
2003-01-27	288			-7.226	0.579
2003-01-28	288			-7.200	0.592
2003-01-29	288			-7.241	0.579
2003-01-31	288			-7.096	0.640
Dosage of Fe and Ni started on February 3rd.					
2003-02-04	288			-7.265	0.582
2003-02-05	288			-7.224	0.604
2003-02-06	288			-7.153	0.631
2003-02-07	288			-7.103	0.648
2003-02-17	288			-7.073	0.663
2003-02-18	288			-7.094	0.666
2003-02-20	288			-7.045	0.682
2003-02-21	288			-7.107	0.669
2003-02-24	288			-7.117	0.665
2003-02-26	200			-7.323	0.695
2003-02-27	200			-7.278	0.709
2003-03-03	100			-7.865	0.614
2003-03-04	100			-7.743	0.656
2003-03-07	20	-8.166	0.699	-8.046	0.637
2003-03-10	20	-8.184	0.646	-7.959	0.657

Table D.2
Values of α-corrected (extrapolated) capacitance and accompanying values of the dispersion factor for the LK3 material.

Date	Temp. (°C)	High frequencies		Low frequencies	
		log $C_{\alpha\text{-corr}}$	α	log $C_{\alpha\text{-corr}}$	α
2002-09-04	20	-8.210	0.836	-7.050	0.817
2002-09-05	20	-8.209	0.827	-7.252	0.773
2002-09-06	20	-8.211	0.825	-7.207	0.784
2002-09-09	100	-8.080	0.874	-7.570	0.667
2002-09-10	100	-8.080	0.869	-7.626	0.648
2002-09-12	200			-7.071	0.649
2002-09-13	200			-7.015	0.661
2002-09-16	288			-7.046	0.512
2002-09-17	288			-6.994	0.545
2002-09-18	288			-6.971	0.567
2002-09-23	288			-7.073	0.574
2002-09-24	288			-7.084	0.575
2002-09-26	288			-7.128	0.570
2002-09-27	288			-7.116	0.578
2002-09-30	288			-7.137	0.581
2002-10-01	288			-7.145	0.583
2002-10-02	288			-7.152	0.584
2002-10-03	288			-7.164	0.584
2002-10-08	288			-7.172	0.593
2002-10-10	288			-7.190	0.594
2002-10-11	288			-7.303	0.565
Dosage of Fe and Ni started on October 14th.					
2002-10-15	288			-7.201	0.601
2002-10-16	288			-7.201	0.604
2002-10-17	288			-7.227	0.598
2002-10-18	288			-7.214	0.603
2002-10-21	288			-7.203	0.611
2002-10-22	288			-7.204	0.612
2002-10-31	288			-7.154	0.637
2002-11-04	288				
2002-11-06	288				
2002-11-18	100			-7.843	0.617
2002-11-22	20	-8.110	0.571	-7.847	0.691
2002-11-25	20	-8.115	0.613	-7.911	0.677

www.ski.se

STATENS KÄRNKRAFTINSPEKTION
Swedish Nuclear Power Inspectorate

POST/POSTAL ADDRESS SE-106 58 Stockholm
BESÖK/OFFICE Klarabergsviadukten 90
TELEFON/TELEPHONE +46 (0)8 698 84 00
TELEFAX +46 (0)8 661 90 86
E-POST/E-MAIL ski@ski.se
WEBBPLATS/WEB SITE www.ski.se